INSITU DETERMINATION OF HYDRAULIC CONDUCTIVITY IN THE VADOSE ZONE USING BOREHOLE INFILTRATION TESTS

by

Daniel B. Stephens
Principal Investigator

and

Scott Tyler, Kevin Lambert, David Watson
Richard Rabold, Robert Knowlton
Elizabeth (Andrews) Byers and Scott Yates
Graduate Research Assistants

Department of Geoscience
New Mexico Institute of Mining and Technology
Socorro, NM 87801

and

Shlomo P. Neuman
Co-Investigator
Department of Hydrology
and Water Resources
University of Arizona
Tucson, AZ

TECHNICAL COMPLETION REPORT

Project No. 1423648

November 1983

New Mexico Water Resources Research Institute
and U.S. Department of Interior Office
of Water Research and Technology

The research on which this report is based was financed in part by the U.S. Department of the Interior, as authorized by the Water Research and Development Act of 1978 (P.L. 95-467).

Project numbers: B-073-NMEX, 1423648, 1345674

The purpose of WRRI technical reports is to provide a timely outlet for research results obtained on projects supported in whole or in part by the institute. Through these reports, we are promoting the free exchange of information and ideas and hope to stimulate thoughtful discussion and action which may lead to resolution of water problems. The WRRI, through peer review of draft reports, attempt to substantiate the accuracy of information contained in its reports, but the views expressed are those of the author(s) and do not necessarily reflect those of the WRRI or its reviewers.

Contents of this publication do not necessarily reflect the views and policies of the U.S. Department of the Interior, nor does mention of trade names or commercial products constitute their endorsement or recommendation for use by the U.S. government.

ABSTRACT

Predicting the rate of water movement above a water table is a crucial problem in hazardous and radioactive waste disposal, in the design of dams, and in the irrigation and drainage of agricultural land. Hydraulic conductivity, the key soil characteristic governing the rate of water movement, was determined in the field using constant head borehole infiltration tests.

Earlier results of numerical simulations of the saturated-unsaturated flow process were verified; these indicate that only a finite zone of soil immediately surrounding the borehole is nearly saturated. Carbon dioxide injected into the borehole prior to water infiltration is an effective means to reduce the amount of entrapped air and reduce the water volume required to complete a test. New empirical solutions were developed to account for capillary effects. The borehole test results generally compared favorably with other field techniques that are restricted in application to near surface, and also with laboratory permeameter experiments on shelby tube samples. Laboratory permeameter experiments on small ring samples (100cc) produced consistently greater values of saturated hydraulic conductivity than other methods.

Keywords: Hydraulic conductivity*, soil moisture movement, unsaturated soils*

TABLE OF CONTENTS

TABLE OF CONTENTS (continued)

LIST OF FIGURES

Figure (continued) Page

Figure (continued) Page

Figure (continued) Page

LIST OF TABLES

INTRODUCTION

Groundwater recharge and movement of pollutants through the vadose zone are of fundamental importance to water resource specialists and environmental regulatory agencies. The physical quantity that characterizes the ability of porous media to transmit fluid is called the hydraulic conductivity. Hydraulic conductivity is dependent upon the water content of the porous medium. Saturated hydraulic conductivity, K_s, occurs when the pores are completely filled with water. Soil scientists developed several methods to determine K_s at very shallow depths. However, due to instrumentation and special construction procedures these methods are not applicable when the thickness of the vadose zone (region between the land surface and the water table) exceeds two or three meters. Borehole infiltration methods are the only means to predict K_s in situ at any depth. The constant head borehole infiltration test simply requires drilling a cased or uncased borehole of known diameter, filling it with water, and measuring the rate at which water must be added to the borehole to maintain a constant water level.

Review of Previous Literature

Analytical solutions for steady infiltration from an open borehole into a homogeneous isotopic soil were developed for deep water table conditions by Glover (1953), and by Terletskata (1954) on the basis of earlier work by Nasberg (1951). According to their concept, the water infiltrating from the borehole into the soil flows radially and downward in response to pressure and gravity gradients. The flow region is assumed to be fully saturated everywhere and is confined within an envelope known as 'free surface'. The latter is a streamline across which no flow can take place and an isobar along which the pressure is everywhere atmospheric. The soil outside the free surface envelope is dry and is not considered to be part of the flow region.

Glover's equation is

$$K_s = \frac{Q_s}{rH} \cdot \frac{1}{C_u} \qquad (1)$$

where

$$C_u = \frac{2\pi H}{r} \cdot \left[\sinh^{-1}\left(\frac{H}{r}\right) - 1\right]^{-1} \qquad (2)$$

and Q_s is the steady infiltration rate, H is height of water in the borehole, and r is the borehole radius. The same formula is recommended in Appendix Des. E-19 of the U.S. Bureau of Reclamation (USBR) Earth Manual (1974) for determining K_s by the well permeameter method. Winger (1960) used equation 1 to prepare a nomogram for K_s to be used with a field technique he called the shallow-well pump-in method. Bouwer (1978) refers to this technique as the reverse auger-hole method. The well permeameter, shallow-well pump-in, and reverse auger-hole methods are essentially the same test.

Equation 1 is based on an analytical solution for a vertical line source whose strength increases linearly with depth in response to gravity. The line source solution is modified in an approximate manner to represent a cylindrical source by prescribing a constant pressure head along the borehole radius at the bottom of the hole. The solution does not account explicitly for the unconfined nature of the flow, i.e., for the presence of a free surface, although the assumption of a linearly increasing source strength is a step in this direction. However, this assumption precluded Glover from guaranteeing that the total hydraulic head along the borehole-soil interface will remain uniform. Another limitation of the analytical solution is that is disregards outflow through the open bottom of the borehole.

According to Glover (1953), when Cu is determined from an electrical

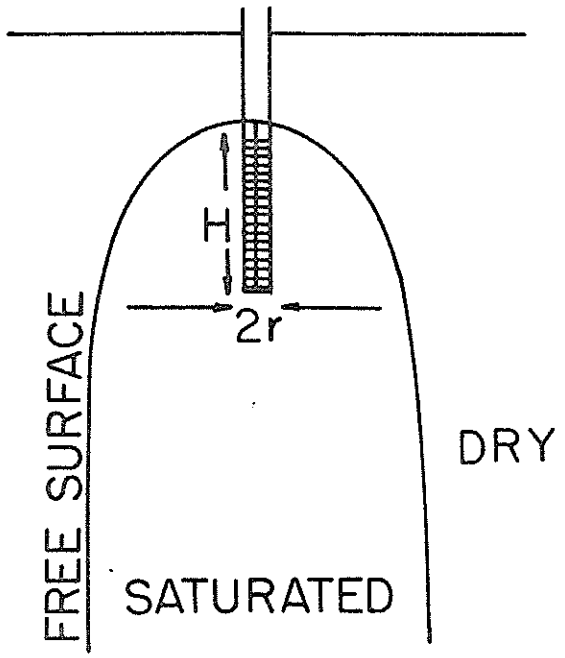

GLOVER $K = \frac{.159Q}{H^2}\left[\sinh^{-1}\left(\frac{H}{r}\right)-1\right]$

NASBURG-TERLETSKATA

$$K = 0.423\,\frac{Q}{H^2}\log_{10}\left(\frac{2H}{r}\right)$$

Figure 1. Free Surface Concept of Flow from a Borehole.

analogue which accounts exactly for all the boundary conditions, including a free surface of the kind shown in figure 1, it exceeds the Cu value defined in equation 1 by 25 percent when H/r = 6, and by 8 percent when H/r = 8. From this, he concluded that equation 1 is reasonably accurate as long as $H/r \geq 10$.

Glover's formula was extended by Zanger (1953) to account for situations where the borehole is partially cased so that the open interval, A, is less than H. Zanger's formula has the form

$$K_s = \frac{Q_s}{2\pi A(2H-A)}\left[\sinh^{-1}\left(\frac{A}{r}\right) - \left(\frac{A}{H}\right)\right] \qquad (3)$$

Its derivation differs from that of Glover only in the limits of integration along the borehole.

One important consideration in performing borehole infiltration tests is the volume of water required to complete the test. According the USBR practice, one computes the minimum volume of water required for an open-hole gravity test, V_{min}, from

$$V_{min} = 2.09\ Sy\ H^3\left[\frac{2}{\sinh^{-1}\frac{H}{r} - 1}\right]^{3/2} \qquad (4)$$

where Sy is specific yield. If Sy is unknown, a value of 0.35 is recommended by the USBR (1974). Equation 4 is derived by noting that, according to figure 1, at some depth below the borehole the flow is everywhere directed vertically downward, in response solely to gravity. Because this implies that all equipotentials (surfaces of equal hydraulic head) are horizontal, and because the free surface is a zero pressure isobar, the vertical hydraulic gradient is equal to unity. Thus, the total rate of flow within the free surface envelope is equal to $Q_s = \pi\ r^2_{fs} K_s$ in which r_{fs} is the radius of this

envelope as defined in figure 1. By comparing this expression with equation 1, one finds that $r_{fs} = H\{2/[\sinh^{-1}(H/r)-1]\}^{1/2}$. Substituting this into equation 4 one obtains $V_{min} = 2.09\ Syr^3_{fs} = 2/3\ \pi\ Syr^3_{fs}$. This is equal to the volume of pores that can be saturated (or desaturated) under gravity within a soil hemisphere of radius rfs. The basis for using the hemisphere volume in computing V_{min} has not been determined.

For open-hope gravity tests, according to USBR (1974), when specific yield is unknown the maximum volume of water required, V_{max}, is given by

$$V_{max} = 2.05 \cdot V_{min} \qquad (5)$$

in which V_{min} is computed according to equation 4 by substituting 15.0 for 2.09, and setting Sy equal to 0.1. Stephens (1979) computed Sy as porosity minus initial water content.

Winger (1965) states that if the volume of water exceeds 1.5 V_{max} " ... without reaching a relatively constant permeability, any permeability selected can be classed as doubtful.

According to Bouwer and Jackson (1974), the volume of soil sampled in the well permeameter test is approximately equal to 0.4 H^3 in which H is in meters. However, this derivation apparently is not published. We are unaware of any methods to predict V_{min}, V_{max}, or sample size for tests with partially cased boreholes, for open-end type tests, or for tests conducted under shallow water table conditions.

Nasberg (1951) developed a formula for K_s based on an analytical solution for a point source above the water table, taking into account the presence of a free surface. Nasberg's approach is similar to that of Glover (1953) except that he has included an image point sink to satisfy more closely the free surface boundary condition and to account for the presence of a stagnation point above the point source. Lamachere (1971) reported that Terletskata

(1954) extended Nasberg's work to the case of a line source by integrating Nasberg's point source solution along the well bore, treating the strength of the source as a constant. (It will be recalled that in Glover's derivation, the strength of the source increases linearly with depth below the water level in the borehole.) Terletskata extended her solution to approximate a cylindrical source by imposing a prescribed pressure head at the bottom of the borehole along its radius, in a manner similar to that of Glover. The Nasberg-Terletskata formula reads

$$K_s = \frac{0.423\ Q}{H^2} \log_{10} \frac{2H}{r} \qquad (6)$$

According to Kozminski (1973), equation 6 is valid in the range $50 < H/r < 200$.

Refer to Stephens and Neuman (1982a) for other details regarding analytical solutions to calculate K_s from borehole infiltration tests.

Using numerical simulations of the constant head borehole infiltration problem which included both saturated and unsaturated flow, Stephens and Neuman (1982b) proposed an empirical solution for the steady state case:

$$\log C_u = 0.658 \log (H/r) - 0.238\alpha^{0.5} - 0.398 \log h + 1.343 \qquad (7)$$

where r = borehole radius, meters,

H = height of water in borehole, meters

α = slope of natural logarithm of the relative hydraulic conductivity, K_r, versus pressure head, ψ, meters^{-1} [ln $0.5/\psi(K^r = 0.5)$]

Their saturated-unsaturated simulations also showed that at steady state, the zone of saturation is limited to a relatively small region surrounding the borehole, outside of which unsaturated flow occurred. This is in sharp

contrast to the free surface flow concept in which the entire flow region is assumed to be saturated and bounded by a zero guage pressure surface. The size of the flow region depends on the magnitude of the capillary effect, which is usually large in fine textured soils and small in coarse textures soils (figure 2). More important perhaps is the conclusion that for tests in homogeneous isotropic soils, existing analytical solutions may overestimate K_s by more than 160 percent in fine textured soils when the height of water in the borehole is small. When the height of water is large and the texture of the soil is coarse, existing analytical solutions may underestimate K_s by more than 35 percent. The value of K_s was also found to be dependent on initial soil moisture conditions or recharge rate. Contrary to what is indicated by existing analytical solutions, Stephens (1979) and Stephens and Neuman (1982b) concluded that in homogeneous isotropic soils, a unique relationship does not exist between K_s, borehole factors, and steady flow rate. They also showed that existing solutions may lead to errors of more than a few hundred percent from tests in heterogeneous and anisotropic soils.

Time dependent simulations of constant head borehole infiltration tests by Stephens (1979) and Stephens and Neuman (1982c) indicated that the time to reach any fraction of the steady infiltration rate and water volume requirements depends mostly upon hydraulic conductivity and specific moisture capacity of the soil, initial moisture content, open area along the borehole, and height of water in the borehole. His numerical experiments showed that USBR (1974) procedures lead to terminating a field test prematurely and overestimating K_s. In addition, the volume of the soil sample was found to be as much as one to two orders of magnitude greater than that predicted by Bouwer and Jackson (1974).

Stephens (1979) suggested that instead of waiting days or weeks for a

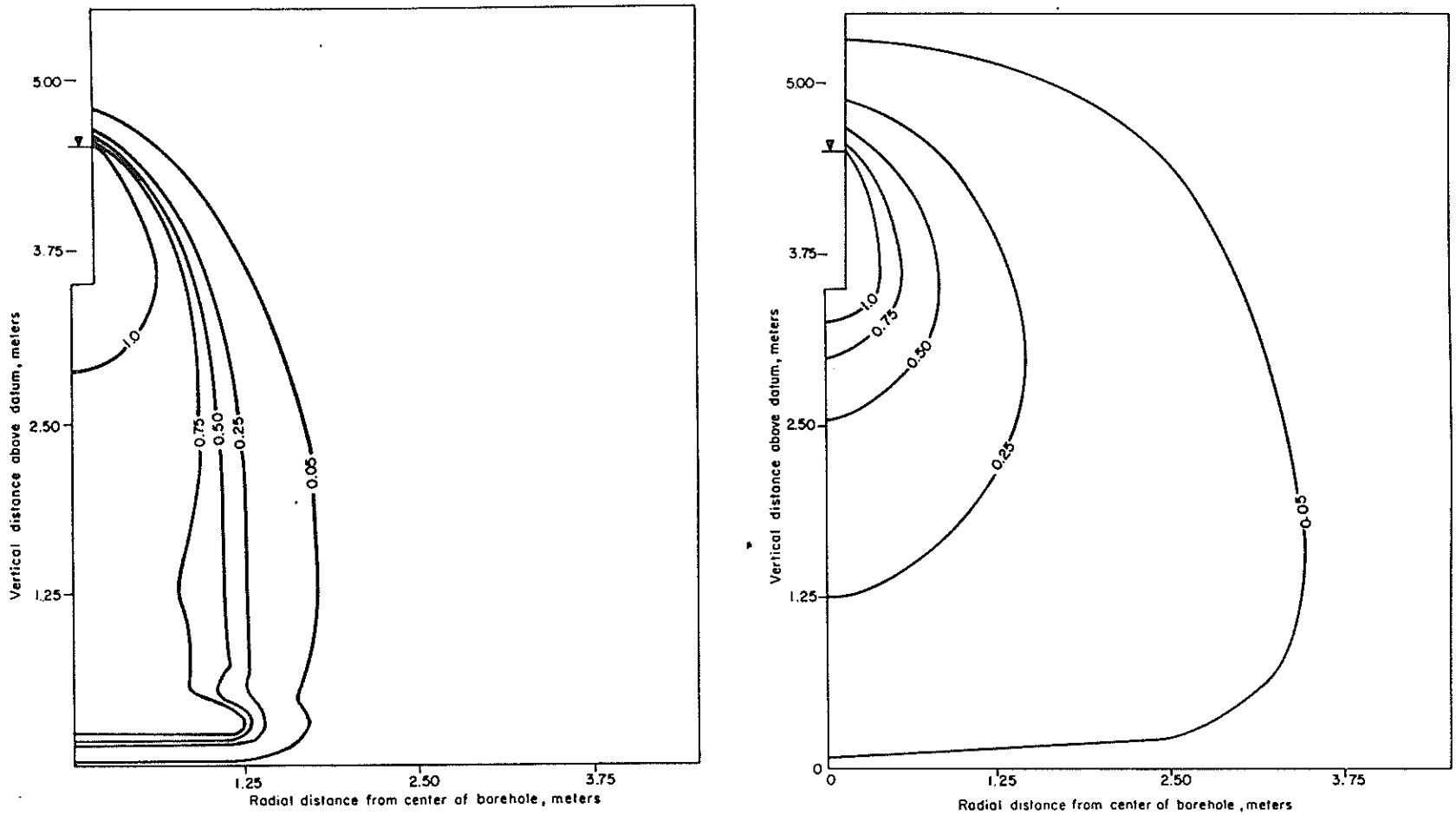

Figure 2. Lines of Equal Relative Hydraulic Conductivity Corresponding to Distribution of Pressure Head Predicted from Saturated-Unsaturated Model.

a) Coarse Sand b) Silt Loam G.E. #3

steady flow rate to occur in low permeable soils, Q_s could be estimated after only a few hours by graphical procedure based on a plot of infiltration rate versus the inverse of the square root of time.

Objectives

The overall objective of the proposed research is to develop a reliable and efficient field technique to determine saturated hydraulic conductivity in the vadose zone for deep water table conditions. More specifically, the project objectives are to:

1) Verify recent theoretical work regarding the reliability of borehole infiltration tests, based on numerical simulations by Stephens (1979). To aid engineers, hydrologists and regulatory agencies, we hope to establish the degree of accuracy with which the various borehole infiltration methods and solutions may be expected to predict saturated hydraulic conductivity under field conditions. We want to evaluate in the field, the effect of capillarity and unsaturated flow, soil heterogeneity, anisotropy, and other factors that may influence the value of saturated hydraulic conductivity obtained from borehole infiltration tests. We also want to know what volume of soil near the borehole is actually sampled during these tests.

2) Apply the new theoretical results to develop improved field procedures and solutions to determine saturated hydraulic conductivity for a wide range of field conditions. We want to test the procedures suggested by Stephens (1979) to reduce the time of testing from days to only a few hours, and to appreciably reduce the injected volume of water needed during the borehole infiltration tests. We will test the approximate solutions proposed by Stephens (1979), which account for capillary effects using empirical

parameters characteristic of the soil (refer to Related Research for details).

3) Compare results of borehole infiltration tests with other methods to compute saturated hydraulic conductivity in the vadose zone used mostly by soil scientists, including shallow depth field techniques and laboratory analyses of core samples.

SITE DESCRIPTION

Location Physiography and Climate

All field experiments were conducted on the Sevilleta National Wildlife Refuge, located about 30 kilometers north of Socorro, New Mexico, about 4.5 kilometers west of Interstate Route 25 and 100 meters south of the Rio Salado (figure 3). The site was selected because of its ease of access by truck, security, close proximity to groundwater for water supply, apparent uniform composition of unconsolidated sand, and sparse vegetation. The test area is situated on an old flood plain adjacent to a narrow sand dune (figure 4). The site is sloped very gently northward toward the Rio Salado and there is little evidence of surface runoff, owing mostly to the high infiltration capacity of the soil. Vegetation consists mostly of saltbush, creosote and grasses and a few juniper. Mean annual precipitation is approximately 20cm and gross annual lake evaporation is about 178cm (U.S. Department of Agriculture 1972).

Geology and Soils

The surficial material at the site was mapped by Machette (1978) as Alluvial Unit B of Holocene age, a silty sand to sandy gravel which forms a low terrace adjacent to the active channel of the ephemeral Rio Salado. The thickness of the unit is reported by Machette to exceed 2m along the mainstem of the Rio Salado. An excavation to a depth of 2.5m at the site just north of

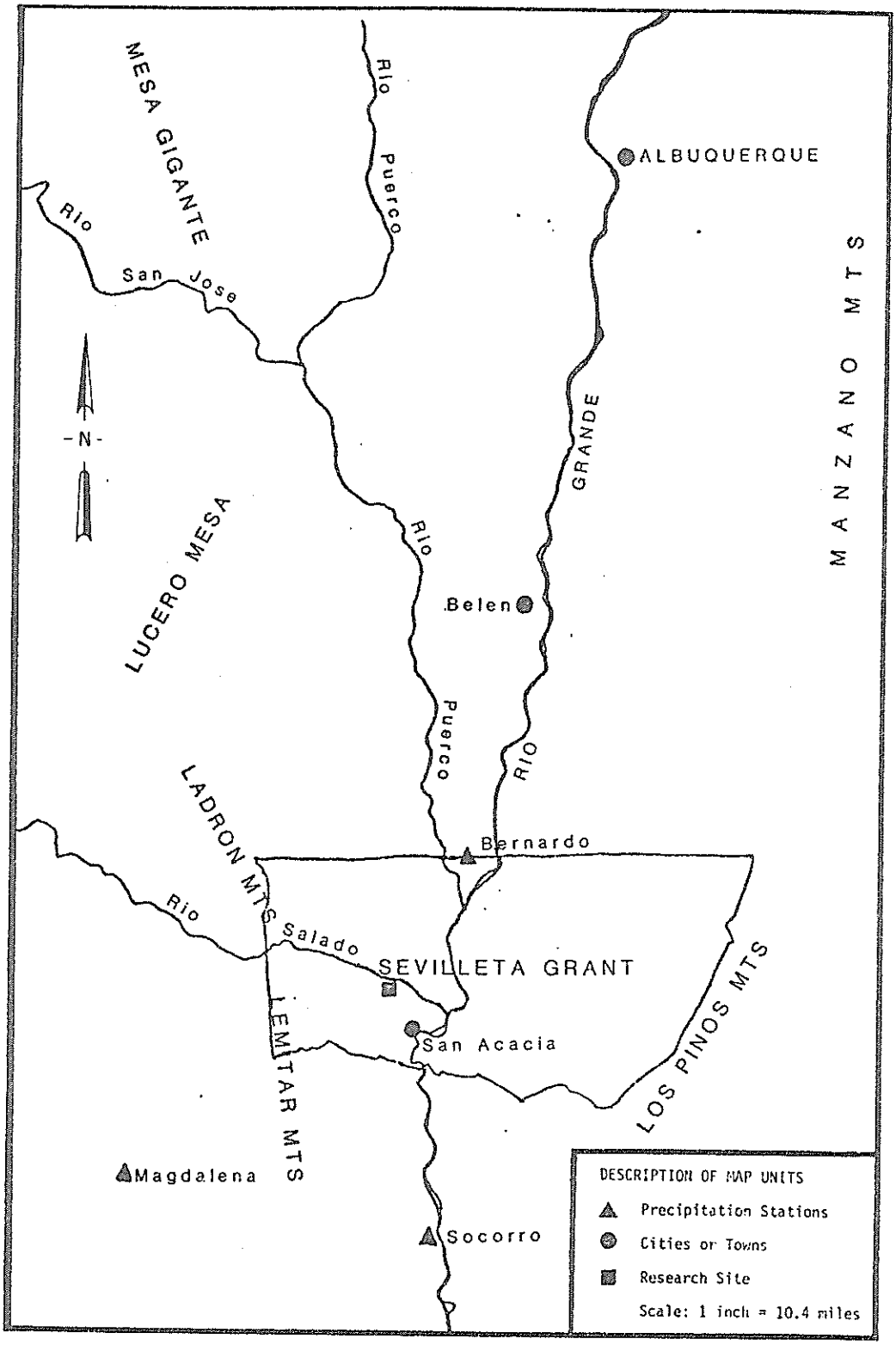

Figure 3. Location Map.

Figure 4. Photo of Dune and Vegetation.
(Left to Right: Kevin Lambert, Scott Yates, Shlomo Neuman, Elizabeth Andrews Byers)

location 5 shown in figure 5 reveals a thick section of sand; silt layers a few centimeters thick occur at depths of approximately 180, 215, and 250cm (figure 6). The 180cm silt layer pinched out within the excavation; however, the lenticular nature of the other layers is not yet established below land surface. Detailed mapping of sedimentary structures in the pit reveals a fluvial depositional environment with some coarse sand and pebbles in the upper 0.7 meters, a stratified zone of fine to medium sand with thin carbonate cemented layers to a depth of about 1.4m, and a relatively unstratified fine to medium sand to the base of the pit. Hand auger samples nearby showed a 15cm-thick clay seam at 4.5 meter depth and a cobble zone at 5 meters.

Fresh excavations of the sand below about 25cm appear moist, and boreholes, trenches and pits do not slough until the sand dries. The depth to water is about 5.5 meters. There was no evidence of a well-developed soil profile. Only occasionally were roots discovered below a few centimeters depth; however, in a few places excavations revealed finger-sized holes of undetermined extent which may represent animal burrows or voids left from decayed roots. An example of such a void is shown if Figure 6 at the 162cm depth to the right of the tape.

HYDRAULIC PROPERTIES

Traditional approaches to characterize the hydraulic properties of the soil are necessary to provide a basis for comparison with borehole test results and to extrapolate results to other soils. Comparative data were collected for particle size distribution, soil-water characteristic curve, porosity, and saturated and unsaturated hydraulic conductivity.

Particle Size Distribution

Stainless steel ring samples 100cc in volume were collected in the site area along three horizontal transects (W, X, and Y) and a vertical transect

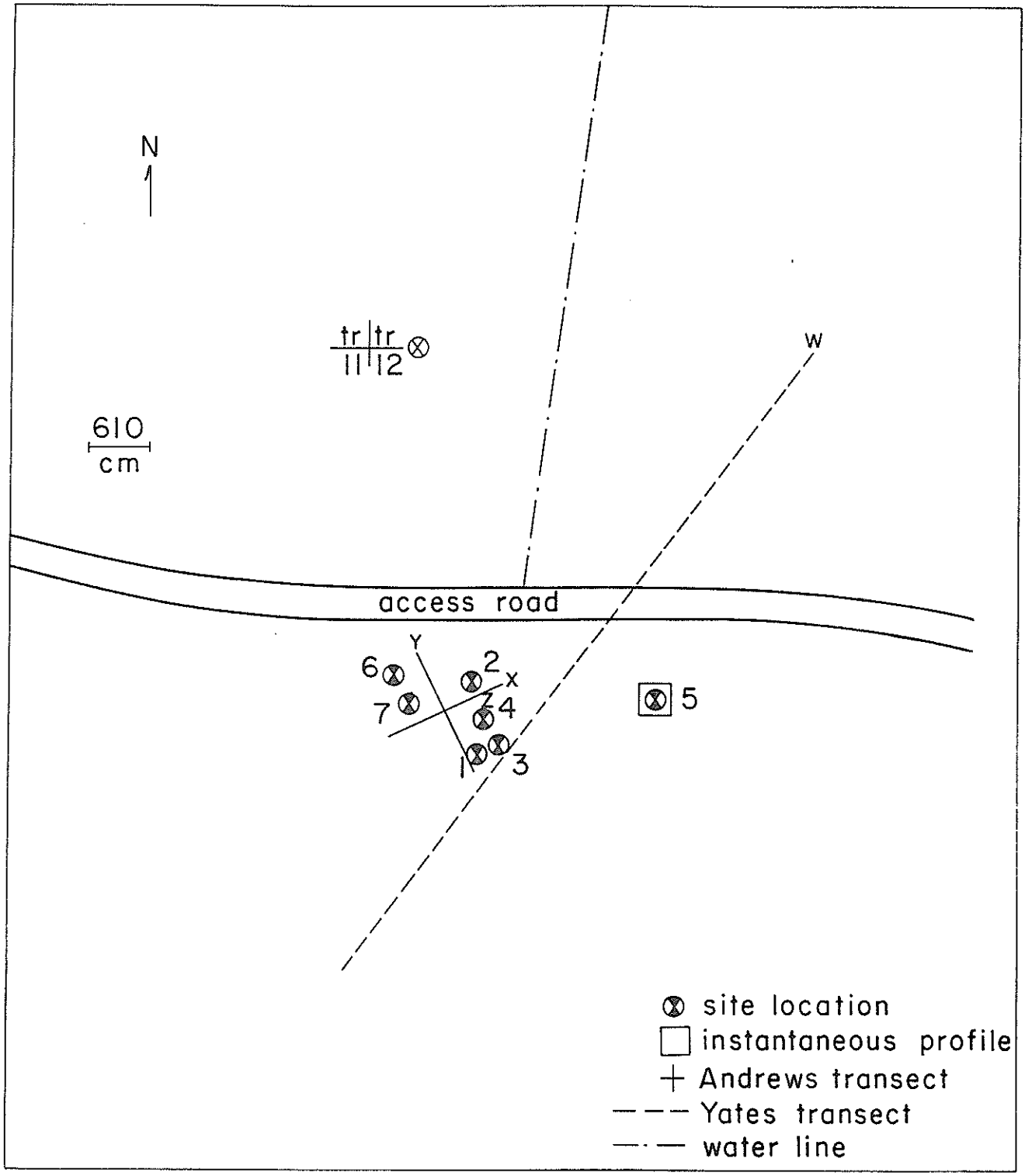

Figure 5. Test Location Map.

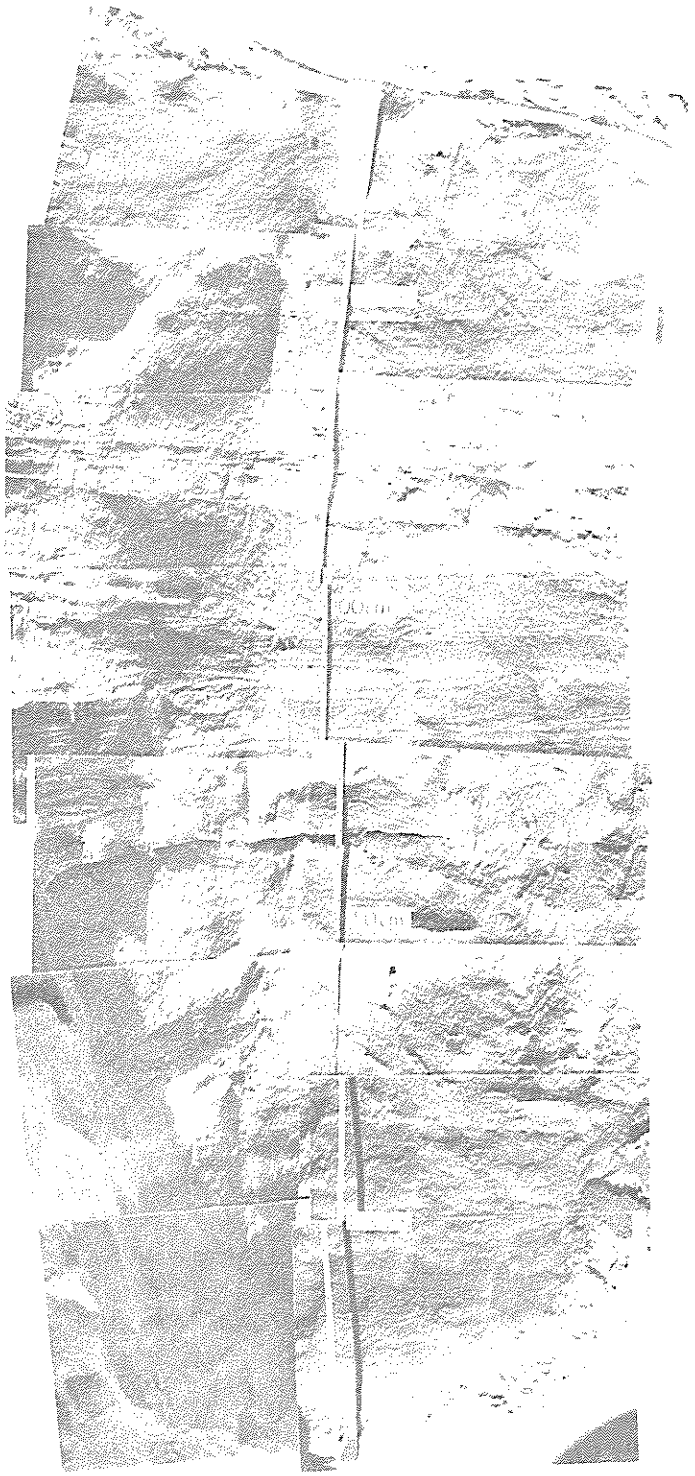

Figure 6. Photo of Trench Wall.

(Z) as shown in figure 5. In transect W samples were taken 1 meter apart over a length of 78 meters at a depth of 30 to 40cm. One hundred samples were collected along the 14.85m long X and Y transects at a depth of 50cm. In the Z transect, located near the X and Y intersection, ring samples were collected about every 7cm to a depth of 4.9m.

Each sample was split and mechanically sieved after the other hydraulic tests were completed. The sample mass collected on each sieve was weighed to calculate cumulative weight per cent retained. Because preliminary testing for silt and clay sizes by the hydrometer method did not reveal a significant fraction of fines, no further hydrometer analyses were run. The arithmetic average of some of the particles sizes are given in table 1. On the basis of particles size analysis, the texture is mostly fine uniform sand. Figure 7 shows the nature of variability in the ten percent finer size, d_{10}, along transects X, Y and Z.

Soil-Water Characteristic Curve

The volumetric water content-pressure head relationship, θ-ψ, was determined in the laboratory by the hanging water column method using the 100cc core rings. Typical results are shown in figure 8 from the borehole at site 5.

Core samples from the side of an excavation (figures 5 and 6) indicate a residual water content for the sand of approximately 6 to 10 percent at pressure heads greater than about -2000cm of water using a pressure membrane apparatus (table 2). Field water content is also in this range, although the corresponding field pressure heads are -60 to -150cm of water. Bulk density was determined by oven drying and weighing 100cc rings. Porosity was calculated from bulk density and an average particle density of 2.65g/cc determined by the pycnometer bottle method. Porosity ranges from about 36 to

TABLE 1

AVERAGE SOIL HYDRAULIC PROPERTIES FROM RING SAMPLES

Transect	Number of Samples	d_{10} (mm)	$\frac{d_{84}+d_{16}}{2}$	$\frac{d_{60}}{d_{10}}$	porosity (%)	bulk density (g/cc)	K_s at (cm/sec)
W	78	0.117	0.244	-	36.06	1.66	0.015
X	100	0.128	0.266	2.428	-	-	0.019
Y	100	0.126	0.259	2.377	-	-	0.018
Z	71	0.117	0.249	2.456	-	-	0.013

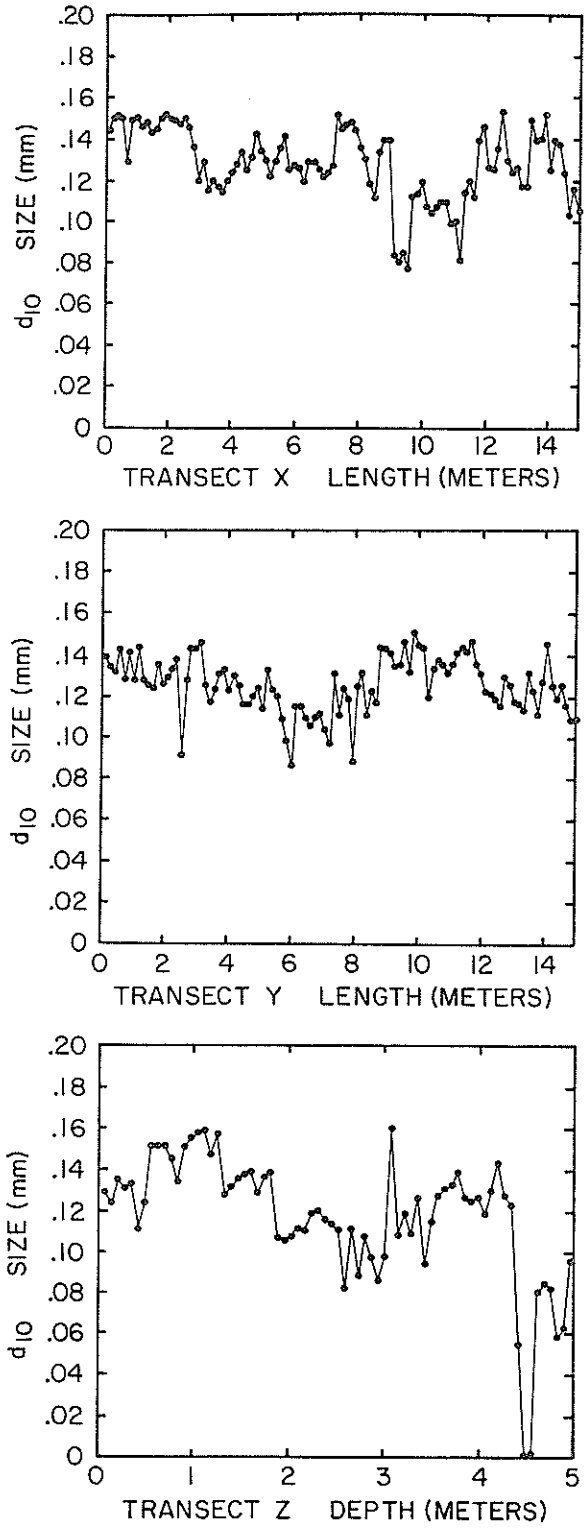

Figure 7. Variability in d_{10} Size Along Transects X, Y, Z.

TABLE 2
HYDRAULIC PROPERTIES FROM CORE SAMPLES PARALLEL TO BEDDING OBTAINED FROM THE FACE OF AN EXCAVATION IN INSTANTANEOUS PROFILE SITE

Depth (cm)	Residual Water Content (vol %)	Porosity (vol %)	Saturated Hydraulic Conductivity (cm/sec)	Description
33	10.8†	45.7	0.029	fine to medium sand
76	9.0†	42.7	0.034	coarse sand
97	6.9*	38.9	0.036	fine-medium sand
157	6.7*	38.9	0.029	fine-medium sand
188	10.6*	38.3	0.018	silty sand
190	8.2*	38.9	0.014	silt and fine sand
190	18.0*	48.3	0.008	silt and fine sand

† 2 bars

* 15 bars

48 percent (tables 1 and 2). The volumetric water content at zero pressure head on the curve is less than porosity for many of the samples owing to entrapped air, incomplete wetting and minor evaporation from the apparatus.

Under field conditions, water content was measured insitu with a neutron moisture probe (model 3222, Troxler Electronics, Inc., Research Triangle Park, NC). The probe was calibrated for field conditions by ponding a 2m diameter area centered on a 5cm diameter aluminum access tube installed in a 6.5cm diameter auger hole; prior to ponding the annulus was backfilled with dry sand and the soil was allowed to equilibrate. Ring samples 100cc in volume were collected during drainage at a depth of about 86cm and at different points located 50cm radial distance from the neutron access tube for determining volumetric water content by oven drying. The neutron probe also recorded water content at the 86cm depth during drainage. Linear regression analysis of the water content calibration procedure shows a linear relationship between the gravimetric determination and the neutron probe measurement in which the slope is 0.895, the intercept is -3.36, and r-squared (R^2) is 0.88.

During drainage following a period of prolonged ponding at the instantaneous profile site (figure 5), water content was measured with the calibrated neutron probe and pressure head was measured with tensiometers at several depths and three different locations within the central part of the impounded area. These simultaneous measurements provided an insitu means to determine θ-ψ on the drainage cycle (figure 9). Comparison of this field method with the laboratory cores (figure 8) shows very good agreement.

Saturated Hydraulic Conductivity

Small Core Samples. In the laboratory saturated hydraulic conductivity, K_s, was determined on small samples collected in the 100cc stainless steel rings and in shelby tubes (thin-walled tubes 76cm long and 7.2cm I.D.). The

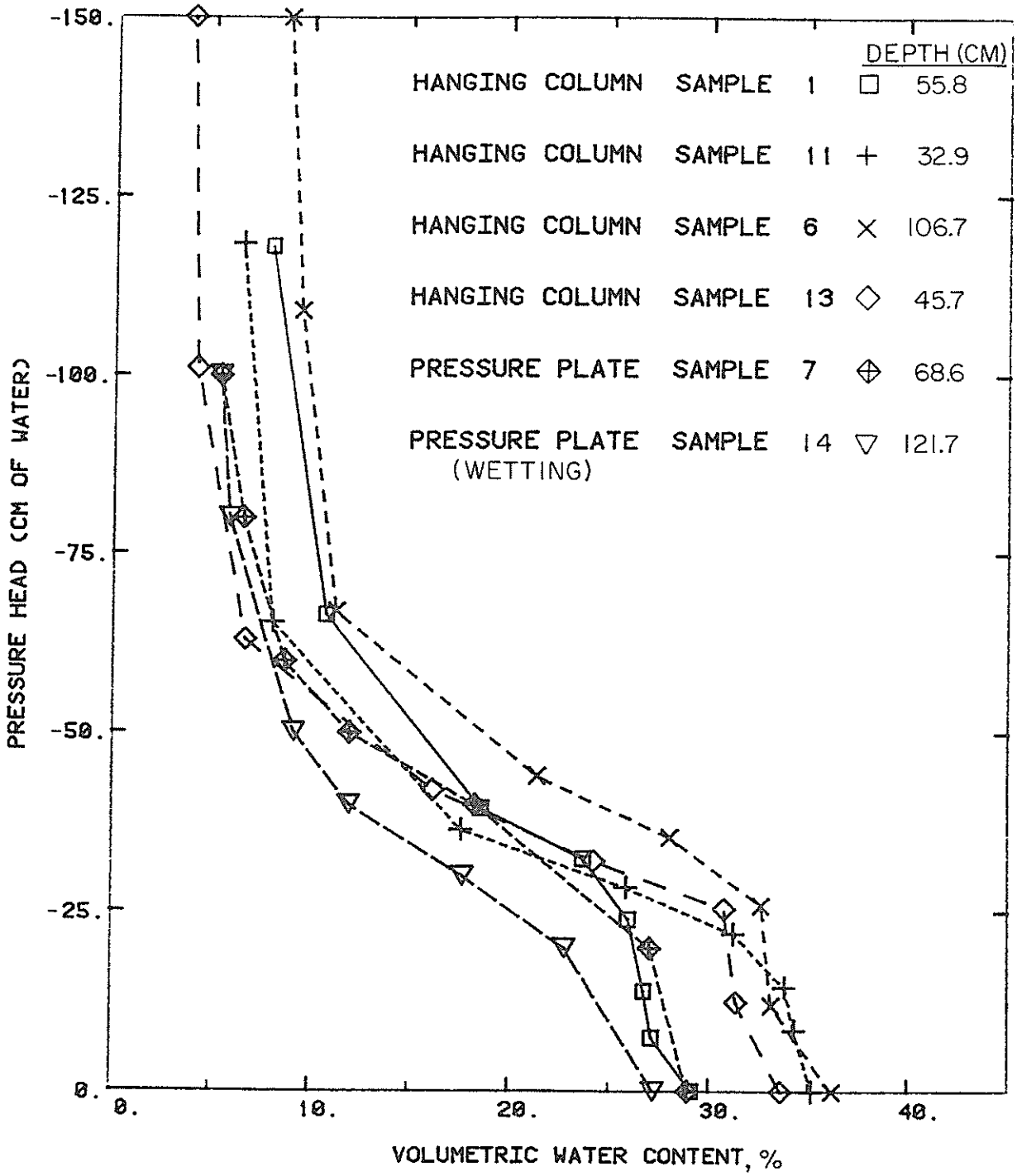

Figure 8. Laboratory Determined Soil-Water Characteristic Curves on Ring Samples from Site 5. All Curves Except Sample 14 are for Desorption.

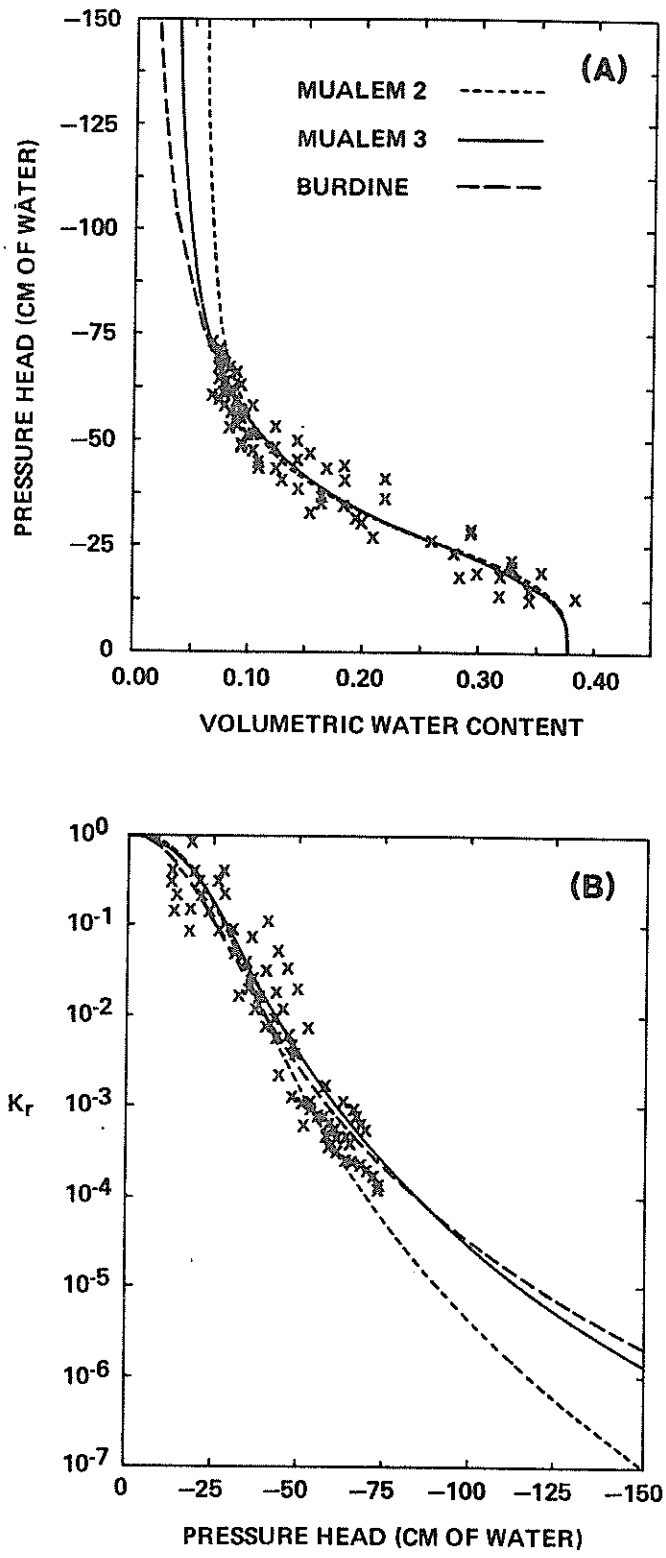

Figure 9. Field Determined Soil Water-Characteristic Curve and Unsaturated Hydraulic Conductivity from an Instantaneous Profile Test. (Lines show the fit of statistical models to field θ-ψ data and predicted relative unsaturated hydraulic conductivity.)

ring samples are especially designed to fit a permeameter which can analyze 15 samples for K_s simultaneously (Eijkelkamp, Giesbeek, the Netherlands). All tests utilized the constant head method and samples were wetted slowly from below. In the permeameter, total hydraulic head difference across the ring samples was only a few centimeters. A number of sets of permeability tests were run at different sites and with both tap water and water pumped from the Rio Salado alluvial aquifer. Results from ring samples adjusted to 20°C are summarized in table 3. These K_s values in the range of 0.01 to 0.03 are typical for clean sand (Freeze and Cherry 1979, p.29). Except where indicated, the results were obtained on rings pushed perpendicular to bedding planes; such an orientation reflects K_s in the vertical direction. The limited data for site 3 (table 3) suggests that the anisotropy ratio, horizontal to vertical K_s, ranges from 0.74 to 4.16.

Some of the initial analyses for K_s from the ring samples indicated that the calculated values decreased with time in the permeameter. This was attributed to bacterial growth clogging the pore space, rather than clay dispersion, because of the relatively coarse texture of the samples. When the permeameter was thoroughly cleaned with detergent, bleach or ethylene alcohol, and rinsed, the calculated K_s values exhibited a typical pattern shown in figure 10 for samples from site 6. In general, the results show an initial increase in hydraulic conductivity followed by a decrease. The initial increase is thought to be due to a removal or reduction in size of air bubbles in the pore space. According to the peaks in K_s in figure 10, there seems to be an inverse correlation between hydraulic conductivity and how long the sample increases in apparent K_s. The sample from the 30cm depth in figure 10 with an average hydraulic conductivity of 0.002cm/sec was still increasing in K_s after 110 hours. This corresponds to about 700 pore volumes passing

TABLE 3
SUMMARY OF LABORATORY RING PERMEAMETER RESULTS
(Vertical K_s Except as Indicated)

Number of Samples	Depth (cm)	$\bar{K}_s$ (10^{-3}cm/sec) Arithmetic	Geometric	Comments
17	30-305	21.6	-	Site 1; Tap water
6	10-26	11.5	11.3	Site 2; Raw field water; 36 hours
6	10-26	13.7	12.1	Site 2; Filtered field water; 8 hours
6	10-26	12.8	11.0	Site 2; Filtered field water; 24 hours
6	10-26	12.0	11.0	Site 2; Flocculated, filtered field water; 8 hours
6	10-26	11.8	11.5	Site 2; Flocculated, filtered, field water; 24 hours
5	10-25	15.5	14.2	Site 2; Tap water; 8 hours
8	30-101	22.6	-	3.7m north of Site 2; tap water
2	71	25.4	-	Site 3; Field water; 24 hours Horizontal K_s
2	71	22.6	-	Site 3; Field water; 24 hours
2	82	20.4	-	Site 3 Field water; 24 hours; Horizontal K_s
2	82	18.9	-	Site 3 Field water; 24 hours
2	92	13.8	-	Site 3; Field water; 24 hours; Horizontal K_s
2	92	15.6	-	Site 3; Field water; 24 hours
2	107	21.2	-	Site 3; Field water; 24 hours; Horizontal K_s
2	107	5.09	-	Site 3; Field water; 24 hours
2	117	14.6	-	Site 3; Field water; 24 hours; Horizontal K_s
2	117	19.8	-	Site 3; Field water; 24 hours
5	25-50	12.0	-	Site 5/IP Site; Field water; 24 hours
6	25-50	27.8	-	Site 5/IP Site; Field water; 24 hours; CO_2 flood
14	30-183	14.0	5.6	Site 6; Tap water;
1	33	29.5	-	Trench at I.P. Site; Horizontal K_s; tap water; 24 hours
1	76	36.0	-	Trench at I.P. Site Horizontal K_s; tap water; 24 hours
1	97	36.2	-	Trench at I.P. Site; Horizontal K_s; tap water; 24 hours
1	157	29.5	-	Trench at I.P. Site; Horizontal K_s; tap water; 21 hours
1	185	17.2	-	Trench at I.P. Site; Horizontal K_s; tap water; 21 hours
1	193	14.5	-	Trench at I/P. Site; Horizontal K_s; tap water; 120 hours
1	193	8.1	-	Trench at I.P. Site; Horizontal K_s; tap water; 120 hours
78	40	16.4	14.9	Transect W; tap water; 48 hours
100	50	19.0	16.0	Transect X; tap water; 20 hours
100	50	18.0	16.0	Transect Y; tap water; 20 hours
71	0-490	13.0	9.0	Transect Z; tap water; 20 hours

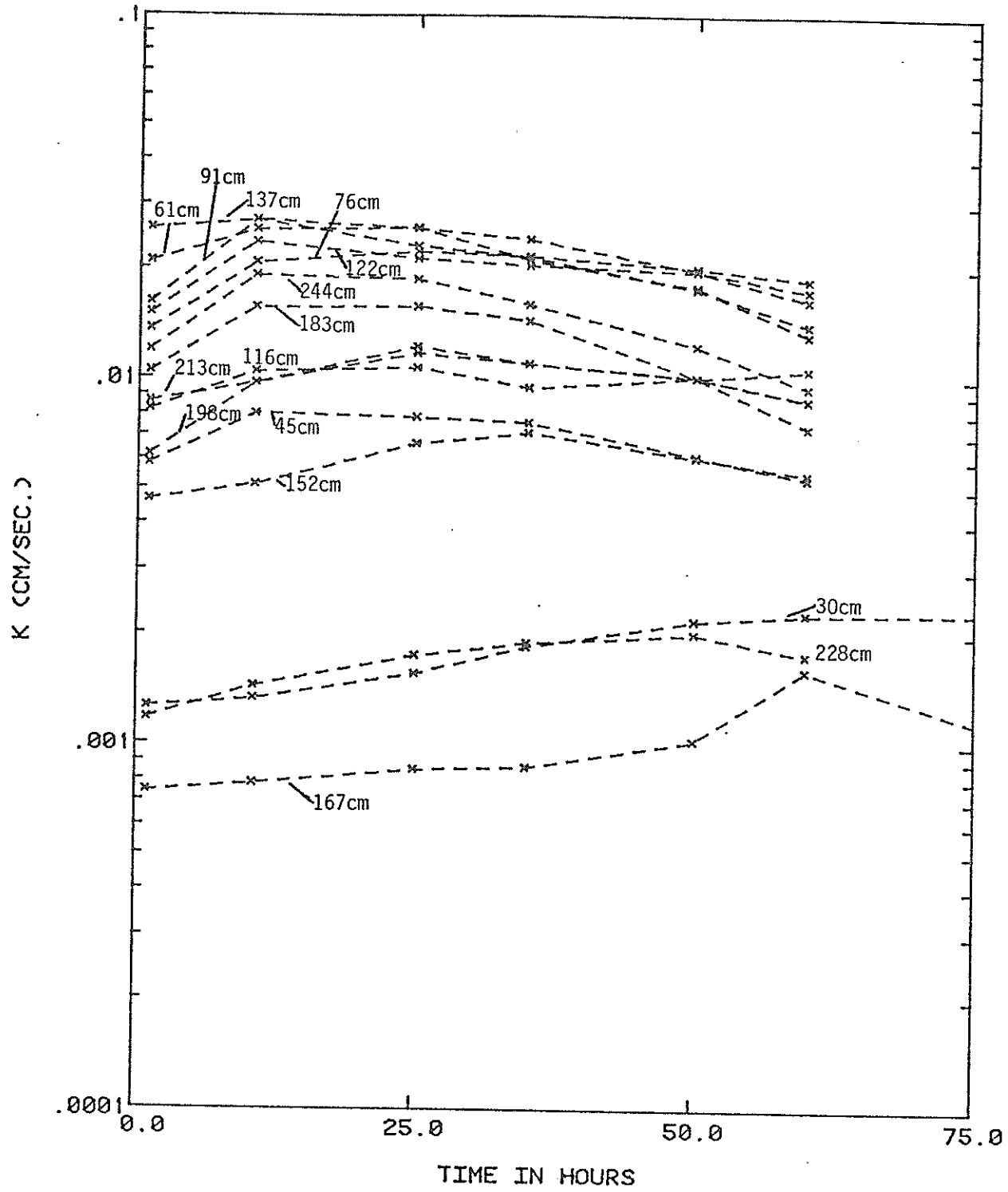

Figure 10. Change in Hydraulic Conductivity with Time in Ring Sample Permeameter.

through the sample. A sample with K_s of about 0.02cm/sec increased until after 10.5 hours; this corresponds to about 667 pore volumes passing through the sample. These results suggest that purging soil of entrapped air is not so much a function of time, but rather, a function of the number of pore volumes of water passing through the soil. The decrease in hydraulic conductivity observed after the initial increase is thought to be due to a growth of organisms in the water. Gupta and Swartzendruber (1962) found a direct relationship between bacteria counts and reduction in hydraulic conductivity. Other causes for a decrease in apparent K_s could include clay mineral dispersion, bubble nucleation, or entrapped air bubble growth with increasing temperature, among others.

An experiment was conducted to determine whether entrapped air influenced K_s of the ring samples. Twenty-one ring samples were collected from the upper 15 to 50cm of sand at the instantaneous profile test site and borehole infiltration site 5 (figure 5). The first group consisted of 10 samples; five of these were flooded with carbon dioxide, CO_2, at a rate of 0.36 lpm for six minutes (approximately 54 pore volumes) prior to wetting in the permeameter, and the other five were not treated with CO_2. Because carbon dioxide is 28 times more soluble than oxygen and 57 times more soluble than nitrogen at 20° (Hillel, 1980), it is hypothesized that flooding with CO_2 will displace original soil air and readily dissolve in the infiltrating water, leaving much less air trapped in the pore space (Seginer and Levine 1964). In this first test group, the permeameter apparently was not thoroughly cleaned, inasmuch as after 48 hours all calculated K_s values decreased by about one-third of the value calculated immediately after wetting. Nevertheless, it was apparent that there was a difference between the initial value of the CO_2 treated group was greater than the untreated group. During about the first 30 to 90 minutes the geometric mean of five ring samples treated with CO_2 was 0.026cm/sec and

the average of the untreated sample was 0.018cm/sec; at about 140 minutes the geometric means were 0.021 and 0.017cm/sec, respectively.

The second group of 11 ring samples was tested in the permeameter after it was cleaned with bleach and rinsed to remove bacteria. Six of the samples were treated with CO_2. The results are shown in figure 11. After 48 hours the geometric mean K_s for the CO_2 treated subgroup was 0.026cm/sec and for the untreated subgroup K_s averaged 0.013cm/sec. There is some suggestions in this figure that fluctuation in K_s may be affected by temperature.

The range of vertical K_s values in the two untreated subgroups described above is similar to the results from other locations within the site indicated in table 3. The results of the ring permeameter tests suggest that CO_2 flooding may cause as much as a two-fold increase in calculated K_s.

In another set of experiments, 15 ring samples were collected at random at a depth of 45cm within a 0.4m x 0.4m area located 80cm north of the instantaneous profile site. These samples were used to test whether CO_2 treatment was as effective in removing entrapped air as vacuum saturation. The laboratory ring permeameter was cleaned thoroughly, filled with tap water, and $HgCl_2$ was added to inhibit bacterial growth (0.005 percent). (Previously, an analysis of water samples from the permeameter, courtesy of Dr. Tom Lynch, New Mexico Institute of Mining and Technology biology department, did not reveal any significant concentrations of bacteria in a 0.005 percent $HgCl_2$ solution.) The vacuum applied to the first sample sucked the sample from the ring and the sample was discarded. The geometric mean of the remaining four samples wetted under a vacuum of 6 to 8mm Hg is plotted as a function of time in figure 12. Vacuum saturated samples all exhibited a slightly murky froth on the downstream end of the sample where outflow to a siphon occurs; the froth slowly dissipated over the duration of the experiment. Figure 12 also

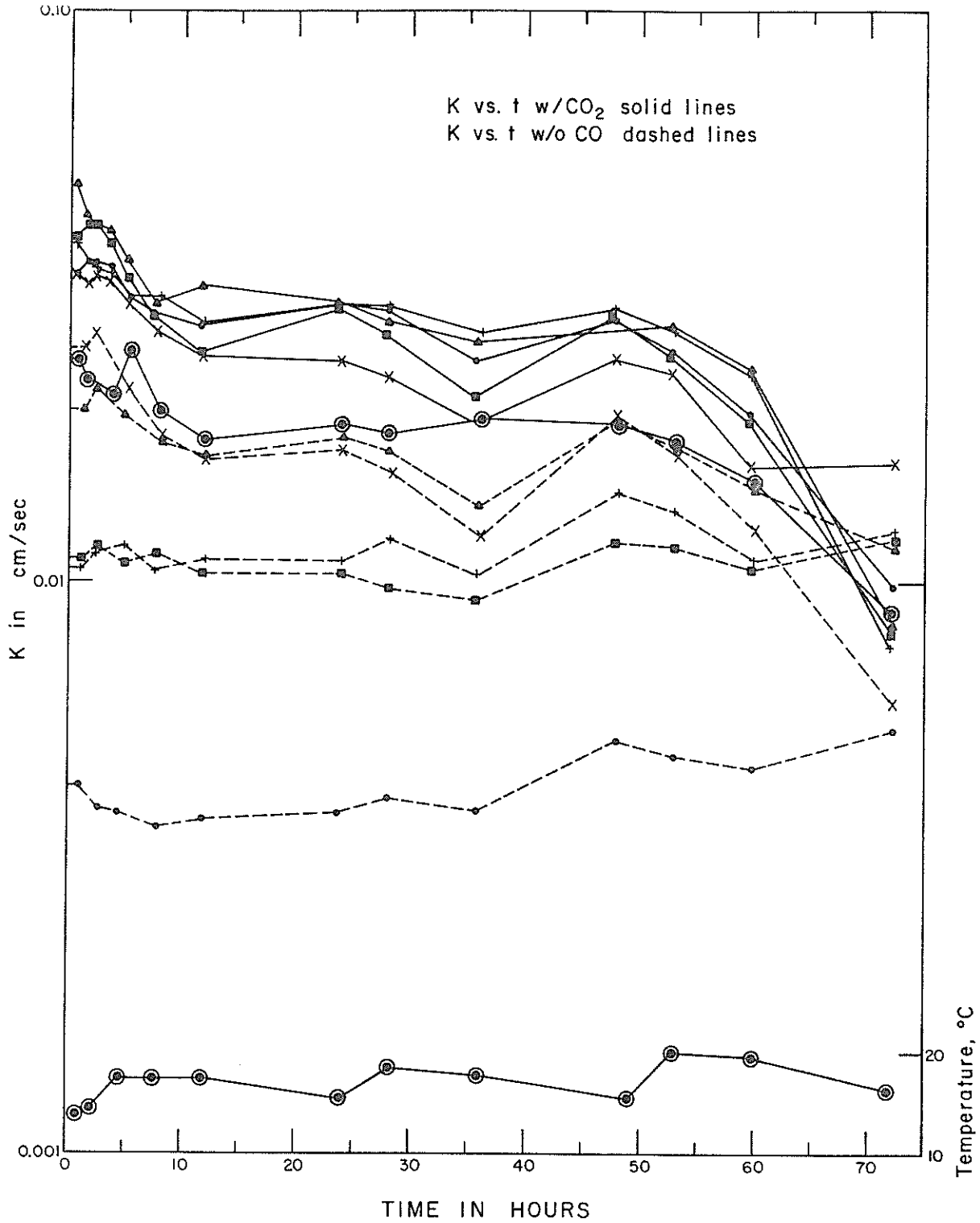

Figure 11. Influence of Carbon Dioxide on Ring Sample Permeability (Solid lines: CO_2 treated).

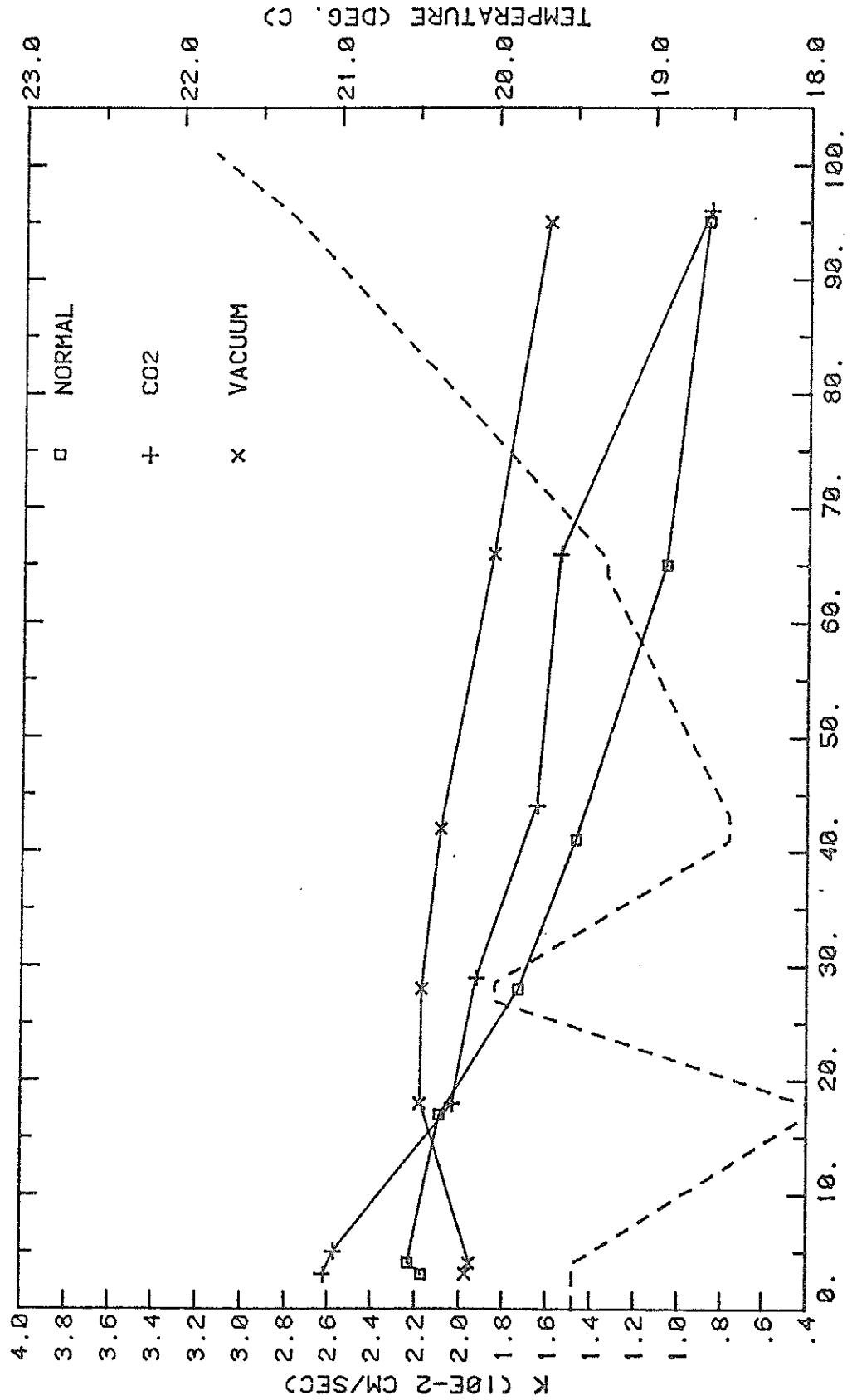

Figure 12. Comparison of Vacuum Saturation and Carbon Dioxide Flooding on Geometric Mean of K_s. (Dashed line is water temperature.)

shows the geometric mean K_s from five of the samples which were flooded with about 4000ml of CO_2 (100 pore volumes) under very low pressure. For comparison, five samples were placed in the permeameter untreated. As indicated in figure 12, the means have generally similar trends to slowly decrease over time. Bacteria growth is not likely due to our precautions in cleaning and adding a bacteriacide. Nevertheless, within the first few hours, the calculated K_s is largest for CO_2 and smallest for vacuum saturation; vacuum saturation is the most commonly used laboratory method to eliminate entrapped air. After about 24 hours, the calculated K_s clearly tends to be largest for the vacuum saturated samples and smallest for the untreated sample group. In this test K_s for CO_2 treated samples is only 10 to about 50 percent greater than the untreated samples. Student's t-tests (Miller and Freund 1965) on all sample measurements over time showed no significance difference in the mean hydraulic conductivity of the CO_2 and vacuum saturated subsets at the 0.05 level. On the other hand, the means of each of these two subsets are significantly different from the untreated subset at the 0.05 level. Figure 12 also suggests that long term behavior may be influenced by temperature. Reasons for differences in the transient behavior shown in figures 10, 11 and 12 are not completely understood at this time. It is apparent that laboratory procedures may have a great deal of influence on calculated K_s.

Shelby Tube Samples. Laboratory permeameter experiments were also conducted on much larger undisturbed samples. Shelby tubes (3094cc volume) were obtained near the southern end of the instantaneous profile site (figure 5). The samples were taken from a depth of 45 to 106cm below land surface by pushing the tube vertically into the soil with a Mobile B-30 drilling rig. Saturated hydraulic conductivity was determined on the undisturbed sample in the laboratory with a constant head permeameter and tap water. Shelby tube samples were tested at different hydraulic heads with and without flooding of

CO_2 prior to water infiltration. The purpose of this experiment was to test the hypotheses that: 1) the size of air bubbles trapped during infiltration is reduced by increasing the hydraulic head, so that calculated K_s is a function of hydraulic head; and 2) injecting water soluble carbon dioxide gas into the pore space prior to infiltration leads to a reduction in volume of entrapped air. Six tests will be described.

For shelby tube test 1, a 66cm long sample was wetted from above by applying water at a head of 185cm above the top of the sample; the lower few centimeters of the shelby tube was immersed in a constant head reservoir. After flow rate stabilized the head above the sample was dropped in 30cm increments. The shelby tube was then drained and purged with compressed air at low pressure (2 to 3 psig) for several days. For test 2 the dried sample was then wetted at a head of 152cm. In test 2 the head remained constant, but K_s was determined over a long period of time. For test 3 the sample was dried in the same fashion as in test 2 and wetted again, except at an increased head of 122cm. For test 4 the effect of variable head was tested again using a new shelby tube sample from the same general site location. This shelby tube sample was 69.2cm long, and the sample was wetted initially at a head of 122cm instead of 183cm. At the end of test 4 the sample was dried with compressed air in preparation for test 5. For test 5, this second shelby tube was flooded with CO_2 in an attempt to purge the soil sample of air . This sample was flooded with 90 liters of CO_2 (about 64 pore volumes) over a 15-minute period at a rate of 6 lpm; the injection pressure was less than 2 psig. After flooding with CO_2, the sample was immediately wetted from above at a head of 183cm. K_s values were then determined at other values of head. Test 6 was a repeat of test five, however, the sample was disrupted after two readings and the experiment was terminated.

Results of these six shelby tube experiments are given in figures 13, 14, and 15. In non-CO_2 shelby tube tests 1 and 4 a decrease of head corresponds to a decrease in calculated K_s (Figure 13); when CO_2 is injected before infiltration (test 5 and 6) there is no obvious relationship between head during wetting and K_s. Figure 14 shows the results of non-CO_2 tests 2 and 3, where a constant head of water is applied. A trend of increasing K_s with time is apparent. For both test 2 and 3 'final' K_s values are approximately 0.0105cm/s. In test 3, it took almost 10 times longer to reach a peak K_s value with the lower head. The greater time to reach the maximum saturation is presumed due mostly to the slower flow rate through the sample and corresponding slower rate of removal of entrapped air. Figures 14 and 15 show that in test 5, when CO_2 is injected, K_s is reached almost immediately after wetting; and K_s remains steady for at least 120 minutes before it slowly decreases, probably because of bacterial growth (Gupta and Swartzendruber 1962). It is interesting to note that the maximum K_s values of CO_2 tests 5 and 6 are nearly identical (figure 13) and are only 20 percent greater than final K_s values from non-CO_2 tests 2 and 3 (figure 14). When the same hydraulic head is applied during wetting of test 4 (without CO_2) and test 5 (with CO_2), the initial infiltration rate is much greater when CO_2 is injected. After nearly 30 hours the value of K_s from the non-CO_2 test 4 reaches nearly the same value as the CO_2 test 5 (figure 15).

These six shelby tube experiments lead to at least three pertinent conclusions. First, when not flooding with CO_2, calculated K_s changes with head. This is consistent with previous experiments by Christianson (1944) who found that variations in K_s with head are caused by the compression and contraction of entrapped air bubbles. Second, when shelby tube samples are not flooded with CO_2, the apparent K_s will increase with time until bacterial growth or bubble nucleation may block the pore space. This suggests a slow

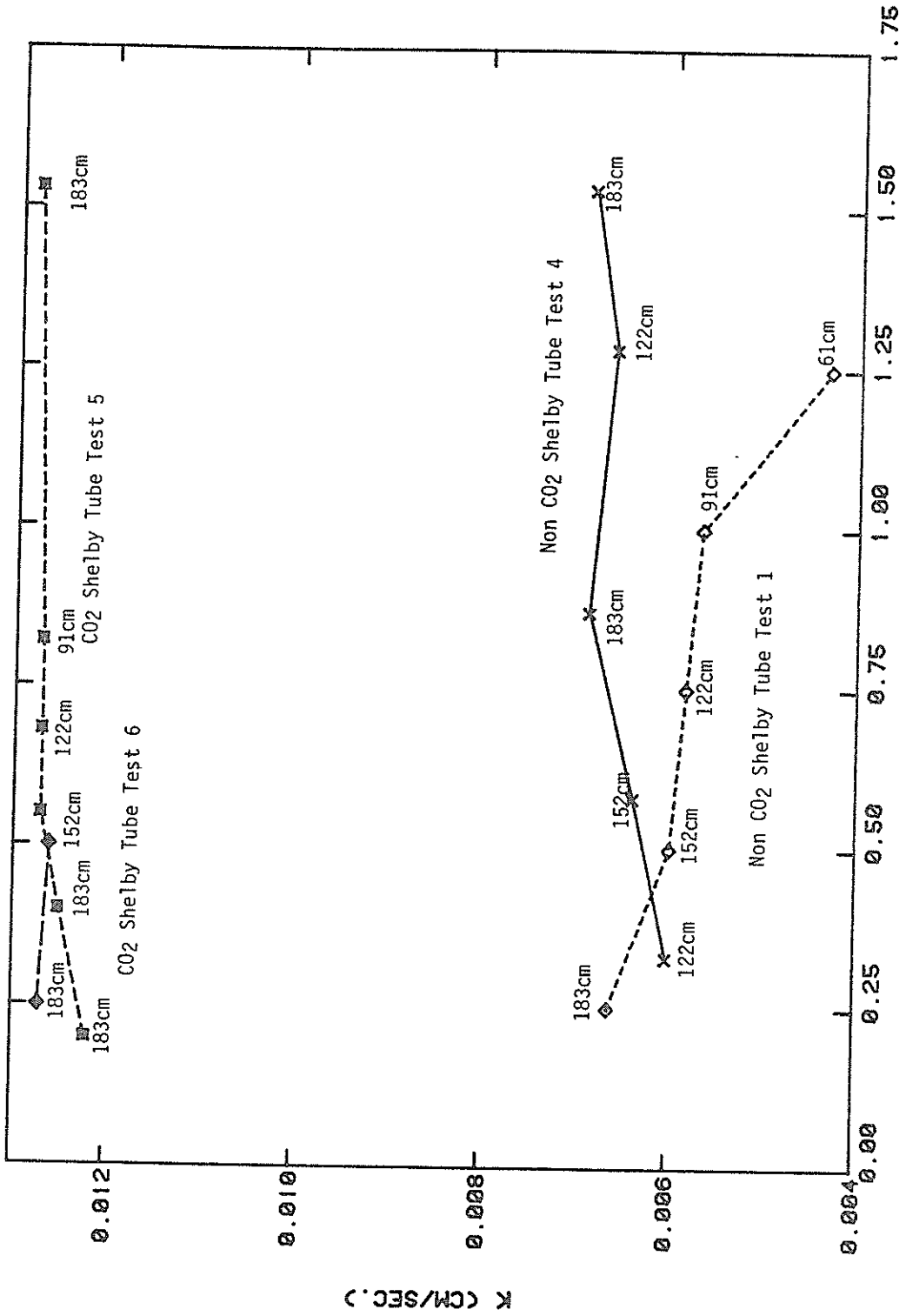

Figure 13. Influence of Hydraulic Head on Calculated K_s.

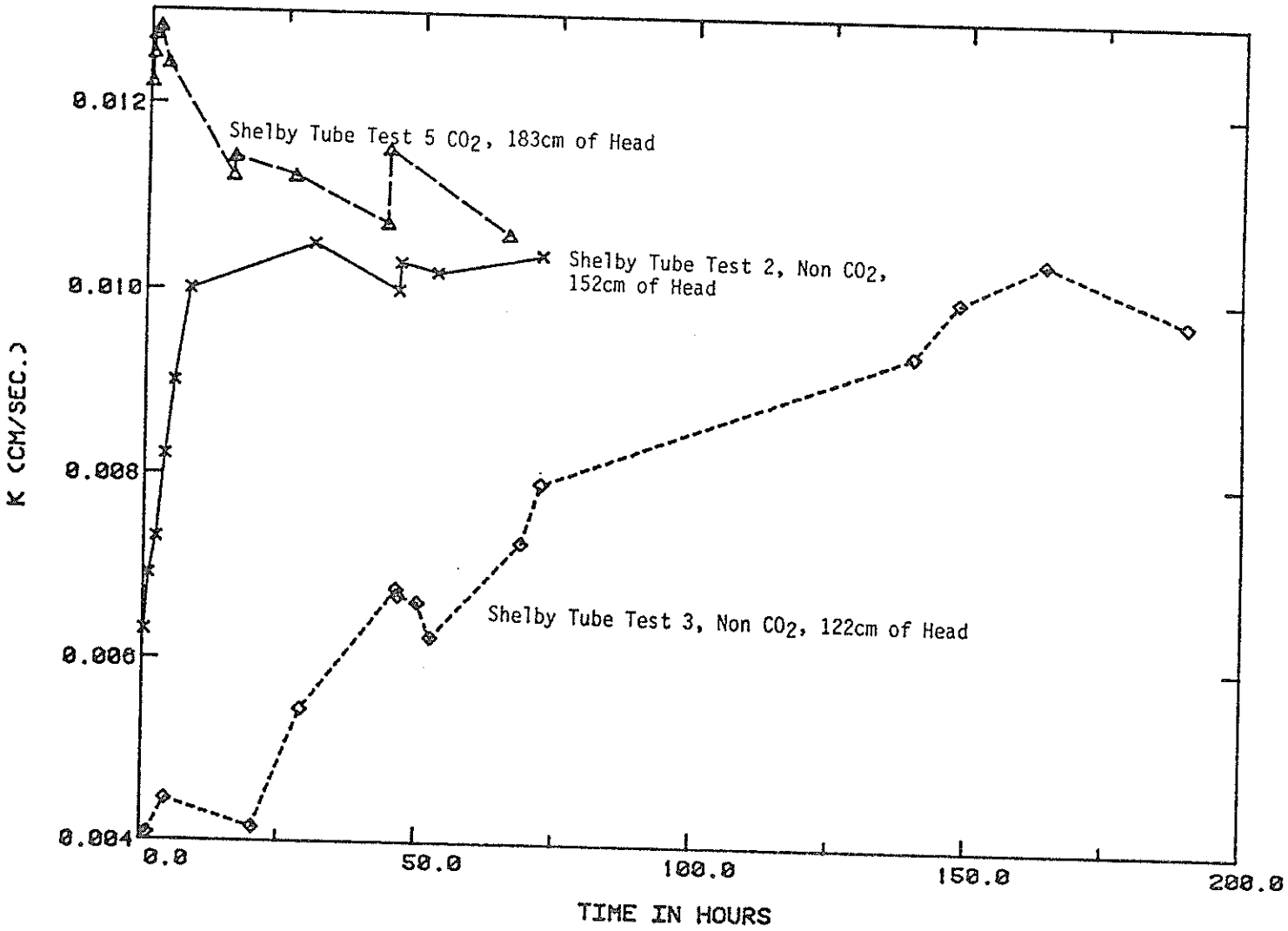

Figure 14. Change in Hydraulic Conductivity with Time in Shelby-Tube Permeameter.

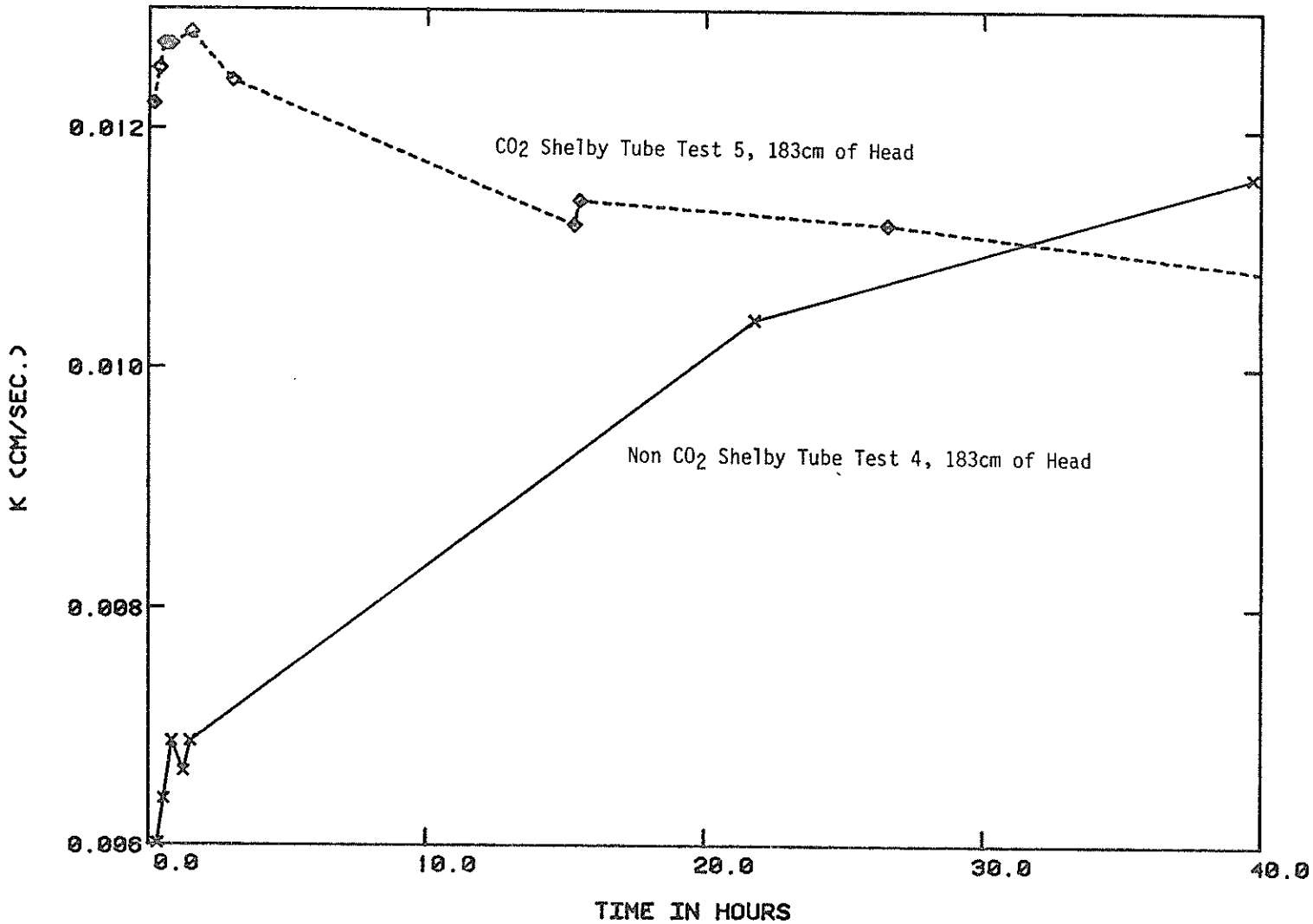

Figure 15. Influence of Carbon Dioxide on Calculated Hydraulic Conductivity in the Shelby-Tube Permeameter.

removal of entrapped air with time, as previously noted by Christianson (1944), Orlob and Radhakrishna (1958), Gupta and Swartzendruber (1964), and others. It has been suggested by Peck (1968) that most of the entrapped air slowly diffuses from bubbles over time and is not entrained or bubbled upward by bouyancy. The observation of bubbles at the downstream end of the shelby tube permeameter points to at least a partial removal by entrainment. Using a Bausch and Lomb oxygen analyzer Spectrokit, the tap water used for the shelby tube permeameter was found to have 6 mg/L of dissolved oxygen compared to a saturated value of 8 mg/L per liter oxygen at an average tap water temperature of 27 degrees Celsius. Because the water is approximately 75 percent saturated with oxygen, entrainment and upward bubbling of air, rather than dissolution, must play a major role in entrapped air removal. The third conclusion is that CO_2 flooding prior to infiltration displaces soil air with the more soluble gas CO_2. The CO_2 is then dissolved behind the wetting front leaving much less entrapped air. This is indicated by the high initial permeabilities shown in tests 5 and 6, and the fact that K_s does not signficantly change with head when CO_2 is applied. Seginer and Levine (1964a) and others report similar results with CO_2.

Standard Field Permeameters. In the field the air-entry permeameter developed by Bouwer (1966) and modified by Topp and Binns (1976) was used to determine saturated K_s within the upper one meter of sand at various locations in the borehole infiltration test study area. Thirteen tests were run according to prescribed procedures; and 11 were run by first injecting CO_2 through the soil in the permeameter ring at low pressures (2-4 psig) before continuing with the usual test procedure. Table 4 summarizes the results of both types of tests. The geometric mean hydraulic conductivity from all 11 samples in group 1 (with CO_2) is 8.78×10^{-3}cm/sec. The mean hydraulic

TABLE 4

SUMMARY OF AIR ENTRY PERMEAMETER RESULTS

Site	Radial Distance and Direction from Borehole (cm)	Depth (cm)	K_s@20°C (10^{-3}cm/sec)	Air Entry Value (cm H_2O)	Group*
1	100 N	0-16	7.26	-21	1
2	110 SW	30-46	2.74	NR	2
2	158 SE	26-42	4.44	-15	2
2	160 NE	32-48	3.81	-26	2
3	100 SE	33-48	6.20	-30	1
3	100 SW	36-52	8.20	-28	1
3	130 N	30-46	4.70	-32	2
3	130 N	30-46	11.00	-16	1
3	130 N	30-46	6.30	-32	2
3	140 S	40-56	5.90	-22	2
3	140 S	40-56	11.00	-22	1
3	160 W	32-48	8.85	-25	1
3	200 E	36-52	2.89	-22	2
3	200 E	36-52	7.64	-25	1
3	200 E	36-52	3.99	-19	2
4	85 E	48-62	9.80	-36	1
4	65 E	83-98	8.50	0	1
5	136 N	0-16	9.10	- 2	1
5	160 NE	0-16	3.90	-19	2
5	160 SE	0-16	8.88	-34	1
5	170 SE	0-16	5.60	-29	2
5	170 NW	0-13	1.20	-18	2
5	175 WNW	0-14	1.50	-11	2
5	175 NNW	0-14	0.44	- 1	2

*

1 Injected CO_2 prior to infiltration

2 Without CO_2; without correcting for entrapped air

conductivity of the group 2 in which CO_2 was not injected prior to infiltration is 4.01 x 10^{-3}cm/sec; and if the anomalously low K_s from the last sample is deleted the mean is 4.04 x 10^{-3}cm/sec.

Statistical tests were conducted on the CO_2 and non-CO_2 treated groups to determine whether the means of the two subsets were different. For the student t-test it was assumed that both samples have the same population variance, that the number of points in each group is small, and that the natural logarithms of saturated hydraulic conductivity are normally distributed. For these data the means are significantly different only at the 0.10 level of significance. However, if the anomalously low value of the last sample is removed from the second group (table 4 - tests w/o CO_2), the means are different at the 0.01 level of significance. It may be justified to omit this one test because a clay layer was encountered only at this particular location and at no others where CO_2 was injected; without this sample the sandy lithologies tested in the two sample groups are considered to be very similar. Another statistical test, the Smith-Satterthwaite test, (Miller and Freund 1965, p.174) is based on the same assumptions previously described, except that the variances of the two populations are not equal. Using all data in each of the two groups, the means are again different at the 0.10 level of significance.

The ratio of the means of the CO_2 and non-CO_2 treated air-entry permeameter tests is about 2.2; this result is very similar to experiments on ring samples shown in figure 11. It is concluded that CO_2 flooding significantly increases the apparent value of saturated hydraulic conductivity obtained from the air-entry permeameter. It is interesting to note that Bouwer (1966) recommended that the calculated value of saturated hydraulic conductivity should be multiplied by a factor of two to compensate for entrapped air. If carbon dioxide flooding does in fact result in 100 percent

removal of entrapped air, then our results substantiate Bouwer's recommendation.

Ring samples from locations at site 5 in table 3 were all obtained within a 3m by 3m area which was previously ponded for about six hours. The hydraulic conductivity from the ponding experiment is assumed equal to the steady flux of infiltration, 7×10^{-3}cm/sec. The average K_s from the ring samples at site 5, untreated with CO_2, is 1.2×10^{-2} cm/sec. Thus, either K_s from the ring samples is in error, is unrepresentative of the ponded area, or air is still trapped in the soil at the ponded site. In contrast to the overestimate of the ponded infiltration rate from the ring samples, limited data available in table 4 suggest that the air-entry permeameter underestimates saturated hydraulic conductivity from ponding unless there is a correction for entrapped air. The mean from the CO_2 treated air-entry permeameter data also suggests that ponding is not sufficient to remove entrapped air; the ratio of hydraulic conductivity from the site 5 ponding experiment to the mean of the five air-entry permeameter tests uncorrected for entrapped air is only about 1.75.

Saturated hydraulic conductivity was also determined using the double-tube method (Bouwer 1961, 1962; and Bouwer and Rice 1967). The apparatus was loaned to us courtesy of Dr. Herman Bouwer and Mr. Robert Rice at the U.S. Department of Agriculture (USDA) Water Conservation Laboratory in Phoenix, AZ. Two successful tests were run; a third test suffered from a leak in the apparatus. Test A was conducted just north of the trench near site 5 at a depth of 0.46m, and test B occurred between sites 6 and 7 at a depth of 0.51m (figure 5). Water pumped from the alluvial aquifer was used in both tests. The double tube test indicates K_s values for test B on the order of 10^{-3} cm/sec, as summarized in table 5; much lower values were found from test A. As a comparison, 100cc ring samples were collected from the zone just beneath

TABLE 5

SUMMARY OF DOUBLE TUBE PERMEAMETER RESULTS

Test #A

R_r = 1.27cm d = 2.44cm

R_c = 6.16cm F_f = 1.18cm

Run #	Saturation time (hrs)	Δy(cm)	$\int_o^t$ ydt(cm-min)	K(cm/sec)
1	5	2.0	15.19	4.87×10^{-4}
2	6.5	1.3	15.41	3.12×10^{-4}
3	7.5	1.8	21.29	3.13×10^{-4}
4	7.7	1.4	21.33	2.43×10^{-4}

Test #B

R_r = 1.27cm d = 3.05cm

R_c = 6.16cm F_f = 1.05cm

Run #	Saturation time (hrs)	Δy(cm)	$\int_o^t$ ydt(cm-min)	K(cm/sec)
1	2	5.9	23.76	1.03×10^{-3}
2	2.5	5.3	15.92	1.15×10^{-3}
3	2.7	5.8	15.89	1.52×10^{-3}
4	3.2	5.9	22.92	1.07×10^{-3}
5	3.5	5.0	22.81	9.11×10^{-4}
6	3.9	5.0	22.69	9.16×10^{-4}

the inner tube at the completion of the double tube tests. In double tube test A, K_s from the one ring sample was 1.51 x 10^{-2}cm/sec, and in test B K_s was 1.78 x 10^{-2} and 1.85 x 10^{-2}cm/sec from samples collected at 3 and 11cm, respectively, below the inner tube. In comparison to these and other laboratory results, (table 3 and figures 13 and 14) the double tube method, especially test A, gives K_s values which are much lower and unreasonable for a soil comprised of fine to medium uniform sand. It is possible, although unlikely, that the double tube penetrated a thin, low-permeable silt layer in both locations and that this layer was not sampled by the cores. The double tube method is cumbersome and time consuming; the low values of K_s could be due to our inexperience with the technique.

Unsaturated Hydraulic Conductivity

Unsaturated hydraulic conductivity, K-ψ, was determined in the laboratory by the pressure out-flow method (Peck 1966, Kunze and Kirkham 1962), in the field by the instantaneous profile method (Watson 1966) and by statistical models based on a combination of the θ-ψ curve and K_s (Mualem 1976a, van Genuchten 1978). The results of the laboratory technique for imbibition are shown for two samples from the site 5 borehole at the 69cm and 122cm depths (figure 16). In the pressure head range of 0 to about -50 cm, the calculated K is too low, owing to the low saturated hydraulic conductivity (about 6 x 10^{-7} cm/s) of the 2 bar ceramic plate used in the volumetric pressure plate extractor (Soil Moisture Equipment Corp, Santa Barbara, California). A 1/2-bar ceramic plate was also used to generate a few θ-ψ data points in the range of observed field moisture conditions on two samples collected within about 3m of the site 5 borehole and within the instantaneous profile site (figure 16). The 1/2-bar ceramic analyses are considered more reasonable.

In the field K-ψ was determined by the instantaneous profile method in

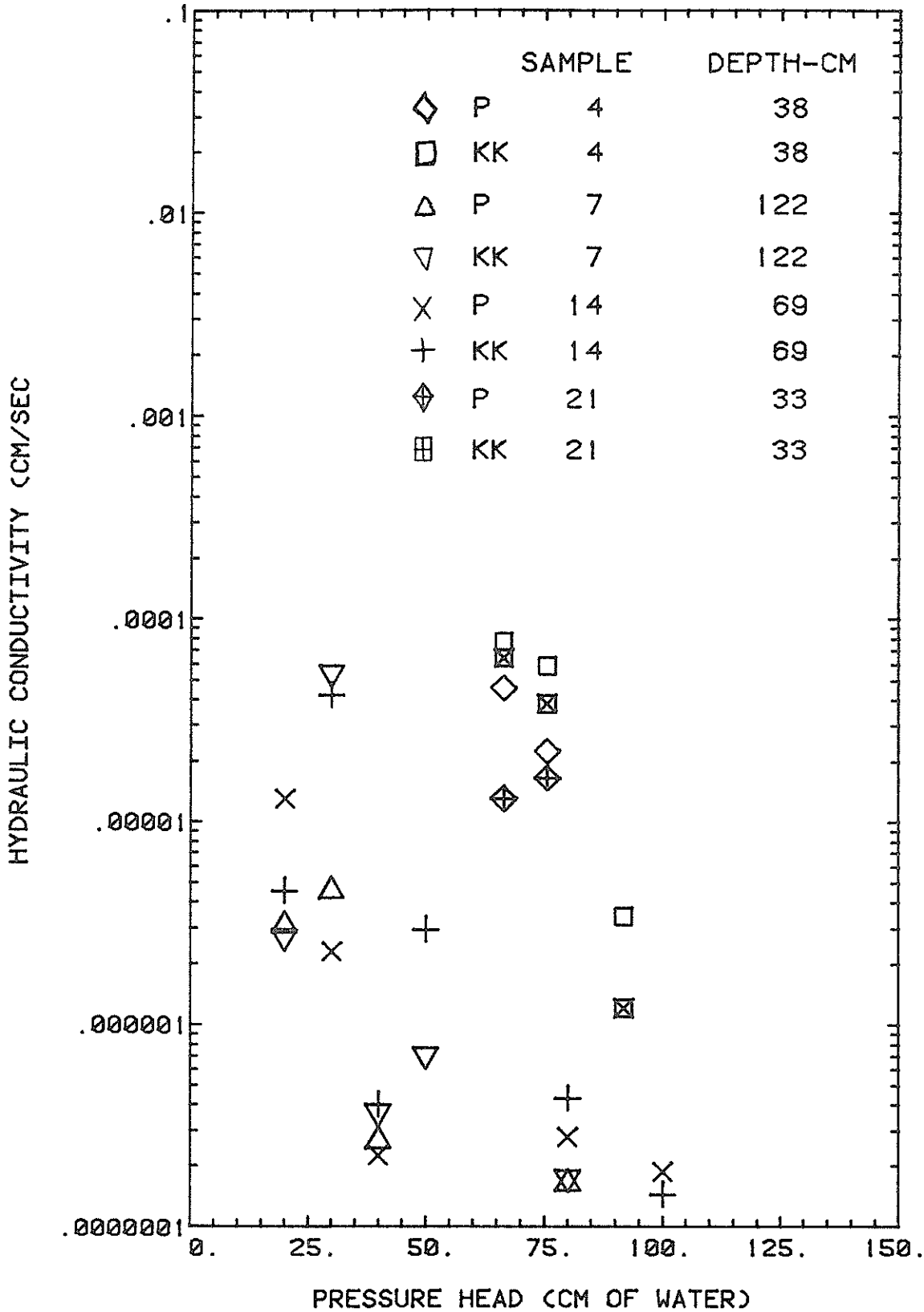

Figure 16. Laboratory Measurements of Unsaturated Hydraulic Conductivity for Imbibition Using Undisturbed Ring Samples from Site 5. (Samples 4 and 21: 0.5 bar ceramics; others 2 bar ceramic.) P = Peck method; KK = Kunze and Kirkham method.

which a 3m x 3m site was leveled and bermed (figure 5). Within this area four neutron-access tubes were installed to measure volumetric water content to a depth of about 2.7m. Four sets of tensiometers, consisting of 5 tensiometers each, were set at 0.3m depth intervals to about 1.52m for measuring pressure head. On July 20, 1982, the site was flooded with water from the alluvial aquifer well point for about eight hours until conditions stabilized. At this time, pressure head ranged between 0 and about -4cm within the 152cm depth. The water was then shut off and the final steady infiltration rate determined by the rate of fall of the ponded water was 7.0×10^{-3}cm/sec. The plot was covered with plastic to prevent significant evaporation losses. During drainage, water content was measured at about 15cm intervals periodically for about 6.25 days. Tensiometer measurements indicated that the hydraulic gradient was within a few percent of unity. The resulting K-ψ data for drainage conditions for one of the stations and all depths are shown in figure 9. Although there is some scatter of data the profile appears to be rather uniform.

Unsaturated hydraulic conductivity was also calculated from the field θ-ψ curves using theory developed by Mualem (1976a) and a procedure developed by van Genuchten (1978), as shown in figure 9. In the Burdine and Mualem 3 models, three parameters are obtained by a non-linear least squares fit to the θ-ψ curve. In the Mualem 2 model, only two parameters are fitted and a third, residual water content, is known. We assumed a residual water content of 6 percent in the Mualem two-parameter model. Saturated hydraulic conductivity was assumed equal to the steady rate of infiltration from ponding, 7.0×10^{-3} cm/sec. Excellent agreement between all models is shown in figure 9b within the range of field conditions. The two-parameter model may give a better prediction of K-ψ in the dry range.

NEW EMPIRICAL SOLUTIONS FOR SATURATED HYDRAULIC CONDUCTIVITY

To incorporate the influence of unsaturated flow on K_s obtained from a borehole infiltration test, Stephens (1979) used empirical procedures to develop an equation which included a parameter α that is a characteristic of the unsaturated hydraulic conductivity versus pressure head curve, K-ψ. In particular, α is simply the slope of a line from ln $K^r(\psi=0)=1.0$ to ln $K^r(\psi)=0.5$, where $K^r=K/K_s$ and $\psi \leq 0$. Practitioners may feel that estimating α is troublesome, owing to the difficulty in measuring K-ψ and the lack of available data to estimate it. Because of this, new empirical solutions were developed which take unsaturated flow into account using other parameters that may be easier to obtain.

Unsaturated flow parameters utilized in formulating the new solutions for K_s from borehole infiltration tests were derived from two procedures designed to predict K-ψ from θ-ψ data. The first is the Brooks-Corey method (Brooks and Corey 1964) and the second is by van Genuchten (1978, 1980). The Brooks-Corey parameters are bubbling pressure head, ψ_b, and λ, the slope of the logarithm of effective saturation versus log of pressure head. The van Genuchten parameters α_v, N, and residual water content, θ_r, are obtained graphically or numerically by a computer program, which obtains these parameters with a non-linear least squares fit to measured θ-ψ data. The calculated parameters in van Genuchten's code can be computed for different theoretical models to calculate K-ψ. The two selected were the three parameter fit models of Mualem and Burdine (Mualem 1976a). Six soils were selected from a catalog (Mualem 1976b) for obtaining the unsaturated soil parameters (table 6). All basic data represent imbibition conditions. No data are available from some of van Genuchten's predictive models because of lack of convergence.

Two other methods of parameterization are also included in table 6. The

TABLE 6
UNSATURATED FLOW PARAMETERS USED TO DEVELOP EMPIRICAL SOLUTIONS FOR K_s

Soil	Mualem Catalog Number	Brooks-Corey		van Genuchten						Stephens I	Stephens II	
				Mualem			Burdine					
		$\lambda(cm^{-1})$	$\psi_b(cm)$	$\alpha_v(cm^{-1})$	N	θ_r	$\alpha_v(cm^{-1})$	N	θ_r	$\alpha(m^{-1})$	$\alpha_3(cm^{-1})$	$\psi_3(cm)$
Del Monte Fine Sand	4108	2.41	55.0	0.016	4.36	0.05	0.017	4.77	0.04	1.24	0.029	12.0
Yolo Light Clay	3102	0.49	28.0	0.027	1.60	0.18	0.044	2.37	0.12	3.96	0.045	1.0
Silt Loam G.E. #3	3310	1.09	200.0	0.004	2.06	0.13	0.006	2.48	0.04	1.05	0.013	11.5
Coarse Sand	4107	1.96	12.0	0.060	2.64	0.04	0.075	3.23	0.03	4.62	0.146	6.0
Gilat Loam	3402	0.16	0.7	0.017	2.30	0.08	-	-	-	1.82	0.040	1.4
Ida Silt Loam	3305	-	-	0.040	1.27	0.00	0.057	2.24	0.00	198.00	0.770	1.0
Sevilleta				0.025	4.70							

Stephens I model parameter α (equation 7) is computed from the slope of the K^r-ψ curve, as indicated above. The Stephens II model parameters include the water-entry value of pressure head and the slope of the K^r-ψ curve, α_3. The latter is calculated from

$$\alpha^3 = \frac{\ln(1) - \ln(0.1)}{0.0 - \psi(K^r=0.1)} \tag{8}$$

where α_3 is in inverse meters and $\psi(K^r = 0.1) < 0$.

Steady flow rate from a borehole into variably saturated media was predicted by computer simulation for various combinations of $0.5 \leq H \leq 10$m and $0.01 \leq r \leq 0.15$m for these six soils by Stephens (1979). He used only the first four of the six soils in table 6 to develop an empirical relationship of the general form: log Cu = f(H,r,soil parameters), such as equation 7. Following this same approach, but with all six soils and the new methods of parameterization for the capillary effect, the SPSS multiple regression technique (Kim and Kohout 1975) was applied to various forms of the independent variables (for example H, H/r, log r, exp (r), etc.) to determine which variables would contribute most to predicting log Cu. The number of data sets (from the variably saturated simulations) input to the Brooks-Corey, Mualem, Burdine, Stephens I, and Stephens II models were 28, 28, 29, 29, and 29, respectively. The five equations developed by this approach, which assumes log Cu is normally distributed, are:

Brooks-Corey:

$$\log_{10}Cu = 0.484 \log_{10}H_D + 0.027 \psi_b^{0.5} - 0.466 \log_{10}H + 0.018H_D^{1.5} + 0.846 (R^2=0.984) \tag{9}$$

where $\psi_b > 0$, and the 95 percent confidence limits on Log Cu are ±0.130 and ±0.098, 0005, 0.084, 0.009 on the other coefficients, respectively;

Mualem:

$$\log Cu = 0.653 \log_{10}H_D - 0.257 \log_{10}\alpha_r - 0.633 \log_{10}H + 0.021 H_D^{0.5} - 0.313 N^{-0.5} + 0.453 \quad (R^2 = 0.993) \tag{10}$$

where 95 percent confidence limits on log Cu are ±0.078 and ±0.066, 0.035, 0.0559, 0.0064, and 0.194 on the other coefficients, respectively;

Burdine:

$$\log Cu = 0.491 \log_{10}H_D - 1.643 \alpha_v^{0.5} - 0.459 \log_{10}H + 0.018 H_D^{0.5} - 0.079 \log_{10} \theta_r + 1.235 \quad (R^2 = 0.986)$$

where the 95 percent confidence limits on log Cu are ±0.107 and ±0.083, 0.235, 0.205, 0.008, and 0.068 on the other coefficients, respectively;

Stephens I:

$$\log Cu = 0.486 \log_{10}H_D + 0.398 \alpha^{-1} - 0.489 \log_{10}H + 0.019H_D^{0.5} + 0.828 \quad (R^2 = 0.983) \tag{12}$$

where the 95 percent confidence limits on log Cu are ±0.104 and ±0.086, 0.061, 0.073, and 0.008 on the other coefficients, respectively;

Stephens II:

$$\log Cu = 0.502 \log_{10}H_D - 0.104 \log_{10}\alpha_3 - 0.467 \log_{10}H + 0.0175(H_D)^{0.5} + 0.0028 \alpha_3^{-3} + 0.794(R^2 = 0.985) \tag{13}$$

where the 95 percent confidence limits a log Cu are ±0.114 and ±0.090, 0.129, 0.0765, 0.0086, 0.0021 on the other coefficients respectively, and $H_D = H/r$.

Only those terms which contributed significantly, on the basis of an F

statistic, are included in the above equations. It should be noted that some of the soil parameters listed in table 6 are not included in the regression equations. This may indicate that the omitted parameter was not highly correlated with Cu or that it was highly correlated with another soil parameter that was included in the equation. The Mualem model (equation 10) seems to give the best fit to log Cu and the Brooks-Corey model the poorest fit, on the basis of the 95 percent confidence interval. The r-square values for all the models are about 0.984, except for the Mualem model which is 0.993.

From a practical standpoint, all these above equations provide similar results. The equation chosen should be that which contains parameters that are easy to determine. In the Brooks-Corey approach, one needs to determine the water-entry value. This can be obtained approximately in the field with the air-entry permeameter described by Bouwer (1966). Clapp and Hornberger (1978) tabulated values of 'saturated suction' for eleven different soil textures; these suctions are essentially equivalent to the air-entry value for desorption. McCuen et al. (1981) also computed mean bubbling pressures and standard errors for a range of soil textures; however, these bubbling pressures are also from drainage experiments and may be about twice as large as one would expect from imbibition. Nevertheless, they are rather easy to determine in the laboratory. In the field about one-half hour is required to complete an air-entry permeameter test very close to land surface. To extrapolate near-surface air-entry permeameter results to the depth of the borehole infiltration test section, the soil profile should be relatively uniform to the depth of the borehole. Particle size analysis of representative samples and soil texture classification on the USDA soil texture triangle are all that are required to estimate the water-entry

pressure head from the results of Clapp and Hornberger (1978) or McCuen et al. (1981). The parameters in van Genuchten's procedure may be obtained by selecting among thirty-four wetting θ-ψ curves for different soils in Mualem's (1976b) catalog. Van Genuchten's (1978) computer procedure was applied to calculate unsaturated flow parameters using Mualem's (1976a) three-parameter model (table 7). The appropriate α and N values may be estimated from this table for soils similar to the soil one may want to test with the borehole method.

Another approach to obtain θ-ψ curves indirectly, and therefore estimate any of the unsaturated soil parameters, is to use the recent work by Arya and Paris (1981), which produces a θ-ψ curve from particle size analyses and bulk density.

Perhaps the best method to obtain the unsaturated flow parameter may be to actually collect θ-ψ data pairs from simultaneous measurements with the neutron probe and tensiometers located around the borehole. Even at steady state the entire moisture content range above background can be determined with proper location of instrumentation, owing to the three-dimensional distribution of moisture content. For example, the field θ-ψ curve could be used to generate Mualem's parameters for equation 10; then, steady borehole infiltration rate, H and r are used to calculate K_s.

PACKER TESTS FOR SATURATED HYDRAULIC CONDUCTIVITY ABOVE A WATER TABLE

Packer testing is a procedure to calculate hydraulic conductivity in boreholes by measuring the flow rate into intervals of the borehole which are isolated by packers. Packer testing is most commonly done below the water table. Furthermore, in conventional approaches the packed-off interval is usually the only one receiving water for injection into the formation. A

TABLE 7

UNSATURATED FLOW PARAMETERS FROM MUALEM'S THREE PARAMETER MODEL USING WETTING θ-ψ CURVES

Soil Type	Catalog Number	α_v (cm^{-1})	N	θr
Silt 'Columbia'	2001	0.015511	1.7676	0.1369
Silt Mont Cenis (limon Silteux)	2002	0.013647	1.3234	0.0000
Silt of Nave-Yaar	2003	0.072010	2.1969	0.3979
Rideau Clay Loam	3101	0.069118	2.0604	0.2863
Yolo Light Clay	3102	0.027000	1.6000	0.1800
Caribou Silt Loam	3301	0.047125	1.6981	0.2956
Grenville Silt Loam	3302	0.030702	1.2878	0.0326
Ida Silt Loam (>15cm)	3305	0.040000	1.2700	0.0000
Ida Silt Loam (0-15cm)	3306	0.089975	1.1768	0.0000
Touched Silt Loam	3308	0.027302	3.5385	0.0993
Silt Loam G.E.3	3310	0.004233	2.0594	0.1313
Gilat Loam	3402	0.017000	2.3000	0.0846
Guelph Loam	3407	0.073566	1.7844	0.2193
Rubicon Sandy Loam	3501	0.052321	1.8570	0.1388
Loamy Sand-Hamra Sharon	4004	0.018695	5.1537	0.1997
Plainfield Sand (210-250μ)	4101	0.045177	3.9979	0.0102
Plainfield Sand (177-210μ)	4102	0.038611	4.0409	0.0099
Plainfield Sand (149-177μ)	4103	0.032170	4.0570	0.0069
Plainfield Sand (125-149μ)	4104	0.024903	5.8327	0.0283
Plainfield Sand (104-125μ)	4105	0.022127	4.4446	0.0148
Sand	4106	0.094490	2.0422	0.0000
Sand	4107	0.060000	2.6400	0.0400
Del Norte Fine Sand	4108	0.016254	4.3600	0.0505
Oakley Sand	4112	0.095194	2.0136	0.0255
G.E. #2 Sand	4115	0.035965	4.4892	0.0409
Crab Creek Sand	4117	0.118896	2.4506	0.0000
Sinai Sand	4122	0.023803	5.3076	0.0326
Sand (50-500μ)	4124	0.019116	4.6747	0.0693
Gravelly Sand G.E. 9	4135	0.015048	2.8391	0.0793
Fine Sand G.E. 2	4136	0.007192	3.8937	0.0608
Plainfield Sand (0-25cm)	4146	0.033730	3.8518	0.1133
Plainfield Sand (25-60cm)	4147	0.031813	4.1948	0.0724
Aggregated Glass Bead	5003	0.039748	6.4676	0.0983
Monodispersed Glass Bead	5004	0.036049	7.6171	0.0363

simple equation will be derived to calculate K_s for discrete zones above the water table by using packers to isolate a segment of the formation during a conventional borehole infiltration test. That is, water is allowed to flow into the formation above and below the packers. The packers serve only to determine the flow rate to a particular zone, or stream tube. If the orientation of the stream tube and the hydraulic gradient along the stream tube are known, hydraulic conductivity can be calculated. Our work at this time is limited to the saturated zone near the borehole, and, in particular, to regions where flow is mostly horizontal. Such areas of nearly horizontal flow along portions of the borehole are predicted by Stephens' (1979) numerical simulations. Furthermore, field experiments S2T4 and S2T5, to be discussed later, suggest that within the zero pressure zone horizontal flow occurs from one-third of the way down the borehole to within 10 centimeters of the bottom. Those regions of the soil above and below tend to have significant flow velocities in the vertical direction. Also, outside of the zero pressure zones, there are large vertical flow components.

The development for a solution to predict K_s with the use of packers, to measure flow rate, and tensiometers, to measure hydraulic gradient, during a borehole infiltration test assumes that the soil is homogeneous and isotropic, and flow is horizontal and steady state. The flow rate, Q', is given by:

$$Q' = 2\pi rbK\ dh/dr \qquad (14)$$

where

r = radial distance from borehole to tensiometer outside the packer zone, [L]

b = distance between packers, [L]

dh/dr = hydraulic gradient in the radial direction

K = zero pressure hydraulic conductivity, $[LT^{-1}]$

The boundary conditions are : $h(r_w) = H$ and $h(r') = h'$, where r_w is the well radius, H is the total hydraulic head in the borehole, r' is some radial distance where the head is measured, and h' is the head at r. Integrating equation 14 and applying the boundary conditions yields:

$$K = \frac{Q'}{2\pi b(H-h')} \cdot \ln\left(\frac{r'}{r_w}\right) \qquad (15)$$

PROCEDURES FOR BOREHOLE INFILTRATION TESTS

Thirty-two borehole infiltration experiments were conducted at seven locations shown in Figure 5. Hereafter, these seven locations are coded S1 to S7; and the tests at each site are referred to as S1T1, for example, to designate the first test conducted in the first borehole site. The objectives of the tests included studies of the effects of capillarity, borehole geometry and construction, influence of the head of water in the borehole, long-term infiltration behavior, anisotropy, and entrapped air. Our procedures are similar to those recommended by the U.S. Bureau of Reclamation (1974). However, our experiments differ from the USBR procedure in the placement of instrumentation in the soil surrounding the borehole to measure water content, pressure head, and temperature. Table 8 is a summary of the experimental conditions. Figures 17 through 23 show the instrumentation layouts.

TABLE 8
SUMMARY OF BOREHOLE INFILTRATION TEST CONDITIONS AND RESULTS

Exp #	H (cm)	R (cm)	H/R	A (cm)	θ_i cm^3/cm^3	Duration (min)	V_{min} (l)	V_{total} (l)	Q_s l/min	K_a (Eq.1) 10^{-3}cm/s	K_b (Eq.6) 10^{-3}cm/s	K_c(Eq.12) 10^{-3}cm/s	K_d (Eq.10) 10^{-3}cm/s	Comments*
S1T1	113.0	3.2	34.9	113.0	10.0	241	438	1014	3.1	2.1	3.2	2.6	2.7	1,2
S2T1	60.2	4.7	12.9	60.2	10.0	232	115	-	2.2	3.6	6.0	3.2	3.5	1,2
S2T2	91.4	5.1	17.9	91.4	10.0	120	327	737	5.1	4.2	6.7	4.5	4.9	1,2
S2T3	103.0	4.7	21.9	103.0	10.0	480	418	1772	3.4	2.4	3.8	2.7	3.0	1,2
S2T4	92.5	5.7	16.2	92.5	10.0	527	360	2342	4.0	3.0	4.9	3.3	3.6	3,5,10
S2T5	94.0	8.9	10.6	94.0	8.0	265	534	1328	4.2	2.6	4.4	2.8	3.0	3,5
S3T1	90.0	6.0	15.0	88.9	10.0	314	347	2005	5.7	4.5	7.4	4.8	5.2	3,6,10
S3T2	96.5	8.9	10.8	88.9	12.5	253	487	1746	5.8	3.4	5.8	3.7	4.0	3,6
S3T3	96.5	8.9	10.8	88.9	12.5	230	487	2214	8.4	5.0	8.5	5.4	5.8	4,5,8,10
S3T4	96.5	8.9	10.8	88.9	13.5	270	470	2176	6.6	3.9	6.7	4.3	4.5	4,5,8
S3T6	96.5	8.9	10.8	88.9	13.0	300	479	4617	15.0	8.9	15.2	9.7	10 3	4,5,7,8
S3T7	97.0	8.9	10.9	88.9	7.0	177	592	1802	9.4	5.5	9.4	6.0	6.4	4,5,8
S4T2	91.4	5.8	15.9	91.4	11.5	280	333	712	6.9	5.4	8.7	5.7	6.3	7
S4T3	91.4	5.8	15.9	91.4	12.5	255	322	532	1.3	1.0	1.6	1.1	1.2	7
S4T4	22.9	5.8	4.0	22.9	12.5	255	17	125	0.3	1.7	3.6	1.1	1.2	10,7
S5T3	76.2	5.8	13.3	76.2	13.0	1560	205	8847	8.0	8.3	13.8	8.1	8.9	9
S5T4	76.2	5.8	13.3	76.2	13.0	312	205	1896	4.9	5.1	8.5	5.0	5.4	7,9
S5T5	76.2	5.8	13.3	76.2	13.0	349	205	2488	6.6	6.9	11.4	6.7	7.3	7,9
S5T6	76.2	5.8	13.3	76.2	13.0	305	205	2252	6.8	7.0	11.7	6.9	7.5	7,9
S5T7	76.2	5.8	13.3	76.2	14.0	375	198	2685	6.9	7.2	11.9	7.0	7.6	7,9
S5T8	76.2	5.8	13.3	76.2	14.5	735	194	4582	9.0	9.4	15.6	9.2	10.0	7,9
S6T1	155.0	5.8	27.0	122.0	8.8	507	1330	11200	18.3	6.0	9.3	8.4	9.1	3,6,7,8
S6T3	121.0	5.8	21.0	121.0	9.8	1295	697	10512	9.1	4.5	7.1	5.5	6.0	3,6,7,9
S6T4	58.0	5.8	10.1	58.0	10.1	1290	121	810	.8	1.2	2.1	1.0	1.1	3,6,7,9
S6T5	57.0	5.8	9.1	57.0	9.7	1275	118	4248	3.0	4.9	8.4	4.2	4.6	3,6,7
S6T6	91.4	5.8	15.9	85.3	8.4	2874	370	8342	3.0	2.3	3.8	2.5	2.7	3,6,8
S7T1	91.4	15.2	6.0	91.4	7.7	1425	801	23101	15.0	7.1	13.7	8.1	7.6	6,7,11

Comments:
1. Test terminated prior to steady state.
2. Gravel filled borehole
3. Johnson PVC screen 0.008 in. slots
4. Hacksaw cut PVC casing w/wire mesh
5. Closed casing bottom
6. Open casing bottom
7. CO_2 injection preceeded test.
8. Open interval slightly less than H.
9. Q_s long duration result
10. θ_i est. from previous tests.
11. Johnson wire wrap screen

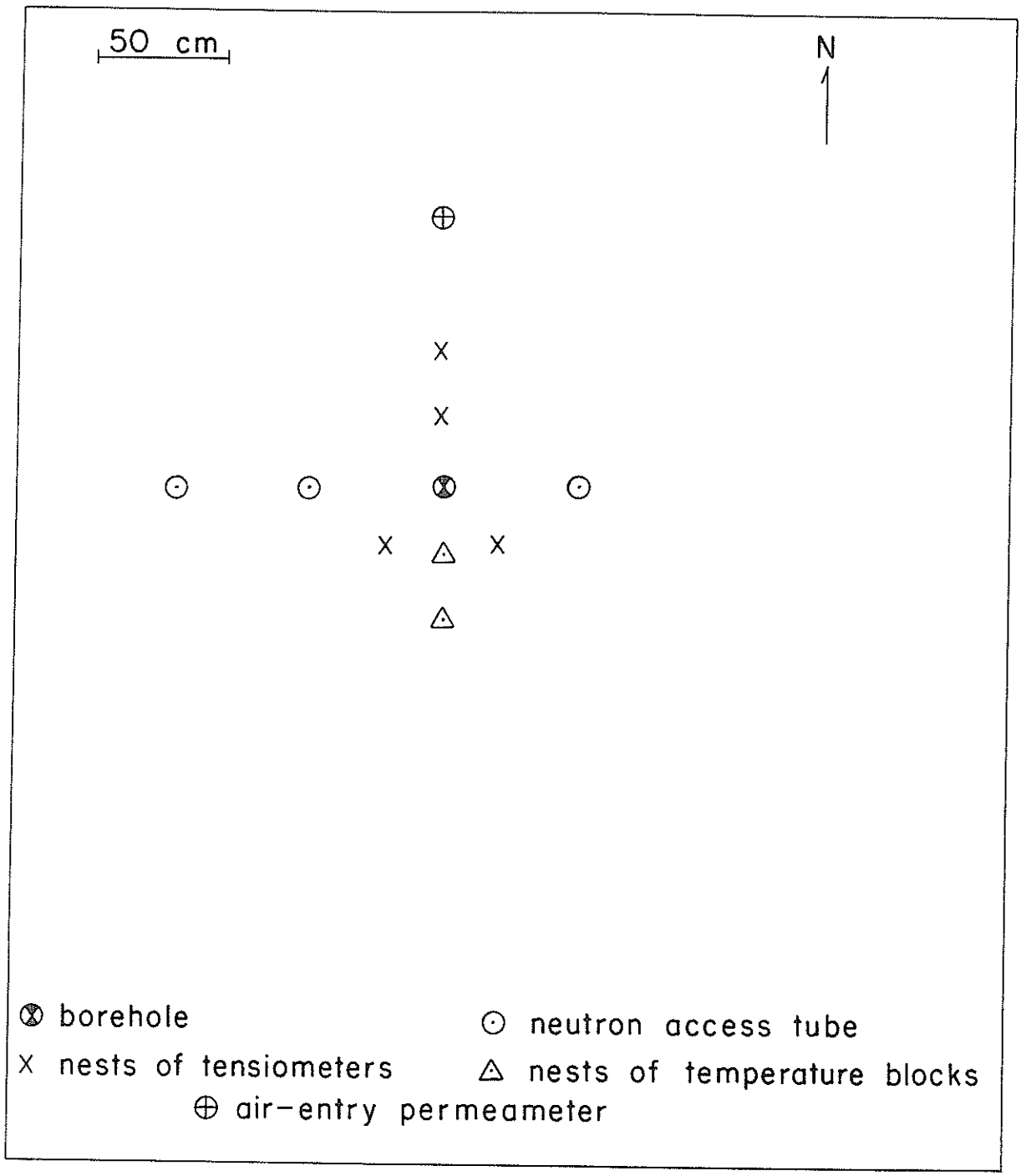

Figure 17. Instrumentation at Site 1.

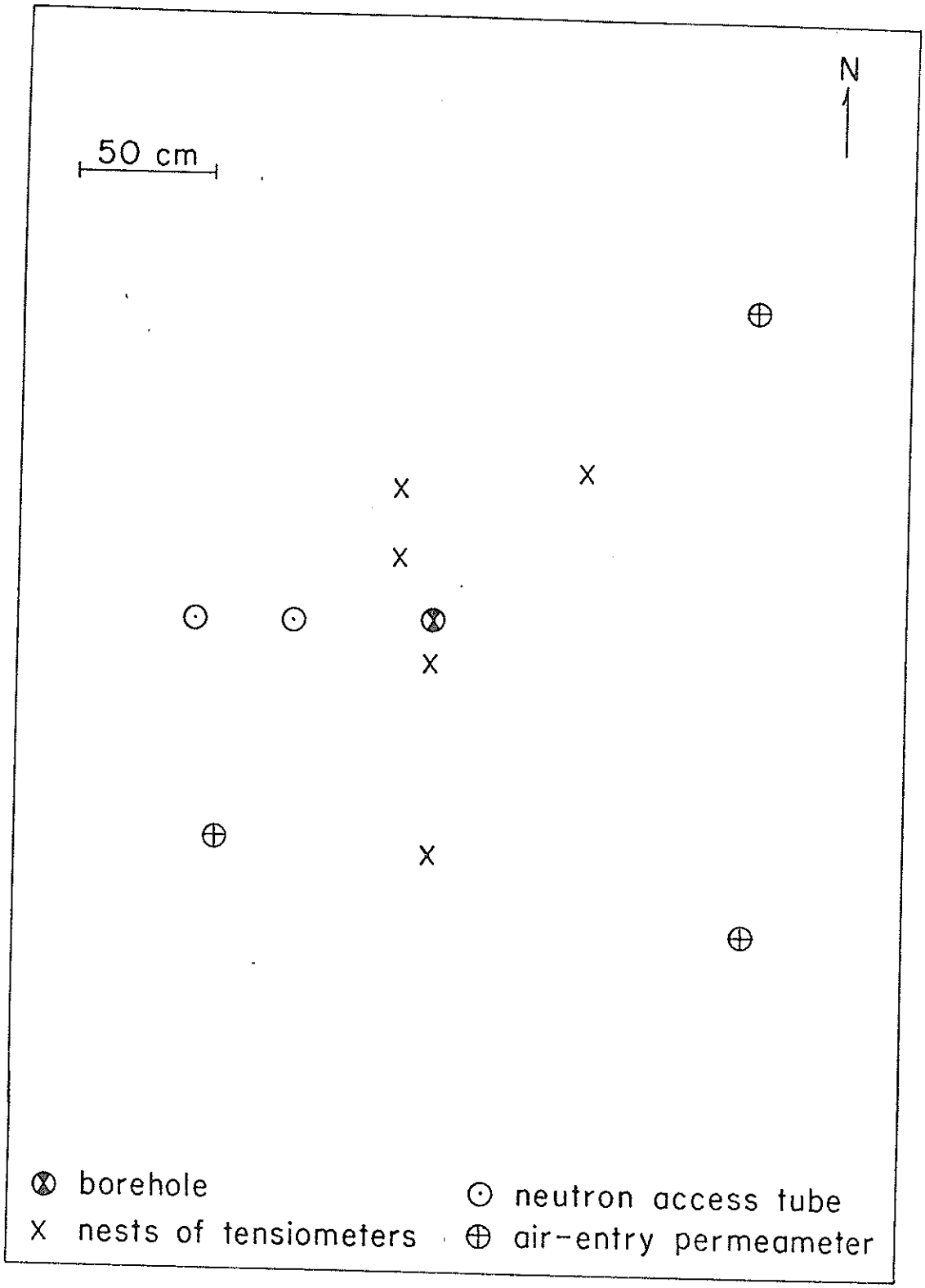

Figure 18. Instrumentation at Site 2.

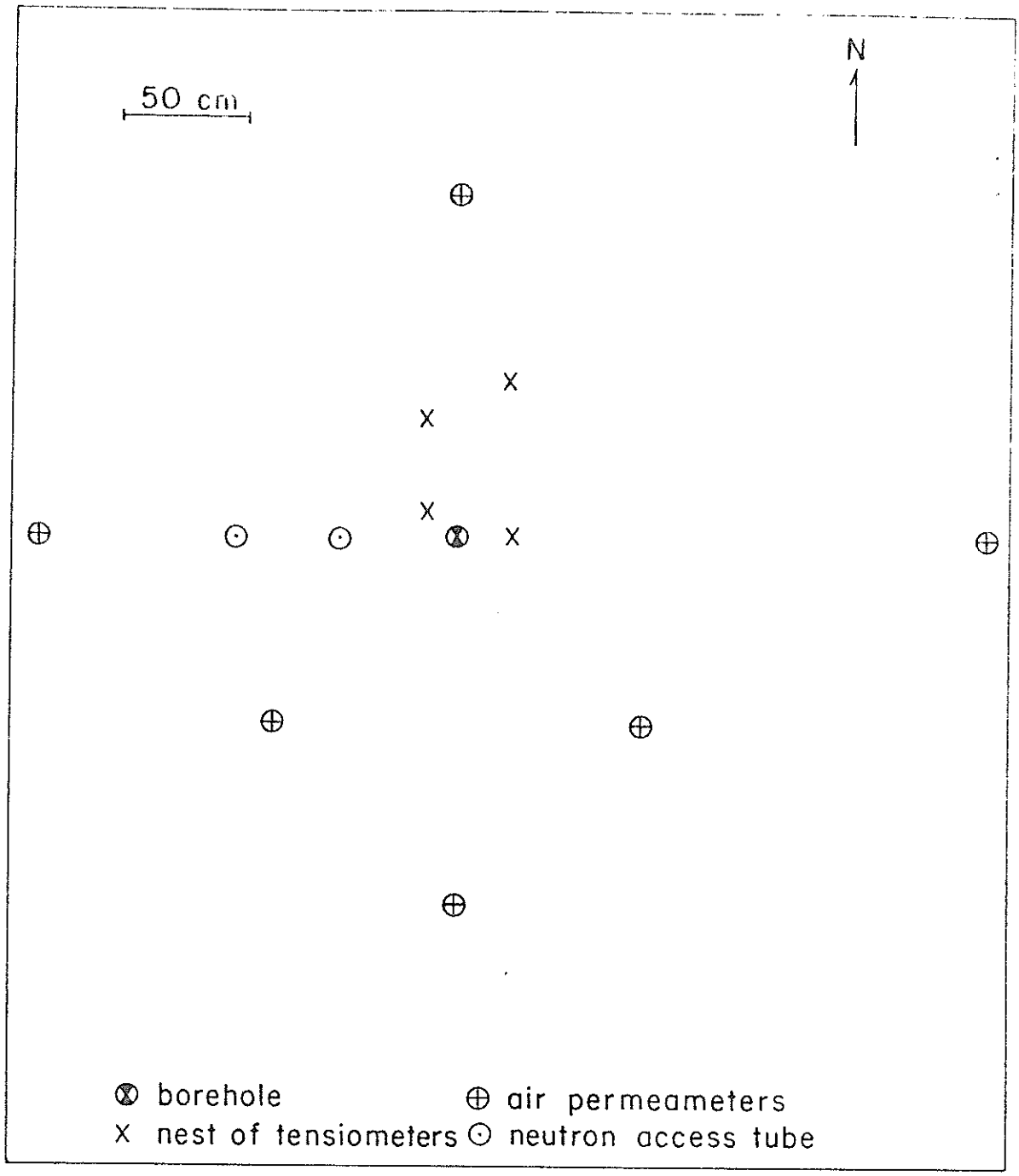

Figure 19. Instrumentation at Site 3.

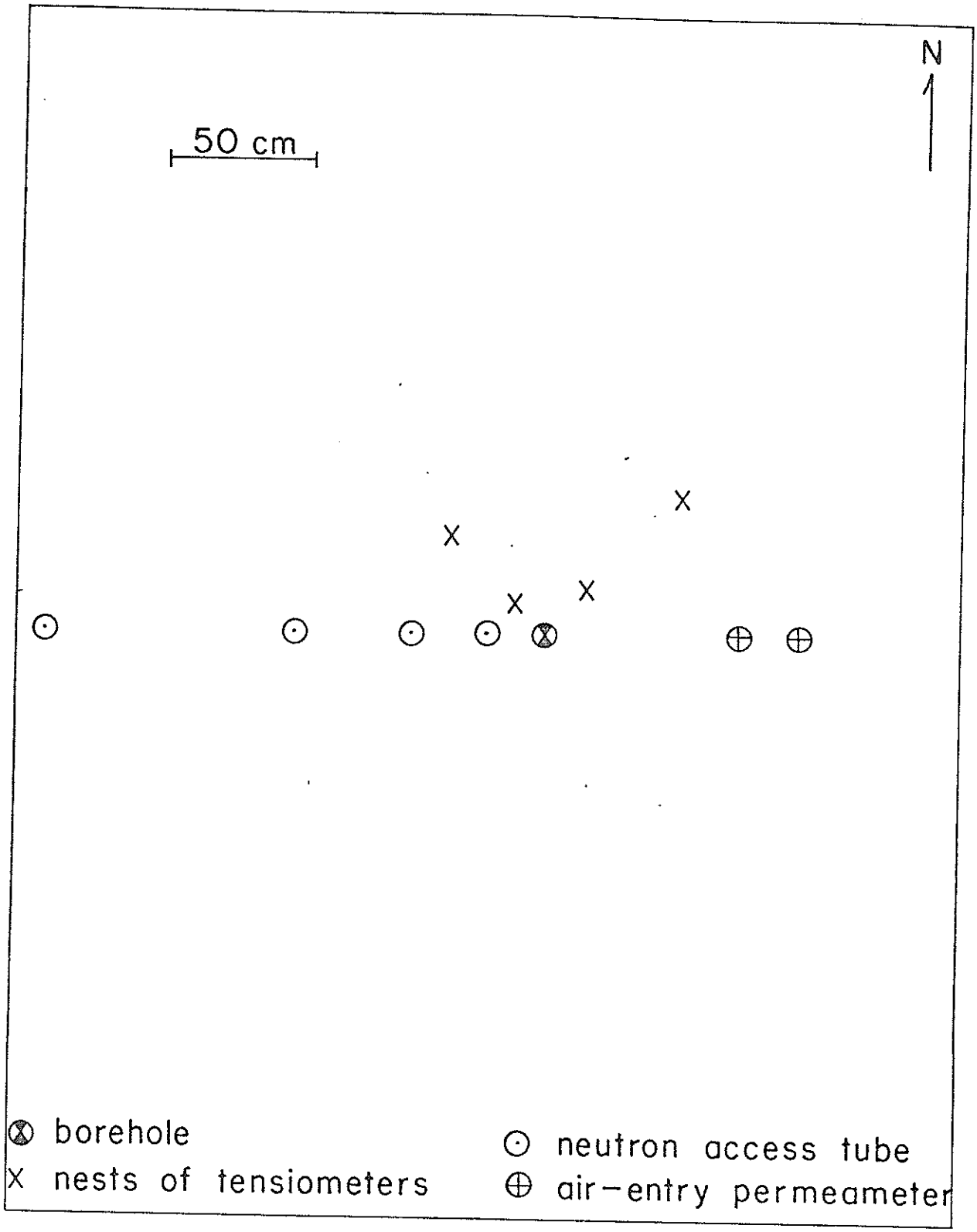

Figure 20. Instrumentation at Site 4.

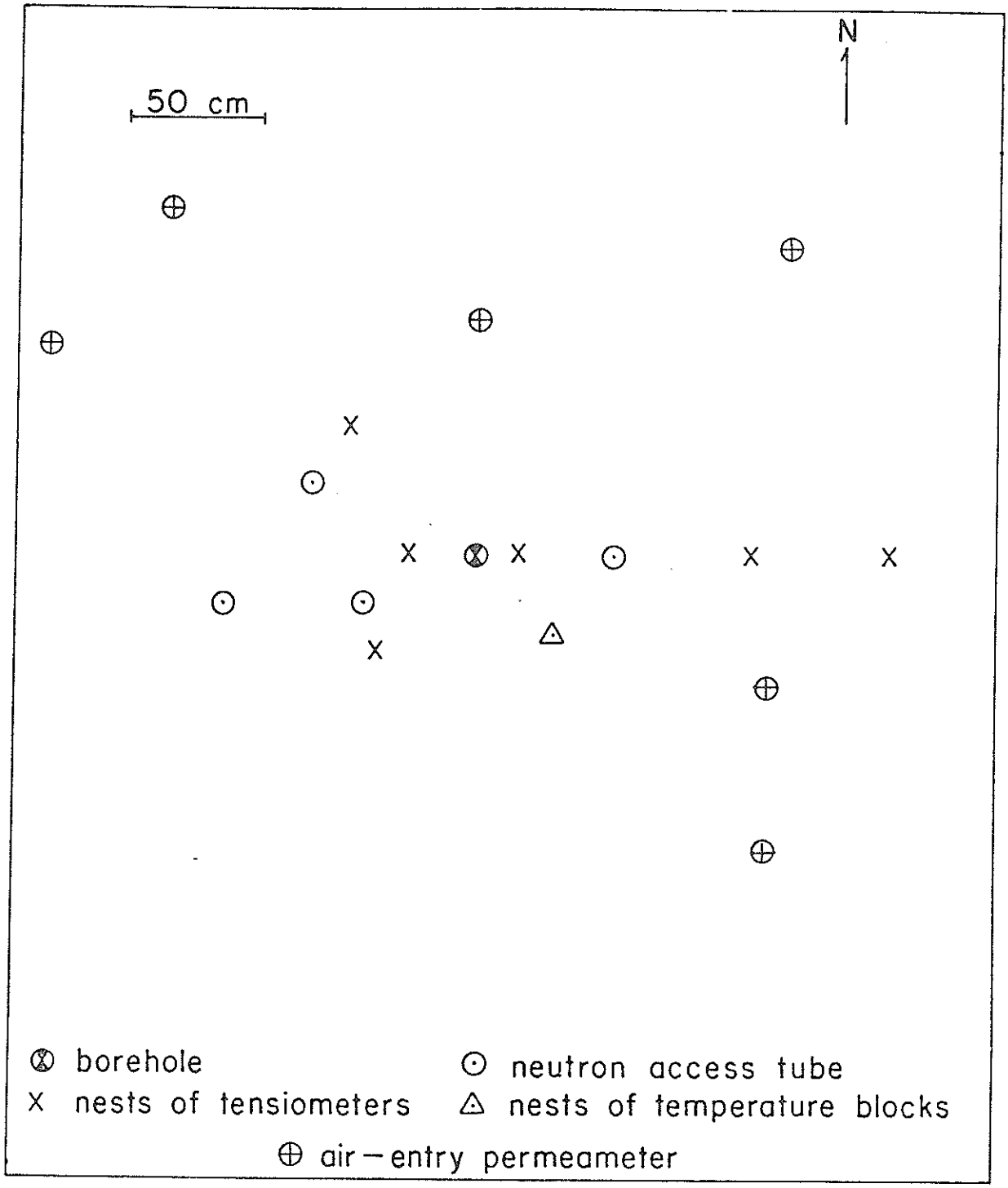

Figure 21. Instrumentation at Site 5.

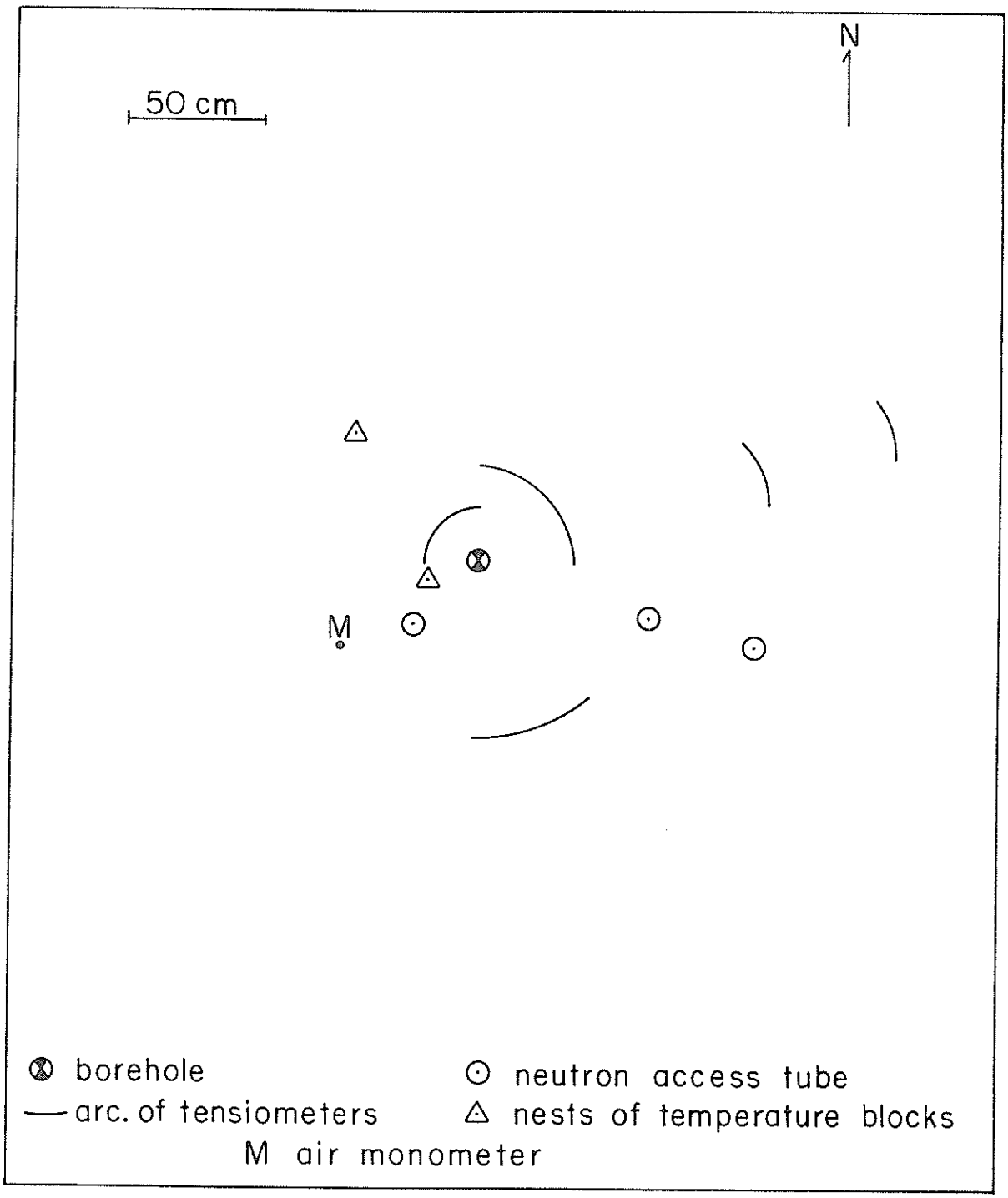

Figure 22. Instrumentation at Site 6.

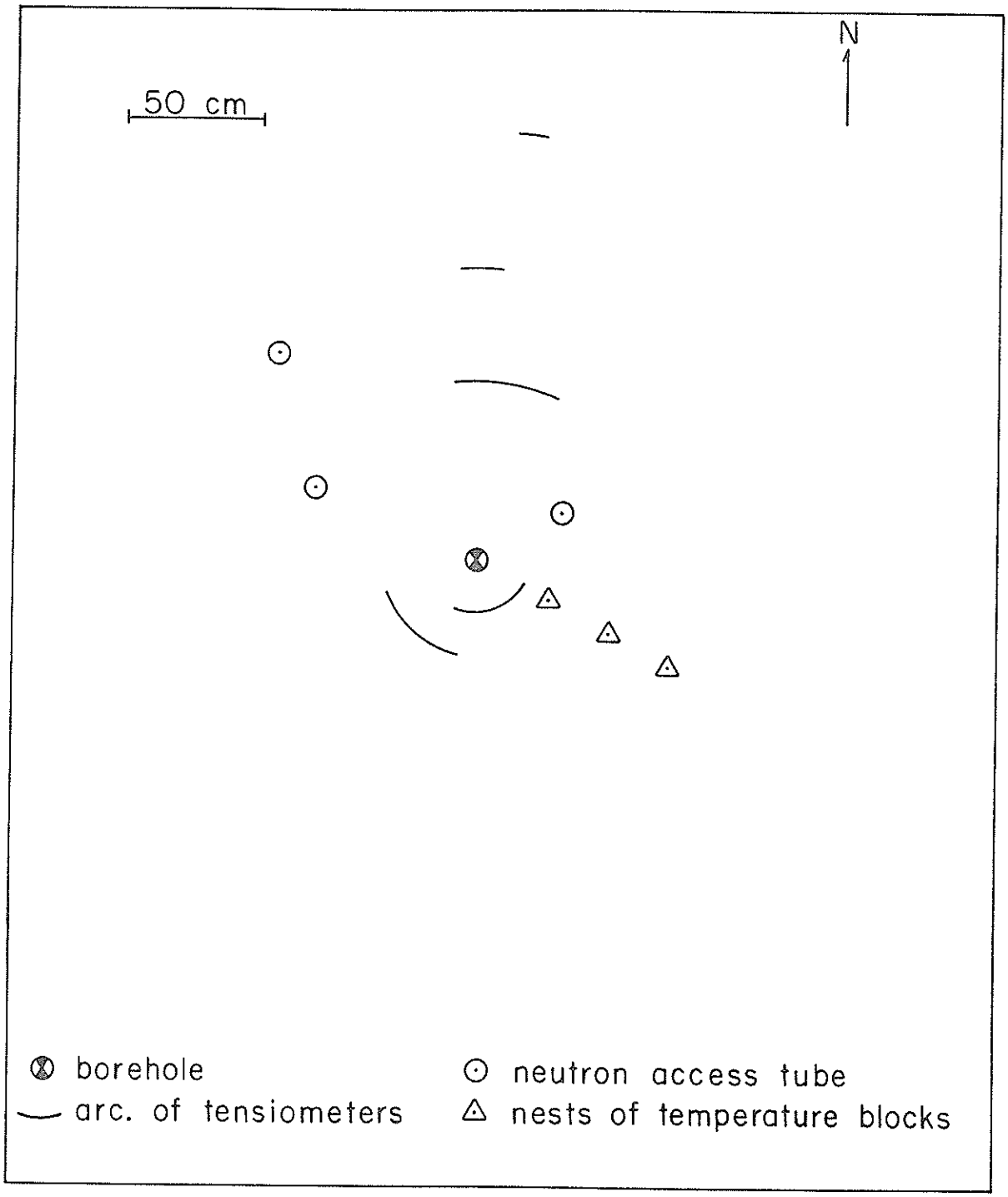

Figure 23. Instrumentation at Site 7.

Borehole Construction

Boreholes of various diameters were constructed with hand augering equipment. In our first four experiments the borehole was filled with gravel, approximately 0.5 to 1.0cm in particle diameter, to maintain an open hole during infiltration. Subsequently, because considerable amounts of formation sand penetrated into the gravel, plastic well screen (Johnson UOP Inc., St. Paul, Minnesota) was used (table 8). The small annular space outside the screen was filled with fine dry sand in most cases, and with gravel on a few of the early tests. The PVC screen slot size, 0.203mm, was selected to keep out most of the formation which has an average particle size of about 0.25mm. Screens having outer diameters of 11.4 and 16.8cm were used. A solid cap prevented sand from entering the bottom of the screen. In some later experiments indicated in table 8, the cap was removed and a fine wire mesh screen was placed at the bottom and inside the well screen to permit water to flow into the formation from the base of the borehole.

Experiments with packers inside the borehole, to be discussed subsequently, employed a hack-saw cut PVC pipe (15.25cm ID). The smooth inside of the PVC pipe helped minimize packer leakage. Slots 1mm wide were spaced at about 1.3 slots per centimeter of casing length, giving an effective open area equal to 474.5cm^2 for a 92cm long section. (By comparison, a 16.8cm Johnson PVC screen has 207.8cm^2 of open area over the same length.) The outside of the hack-saw cut casing was wrapped with a fine wire mesh with 0.7mm openings to restrict sand movement into the borehole. The hack saw cut casing was used for a number of experiments which did not use packers (table 8).

A wire wrapped galvanized steel well screen was used in the final experiment, S7T1. The screen diameter was about 30cm and the slot size was about 1.0mm. The bottom of the well screen was open to the formation via a

fine wire mesh.

Water Supply

Water for all the tests was supplied from a 7-meter deep well-point located north of sites in the Rio Salado floodplain. A chemical analysis of the groundwater is given in table 9. A gasoline-driven suction pump connected to 200 meters of 1 3/4" (4cm) and 1" (2.5cm) PVC plastic pipe brought water to the site (figure 5) at a rate of approximately 12 to 20 liters/min (lpm). The use of such a long above-ground pipe caused significant diurnal water temperature fluctuations during the summer months.

For test sites 1 and 2 and S6T4, water was stored in two elevated 55 gallon barrels. Each barrel was volume calibrated in the laboratory, and water levels in the barrels were noted on manometers on the outside of the barrel. The drums were alternated into service. As the level in one drum became low, it was valved out of the injection system and refilled from the well supply. At the same time, the remaining drum was valved into the system such that flow to the borehole was not interrupted. In other experiments the barrels were eliminated because of flow rate fluctuations caused by differences in head before and after a switch. The water was then pumped through an in-line filter and totalizing flow meter before entering the constant head control valve.

To maintain a constant water level in the borehole, a 1.9cm diameter stock tank valve was used. A float and float arm of the design of the USBR (Earth Manual, 1974, p. 579) was attached to the stock tank valve. The valve/float system functioned adequately, although this assembly did cause flow surges which resulted in occasional fluctuations of the water level in the borehole. Water levels in the borehole were measured periodically with a meter stick. In some experiments a piezometer located just outside the screen

TABLE 9
CHEMICAL ANALYSIS OF WATER USED FOR FIELD TESTS
SAMPLE COLLECTED 10/7/81

pH	7.9
CO_3	0.0 mg/l
HCO_3	137.0 mg/l
Cl	297.0 mg/l
SO_4	462.0 mg/l
Na	290.0 mg/l
K	8.2 mg/l
Mg	42.0 mg/l
Ca	142.0 mg/l
Conductivity	2000 micromhos
Temperature	16°C

was used to monitor water levels. There was no appreciable head loss across the screen.

Injection of water into the borehole was through a 1.87cm diameter PVC pipe or garden hose that ran down the inside of the borehole to within 15 to 30cm of the bottom of the hole. This tubing was perforated and plugged at the bottom to disperse the injection water momentum within the borehole.

Instrumentation

Pressure Head and Total Hydraulic Head. Each tensiometer nest or arc shown in figures 17 to 23, consists of five to eight 1.9cm OD tensiometers.

For S1T1 and S2T1 to S2T3 pressure head was measured by a mercury manometer connected to each tensiometer (Soil Moisture Equipment Corporation, Santa Barbara, California). An insertion tube available from the tensiometer manufacturer was used to install the tensiometers.

For S2T4 through S5T3, pressure head measurements were obtained from as many as 22 tensiometers connected to a scanning valve (Scanivalve Corp., San Diego, California) and a differential pressure transducer (Model PDCR22, Druck, Inc., London, England). Data from the 22 tensiometers was collected by a data logger (Model CR 21, Campbell Scientific, Inc., Logan, Utah) which controls the frequency of data recording and storage. For these tests, the data logger signaled the scanning valve to switch between tensiometer ports at pre-determined time intervals. Following a switch, the pressure was allowed to equilibrate before the voltage was measured by the transducer. Time of measurement, port number, and output voltage were stored on paper tape with a thermal printer and on magnetic cassette tape for convenient data transfer to a DEC-20 computer system. To reduce instrument error due to temperature fluctuations, all tensiometers, tubing, and instruments were insulated. To further reduce errors, the transducer was calibrated during each scan by the use of two reference ports on the scanning valve connected to standing water

columns located at the transducer level and 200 centimeters below. Pressure heads from the transducer/scanning valve system are estimated to be accurate to within 5 centimeters of water. Figure 24 illustrates the instrumentation associated with experiments which utilized this pressure head data acquisition system. Other equipment and instrumentation shown in figures 17 through 23 is as described previously.

Upon completion of S5T3, total hydraulic heads from the automatic data collection system were found to be in error. The entire electronic system was returned to the laboratory for inspection, where it was discovered that the scanning valve, which switches between tensiometers, leaked. To avoid delay, the automatic data collection system was replaced with mercury manometers. The mercury manometers were found to be more durable and less temperamental than the electronic system. Also, no unnecessary data was recorded, and at early time pressure changes in one tensiometer can be read faster than with the electronic system, which can continuously scan all tensiometers only once every 24 minutes.

Water Content. Water content in the vicinity of the borehole was monitored by a neutron probe (Model 3222, Troxler Electronic Laboratories Inc., Research Triangle Park, North Carolina). The neutron probe determines the water content by counting the number of thermalized neutrons returning to the detector (the neutrons become thermalized or slowed by their collision with hydrogen atoms). The source and detector are located at the same depth in this instrument. The precision of the gauge at 20.0 percent water content by volume for the fast count (15 seconds) position is ≈0.66 percent, according to the manufacturer. Moisture content was almost always measured when the gauge was set in the fast count position. This allowed for more rapid data collection with minor reduction in precision. For example, if counts are

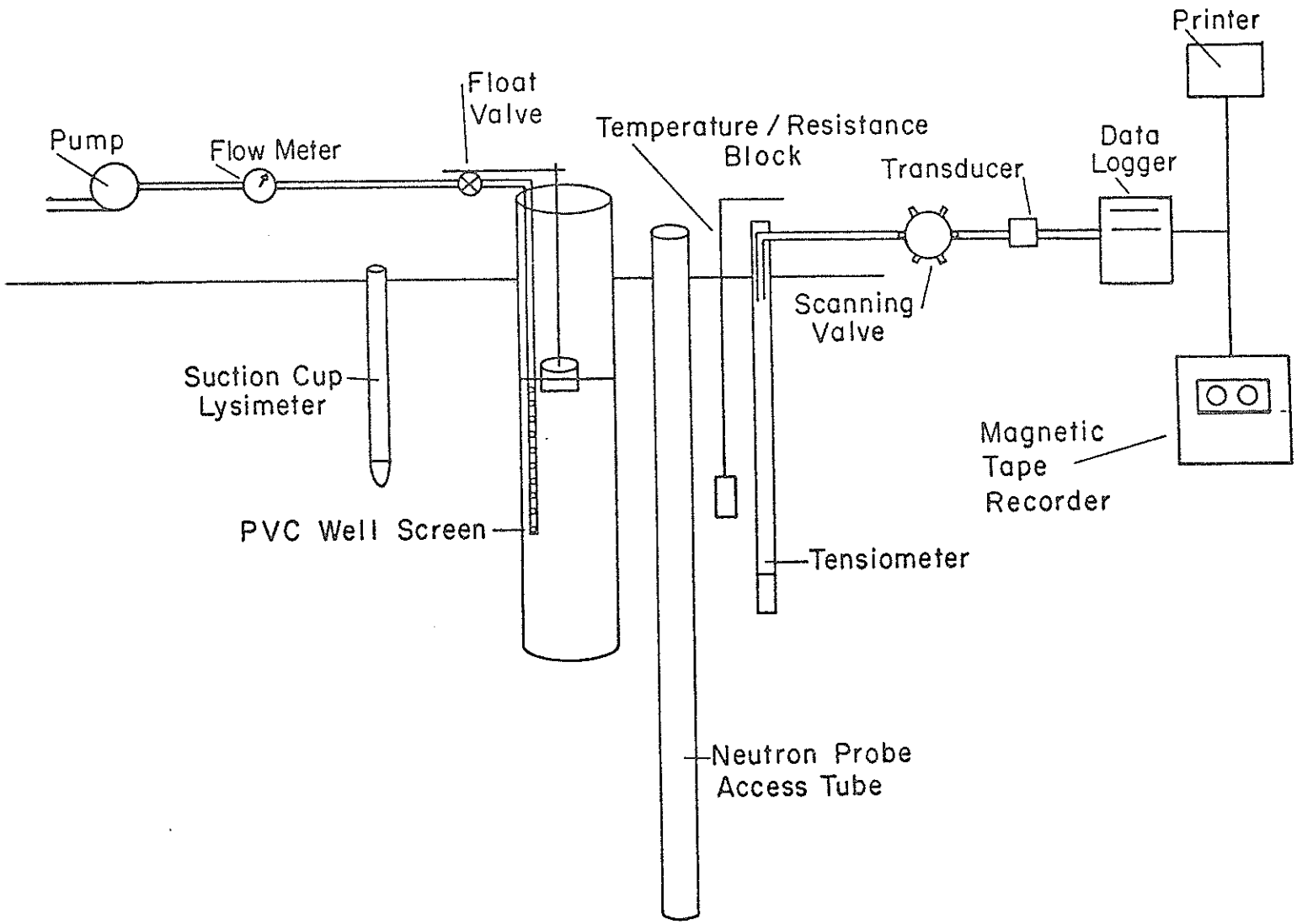

Figure 24. Schematic Diagram of Instrumentation.

accumulated for one minute or four minutes the precision at 20.0 percent water content by volume is ≈0.33 percent and ≈0.17 percent, respectively. The 5cm OD, 305cm long aluminum access tubes for the neutron probe were installed in holes dug by an Eijkelkamp hand auger (Eijkelkamp, Equipment for Soil Research B.V., Giesbeek, The Netherlands). The excavated soil was used to backfill around the access tubes to insure they fit securely in the hole. The access tubes were allowed to equilibrate over several days; this gave the backfilled material an opportunity to equilibrate with the background moisture content. Approximately 30 centimeters of each access tube were left above ground to accommodate the moisture probe box, which would be set on top. The moisture probe was then lowered down each access tube at known intervals, before and during the experiments, so that content profiles could be determined. Records were kept of count ratio, and water content was calculated from the factory calibration curve by the microprocessor. Data collected after site 4 were corrected using the calibration curve described in the Site Description. A slightly different calibration curve was used prior to site 4.

Temperature. Soil temperature was recorded to an accuracy of 0.56° C (1° F) by thermistors (Model MC-312, Soiltest, Inc., Evanston, Illinois) placed in the soil at 30 centimeter depth intervals to a total depth of about 3 meters in most tests. One thermistor was also placed in the borehole.

Carbon Dioxide. The equipment required to inject carbon dioxide into the borehole includes a carbon dioxide tank, pressure regulator, flowmeter, and connecting hoses. A standard commercial carbon dioxide tank was used as the source of gas. Pressure regulator gauges calibrated from 0 to 5 pounds per square inch and 0 to 30 pounds per square inch were used.

The rate of carbon dioxide flowing into the borehole was measured with a Sho-Rate Flowmeter (Model 1355, Brooks Instrument Division, Emerson Electric Company, Hatfield, Pennsylvania). The flow rate is determined by the height

of rise of a steel ball within the graduated glass tube inside the flowmeter and the factory-supplied calibration curve. Knowing the flow rate and elapsed time, the volume of carbon dioxide injected is determined. The flowmeter is designed so that glass tubes of different diameter can be placed inside, giving a broader range of flow rates. The manufacturers glass tube number R-6-15-B was used for all carbon dioxide injections in the field.

Air Pressure. Air pressure ahead of the wetting front was monitored by inserting open-bottomed pipes (about 1.3cm OD) into a tightly fitting hole about 50 to 100cm from the borehole and about 1 meter deep. Tygon tubing was attached to the top of the pipe and connected to a water manometer (Dwyer Instruments Inc., Michigan City, Indiana). The manometers were read periodically during the early stages of infiltration at site 2 and S6T6.

At site 5, the build up of soil gas pressure during CO_2 injection was monitored with four small diameter (1cm) steel access tubes, at distances of 10, 15, 20, and 25 centimeters, from the borehole. Two pressure indicators were used to determine the pressure front. The first device was the Dwyer water manometer which remained attached to the 10 centimeter access tube during the injection of carbon dioxide. The second was a Druck null-type pressure indicator (Model DPI 201, Druck Inc. London, England) that was rotated among the remaining access tubes during carbon dioxide injection.

Packer Testing

A packer assembly was designed to measure flow rate out of separate sections of the borehole during a constant head borehole infiltration test. Thus, the packer had to be designed to allow water to pass from the source to the zone below the packer, and also to maintain a tight seal with the hack-saw cut PVC casing to prevent leakage.

The packer was constructed for use in a 15.25cm inside diameter casing.

The packer consists of an upper plate to which a 4.5cm inside diameter, 183cm long PVC standpipe was attached. The lower packer plate is attached to the upper plate by four 15.25cm stainless steel bolts. Each packer plate consists of two 0.7cm aluminum plates with a rubber gasket sandwiched between. This rubber gasket protrudes from the edges of the plates and seals the packer against the walls of the well screen. The distance between the bottom of the top plate and top of the bottom plate is adjustable from 12.7cm to 3.8cm. To allow flow to the unpacked section below, a 1.9cm I.D.PVC pipe passes from the upper to the lower plate. To allow flow of water into the packer prior to a test, a 0.7cm valve is located 5cm above the upper plate on the standpipe. This valve is operated from the land surface by a 178cm key.

The best practical method of measuring the flow rate out of the packer is to separately monitor the flows to both the packed and the unpacked sections of the borehole, while maintaining a constant and equal height of water in each. This method requires the use of two flowmeters and two float control valves. For the experiments conducted, a carburetor float valve was placed down the packer standpipe and the flow from a calibrated barrel was recorded.

For the packer as designed, the flow rate is recorded as follows: With the packed to unpacked section valve (PUPS valve) open, the borehole test is conducted until a steady infiltration rate is achieved (the PUPS valve hydraulically connects the packed and unpacked sections and permits the continuation of a standard borehole infiltration test). Upon the achievement of a steady infiltration rate, the PUPS valve is closed and the test section is isolated from the unpacked borehole. A constant head is maintained in the unpacked section through the float control valve. As soon as the PUPS valve is closed, the inner float valve control valve is opened, and water is injected into the packer from the calibrated barrels. During this time, the fluid level inside the packed interval is kept equal to that level of water

above and below the packer. After sufficient time has passed to record a flow rate into the packer, the PUPS valve is opened and the inner float valve control valve is closed. The test is then continued as a standard borehole test. The packer assembly is then slowly lowered to the next interval to be tested and flow rates are measured as above.

During the field testing of the packer, fast-response tensiometers (Soil Moisture Equipment Corp. Santa Barbara, California) were used to record soil pressure heads (both positive and negative). Elevation head was measured as the distance from the datum (the transducer level) and the center of the tensiometer cup. The total hydraulic head is the sum of these two heads. For other experiments, land surface datum is used to compute total hydraulic head. The hydraulic gradient is then calculated along the flow tube by taking the difference in total head between any point in the borehole and the total hydraulic head as measured at the tensiometer and dividing this quantity by the radial distance between the borehole face and the tensiometer.

At S3T4 tensiometer locations are shown in figure 19. Prior to the packer test phase of the S3T4 experiment, approximately 1750 liters of water were injected through the borehole into to the soil during conventional borehole infiltration tests. The water level in the borehole was kept 5 to 10cm above top of the screened interval. Earlier, screened borehole tests had shown soil formation erosion at the top of the water level in the borehole. It was postulated that the water level fluctuation within the borehole had caused this erosion. By keeping the water surface above the top of the screen, it was hoped to reduce the erosion. Removal of the casing following the experiment showed little reduction in soil erosion however.

FIELD RESULTS AND DISCUSSION

Short Duration Experiments

For purposes of discussion, three short-duration experiments will be presented in detail. These three tests were conducted at site 3 in April 1982. In general, the behavior and duration are similar to the many experiments conducted previously for slightly different conditions. The initial soil temperature was about 18°C and the injection water temperature was about 23°C. Initial soil pressure head was in the range of -60 to -80 centimeters of water. The initial hydraulic gradient was about 1.1, indicating downward vertical flow.

The infiltration rate for experiments from S1T1 through S3T4, as well as all others where no CO_2 was injected, followed a similar pattern to that shown in figure 25 for S3T4. At very early time the infiltration rate is limited by the capacity of the pump to about 20 lpm. For our soil this period usually lasts 5 to 10 minutes until the borehole is full. Thereafter, a constant head is maintained by the float valve and infiltration rate gradually decreases to a near-steady value. The cumulative infiltration rate is shown in figure 26. The maximum and minimum volume to be infiltrated according to equations 4 and 5 is shown for comparison to actual field data. For S3T4 the minimum required volume is injected after about 60 minutes and the maximum occurs at about 120 minutes; at these times the infiltration rate in figure 25 appears to be fairly steady. Data from S3T4 suggests that the USBR criteria to terminate a test are reasonable; however, results of other tests summarized in table 8 indicate that the steady infiltration rate may not be reached until long after the calculated maximum volume (V_{max}) has been injected. The short-duration experiments were all completed within a few hundred minutes.

For test S3T4, the height of water in the borehole was 96.5 centimeters;

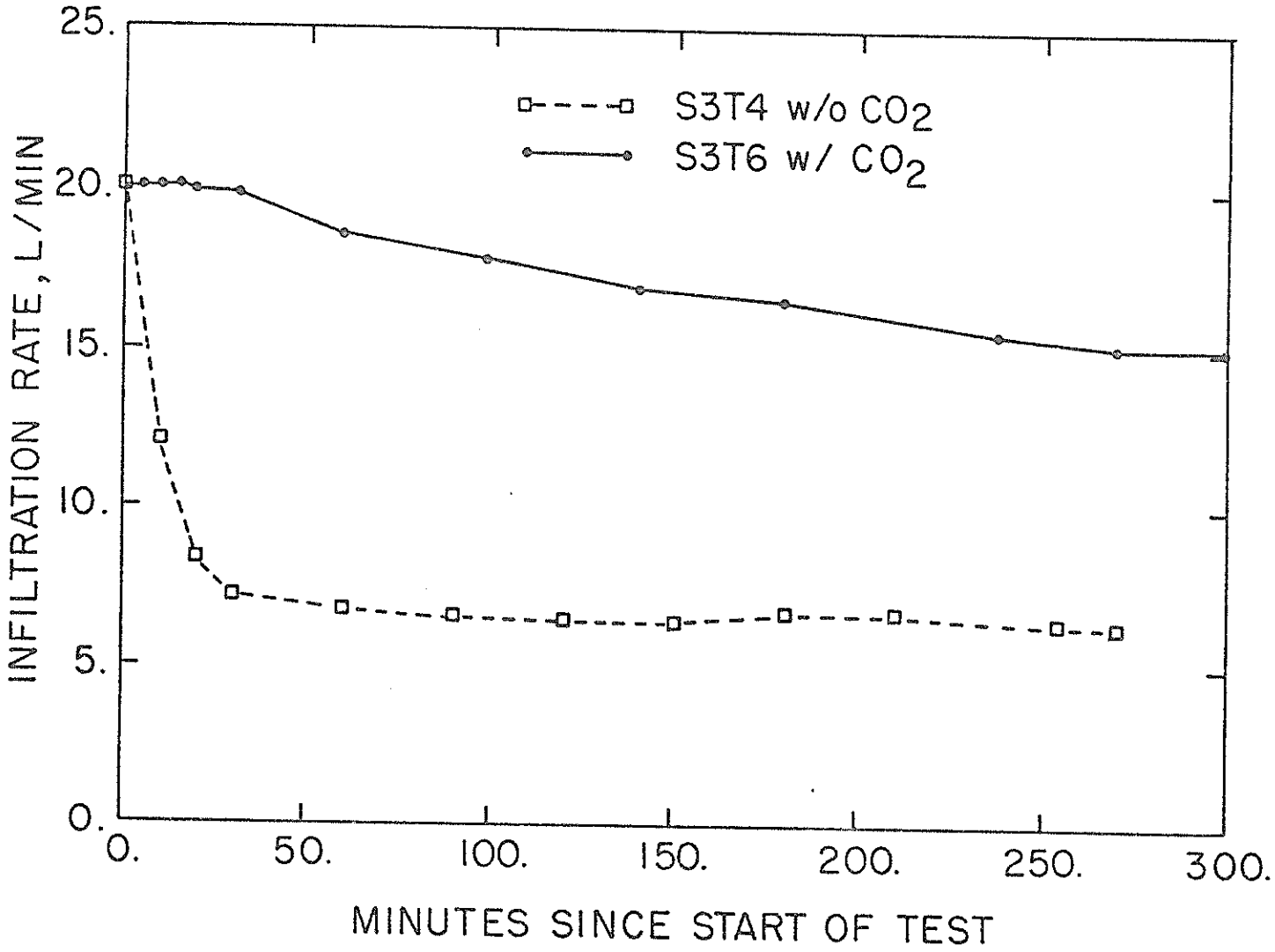

Figure 25. Infiltration Rate into Boreholes for S3T4 and S3T6 Showing the Effect of CO_2 Flooding.

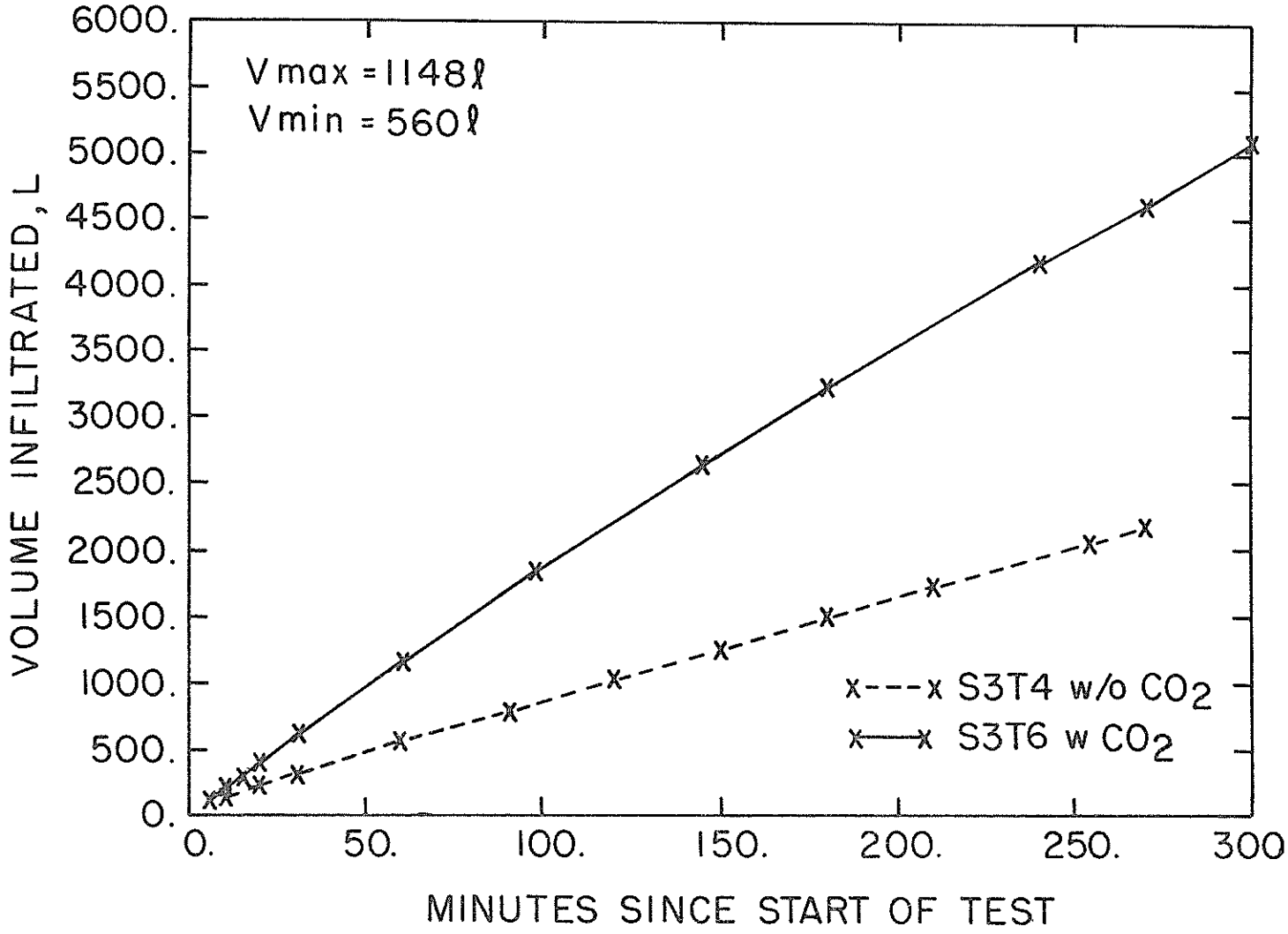

Figure 26. Cumulative Infiltration Rate for S3T4 and S3T6.

however, only 88.9 centimeters of the borehole was screened. Total hydraulic head from tensiometers at 15 centimeters from the borehole practically stabilized 15 to 20 minutes after the test began and did not change appreciably for the six hour duration of the test (figure 27). A contour of total hydraulic heads for this test is shown in figure 28. Hydraulic gradients increase toward the base of the borehole, as would be expected if flux increases with depth along the borehole, as presumed by Glover (1953) and indicated by numerical studies of Stephens (1979). Therefore, in heterogeneous materials hydraulic conductivities near the base of the borehole are likely to have a strong influence on the average value of K_s which one assumes the borehole method provides.

Figure 28 also shows the approximate location of the theoretical free surface predicted from analytical solutions. Observed gradients in figure 28 indicate that the actual flow field is larger than expected by the free surface approach. Most of the lateral spread is caused by capillarity and probably a small degree of anisotropy.

At 90 minutes into S3T4, the flow rate and pressure head within 75 centimeters of the borehole was steady. For this time the pressure head distribution is shown in figure 29. A comparison of figures 28 and 29 indicates that water flowing from the borehole along any path will pass from a saturated to an unsaturated region. This observation contradicts the free surface approach, and supports the results of saturated-unsaturated numerical simulations conducted by Stephens (1979).

Due to capillarity the volume of saturated soil sampled is only a small part of the flow domain. This particular sand has hydraulic properties which are very similar to the coarsest soil used by Stephens (1979) in his numerical studies. That study suggests that for a particular borehole construction, the region where saturation exists becomes smaller as α decreases (equation 7).

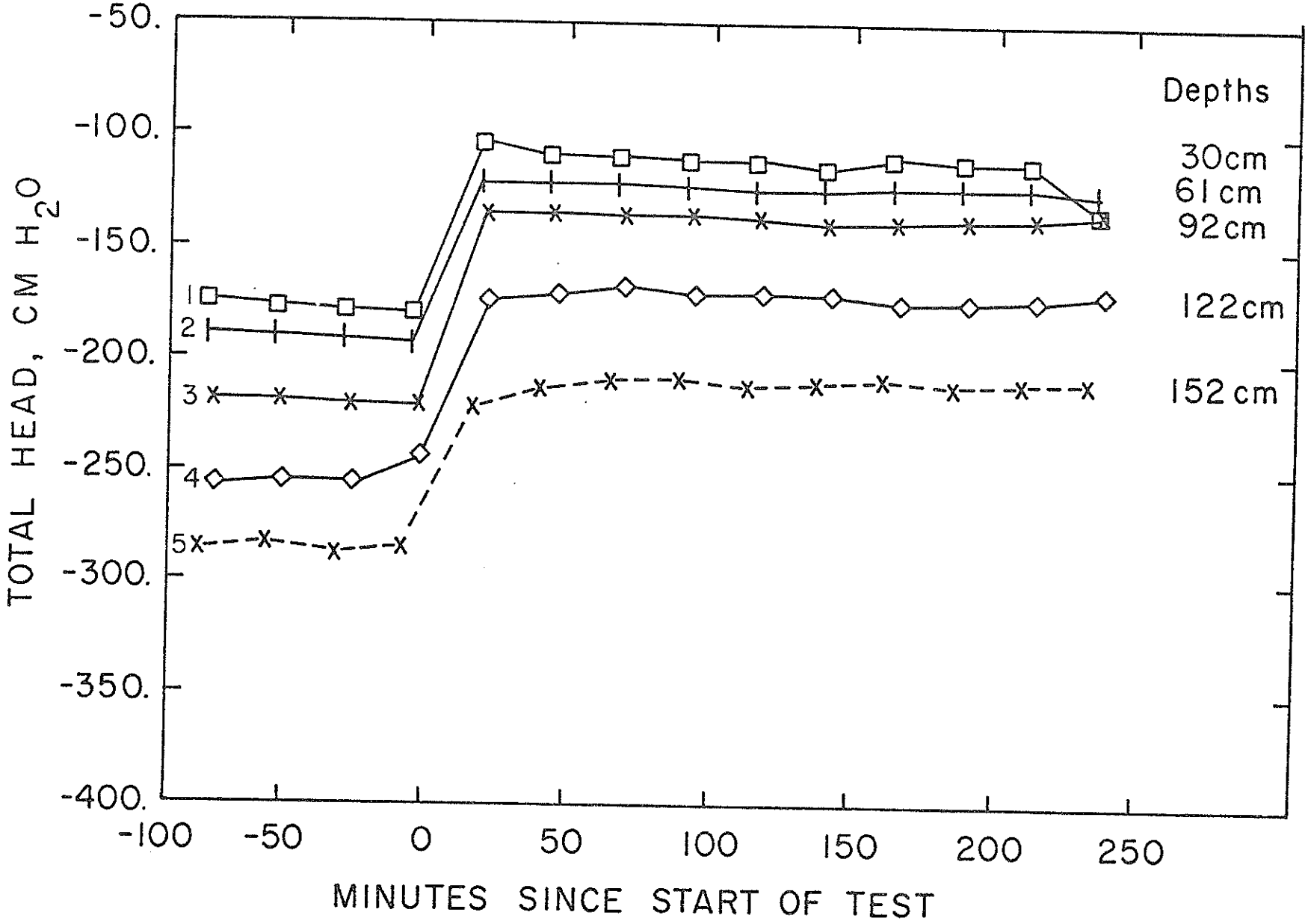

Figure 27. Total Hydraulic Head Response at S3T4.

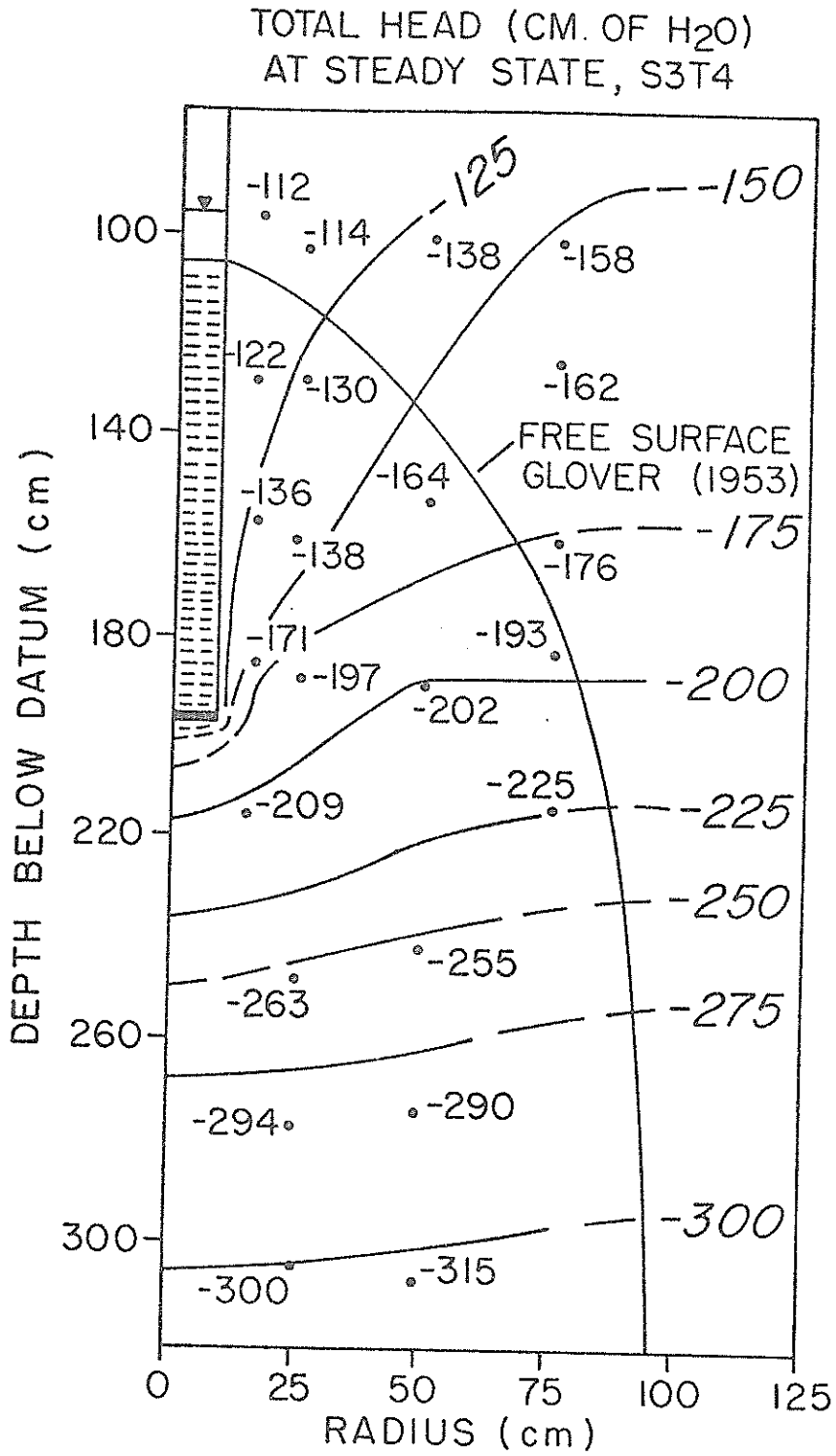

Figure 28. Flowfield for S3T4 and Approximate Position of the Free Surface Predicted by Glover (1953).

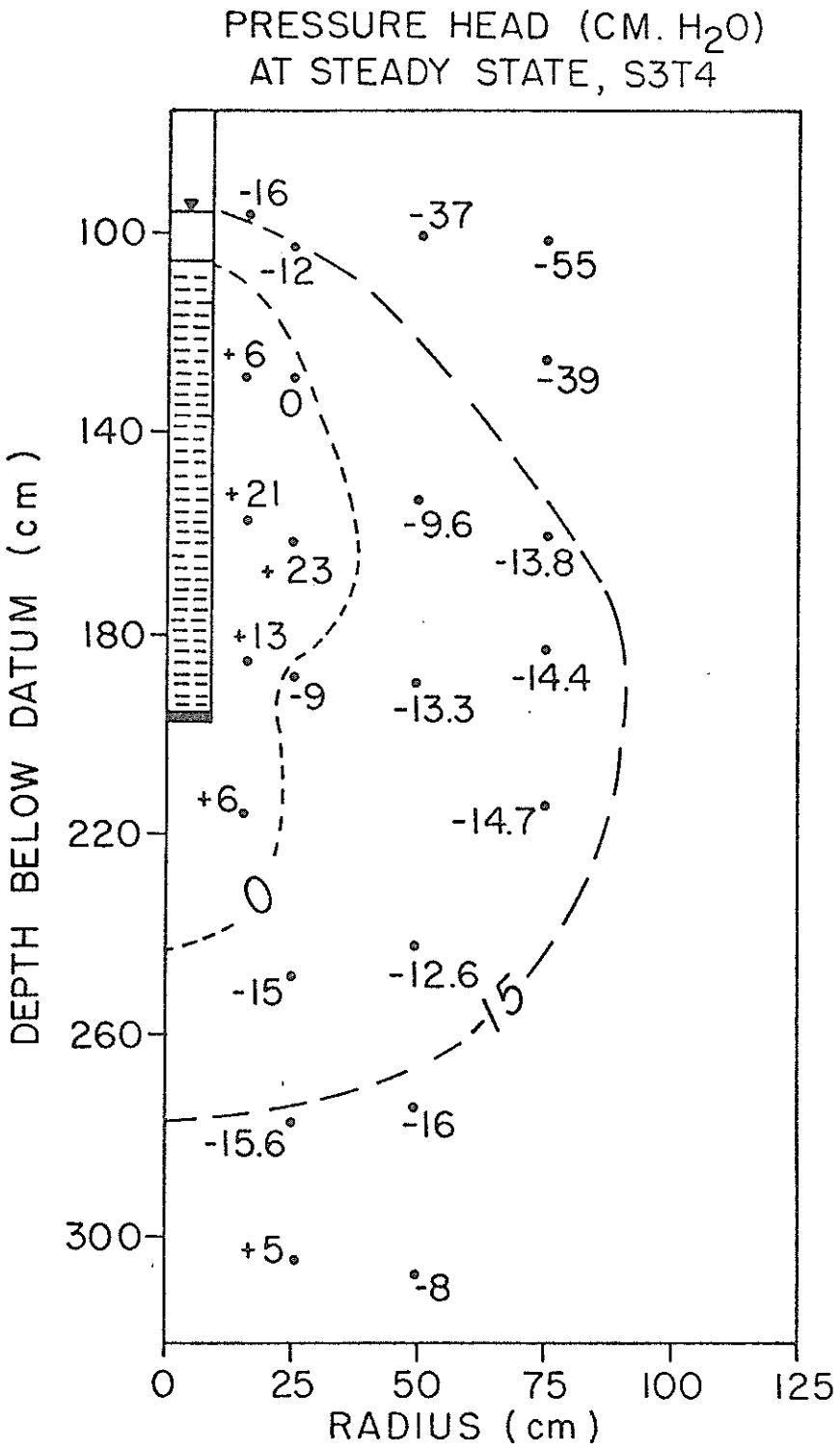

Figure 29. Pressure Head Distribution S3T4.

This observation implies that the volume of soil sampled may depend on the properties of the soil as well as on borehole conditions.

The preceding discussion of the zone of saturation does not account for any gas which may be trapped in the pore space during infiltration. If air were entrapped, the hydraulic conductivity at pressure heads greater than the water-entry valve would be less the K_s and the saturation percentage associated with this region would be less than 100 percent.

Table 8 summarizes the results of the borehole infiltration tests. In general, for all non-CO_2 tests, the values of K_s calculated from all borehole solutions fall between about 2×10^{-3} and 8×10^{-3} cm/sec. According to Bouwer and Jackson (1974), these values represent hydraulic conductivity primarily in the horizontal direction.

As a comparison to K_s values obtained from the borehole tests, several air-entry permeameter tests (Topp and Binns 1976) were conducted within the site (table 4). This permeameter only measures hydraulic conductivity in the vertical direction. These results are not adjusted for entrapped air as suggested by Bouwer (1966) and are comparable to K_s values obtained from the borehole method. Therefore, preliminary conclusions may be that the soil is not highly anisotropic, and that the borehole test may be influenced by entrapped air.

As indicated in table 3, most laboratory values of K_s at sites 1, 2, and 3 fall in the range of 1×10^{-2} to 3×10^{-2}cm/sec, significantly greater than all field-measured values. (No carbon dioxide was used in laboratory or field experiments at these sites.) Some of these cores were obtained from the same soil volume sampled by the air-entry permeameter. These laboratory tests were carefully monitored for sources of error due to sample handling and water chemistry; however, it was apparent that these factors were relatively

insignificant. This implied that if the laboratory results represent the "true" value of K_s, then either all the solutions for the borehole infiltration and air-entry permeameter tests are in error, or that the field methods obtain an average K_s over an area which is not represented by the average K_s from small ring samples, or that air entrapment is much more significant in the field than in the laboratory.

To check the latter possibility, the top of the borehole at S3T6 was capped with the packer assembly and approximately 5000 liters of carbon dioxide was injected into the borehole over a 16 hour period. It was presumed that the carbon dioxide would displace the soil air and then dissolve into the infiltrating water, thereby leaving the soil closer to complete saturation.

Figure 25 shows the infiltration rate versus time for test S3T6. Rates have been corrected for fluid viscosity at 20°C. For about the first 30 minutes during S3T6, the borehole was taking on water as fast as the pump could supply, and the borehole was only partially filled with water. After about 60 minutes, the water depth in the borehole stabilized at the designed depth, 97cm, and the flow rate then slowly diminished. The infiltration rate for the case where CO_2 was injected prior to testing was more than twice that of S3T4 under practically the same test conditions. The S3T6 values of K_s from equations 1, 6, 10, and 12 range from 8.9×10^{-3} to 1.5×10^{-2}cm/sec, and are considerably closer to the laboratory values (table 3) than borehole tests without CO_2 injection.

During the period prior to flow rate stabilization at S3T6, water content and pressure head data indicated that the soil reached a maximum wetness and then drained slightly. Such behavior is not predicted from numerical simulations or analytical solutions. This drainage pattern could be attributed to the build up of silt on the face of the borehole or to gas coming out of solution from the injected water. The drainage phenomenon was

observed in many other tests and will be described in more detail subsequently.

To check whether a piping channel had developed during the time interval between tests S3T4 and S3T6 to explain the increase in infiltration rate shown in figure 25, the soil was allowed to drain and S3T6 conditions were repeated without prior injection of CO_2. In this test, S3T7, the final infiltration rate was 9.4 liters per minute; and K_s fell between the values from tests S3T4 and S3T6. At the end of testing, the average water content measured in the neutron probe access tube closest to the borehole (50cm) was 24 percent, 31 percent, and 26 percent for tests S3T4, S3T6, and S3T7, respectively. The greatest water content is observed when CO_2 is flooded prior to the infiltration test, and the smallest water content occurred for S3T4. There is less air trapped at the end of S3T7 than at S3T4 probably because the S3T7 soil was initially wetter (slower wetting front advance) and many of the fine pore spaces which trapped air in S3T4 contained water at the end of S3T6.

A comparison of flow rate and water content data for S3T4, S3T6, and S3T7 clearly shows that air is entrapped during infiltration from the borehole. Flooding the soil with a highly water soluble gas, such as carbon dioxide, prior to the infiltration test seems to be an effective means of removing a significant portion of the entrapped air.

The cause of air entrapment in the field may be due in part to the large hydraulic gradients (on the order of 100 near the borehole at early time) imposed on the soil during the rapid filling of the borehole. In the laboratory where K_s values are generally greater, the 100 cm^3 rings were wetted slowly from below under gradients which were much less than those found in the field.

In spite of the marked increase in K_s from borehole methods with CO_2, the

laboratory ring permeameter results are considerably greater than all other methods by a factor of about two. It is believed that this is due to a boundary effect between the ring and soil. The soil disturbance along this boundary may cause an increase in the overall K_s, due to the relatively small sample size of the ring.

Long-Duration Experiments

Effect of Entrapped Air. Owing to the discrepancy in K_s between the short-duration field tests and laboratory permeameter results, borehole infiltration experiments were conducted to determine whether additional entrapped air could be removed from the soil by running the field tests for extended periods. In the center of the instantaneous profile plot (figure 5), a borehole infiltration test was run on October 15-16, 1982, for 1560 minutes without CO_2 injection (S5T3). In five subsequent experiments at this site CO_2 was injected (table 10). Test S5T8 began on December 16, 1982, and infiltration continued for 735 minutes; prior to this, 2710 liters of CO_2 was injected at a pressure of about 1.4 bars for 79 minutes. This CO_2 volume represents approximately 39 pore volumes, assuming 40 percent porosity, and a bulk soil sample volume equal to 0.4 H^3 where H (Bouwer and Jackson 1974), is 0.76m.

Figure 30 shows the infiltration rate corrected to 20°C for both S5T3 and S5T8. During the initial phase of infiltration both tests show a gradual decrease in infiltration rate which is attributed to a reduction in hydraulic gradient during wetting. This type of infiltration behavior will be referred to as phase 1. During phase 1 carbon dioxide injection causes a significant increase in flow rate.

It may not be necessary to inject as much CO_2 as we used in S5T8. Nearly the same infiltration rate near the end of phase 1 at S5T8 occurred at S5T5 when about 10 pore volumes of CO_2 were injected (table 10).

TABLE 10
INFLUENCE OF CO_2 PORE VOLUMES INJECTED ON PHASE 1 INFILTRATION RATE AT SITE 5

Test	CO_2 Injection Pressure [Bars(psi)]	CO_2 Injection Rate (l/Min)	Duration of Injection (Min)	CO_2 Vol (l)	Pore Volumes	Q at 300 Min (l/Min)
S5T3	0	0	0	0	0	3.72
S5T4	0.165(2.4)	3.5	20	70	1.0	4.99
S5T5	0.323(4.7)	14.5	51	739.5	10.5	6.49
S5T6	0.332(4.8)	14.5	80	1160	16.5	6.97
S5T7	0.936(13.6)	27.2	85	2313	32.9	6.86
S5T8	0.389(20.2)	34.3	79	2710	38.6	6.36

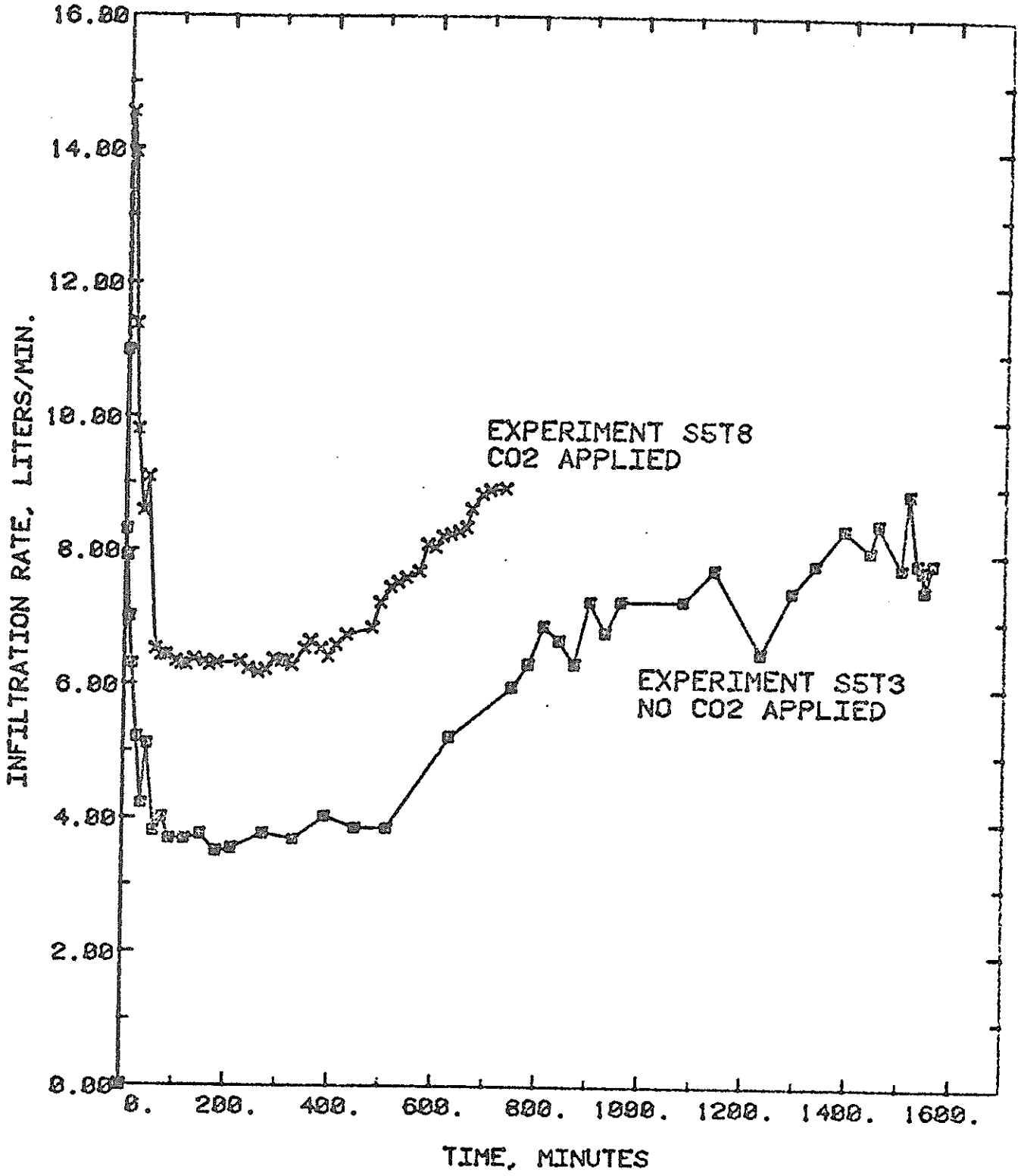

Figure 30. Long-Term Infiltration Rate Versus Time for S5T3 and S5T8.

Both tests S5T3 and S5T8 also exhibit a second phase when infiltration rate increases . This second phase may be attributed to expulsion of entrapped air, as observed in field experiments with water spreading basins (Todd 1980) and laboratory column experiments (Christiansen 1944).

In S5T3 (without CO_2) the infiltration rate begins to increase at approximately 500 minutes, and at S5T8 (with CO_2) it begins to increase at approximately 400 minutes (figure 30). For S5T3, from the end of phase one to the plateau in phase two, infiltration rate approximately doubles, and for S5T8 the infiltration rate increases by about a factor of 1.3. If this increase is due to expulsion of trapped air, then there seems to be less air trapped during infiltration tests preceded by CO_2 injection. Because freezing temperatures forced the premature termination of S5T8 the increase in infiltration rate could have been even greater between these phases. However, a significantly greater final Q for phase 2 is not expected because shelby tube experiments described previously showed that the K_s from CO_2 treated samples was about the same as for treated samples when sufficient time was provided for the latter to reach a plateau. The final phase 2 infiltration rate for S5T8 exceeds S5T3 by only 13 percent. Hydraulic conductivities calculated from equation 10 (table 8) are 0.0089 and 0.010cm/s for S5T3 and S5T8, respectively. The difference is not significant in practical terms. A very important practical application, however, is that when CO_2 is injected, the plateau infiltration rate during phase 2 is reached in nearly half the time and with about half the water volume compared with the traditional non-CO_2 procedure. Furthermore, by using the phase 2 peak infiltration rate in equation 10, calculated K_s is in reasonably good agreement with the shelby tube permeameter results (figures 13, 14, 15); K_s is also closer to the 100cc ring permeameter results than if one used the Q corresponding to the time when

V_{min} or V_{max} occurred.

At S5T3 and S5T8, a third phase of infiltration occurs after the rapid increase in infiltration rate which characterizes phase 2. During phase 3, infiltration rate may remain steady or gradually increase or decrease. This behavior will be described later in this section.

From the previous discussion of phase 1 and 2 infiltration and from the analytical solutions to determine K_s, one may infer that K_s approximately doubles when infiltration rate doubles, due to removal of entrapped air for example. However, from Darcy's law it is clear that K_s depends on the hydraulic gradient as well as on the flow rate. In fact, if there is air entrapped in a transient state then K_s is not constant, and one should expect to observe changes in hydraulic gradient concommitant with Q and K_s. During S5T3, S5T5, and S5T7, the average negative hydraulic gradient is shown in figure 31. The average gradient is determined by averaging the difference in the total head between the borehole and the tensiometers located at the 15 centimeters radius from borehole center divided by the distance between the borehole wall and the tensiometers. (The negative of this quantity is used so that infiltration rate, as calculated by Darcy's Law, is positive; thus Q is proportional to the negative of i as well as K_s.) From figures 30 and 31 it is apparent for S5T3 that the hydraulic gradient is smallest at the end of the test when flow rate is greatest. This can only be explained by an increase in hydraulic conductivity during infiltration. Figure 32 indicates that when the change in hydraulic gradient is taken into account, hydraulic conductivity increases by a factor of about 3.4 between the end of phase 1 and the end of the experiment; this is in contrast to only about a two-fold increase in infiltration rate over the same period. The brief increase in hydraulic gradient within the first few hundred minutes of the experiments of S5T3 could be due to an increase in head in the well, inasmuch as K_s appears to be nearly

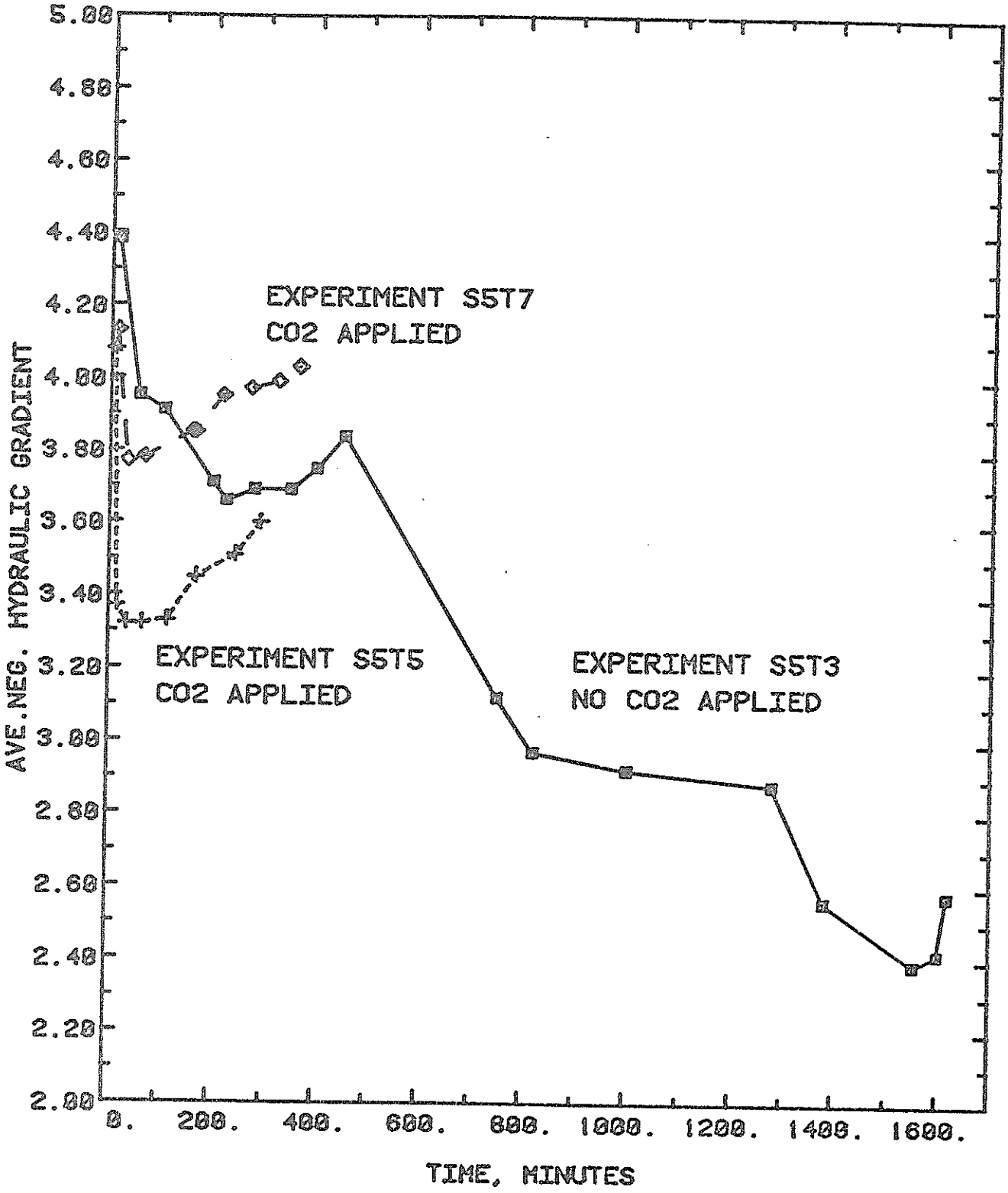

Figure 31. Average Hydraulic Gradient Versus Time for S5T3, S5T5, and S5T7.

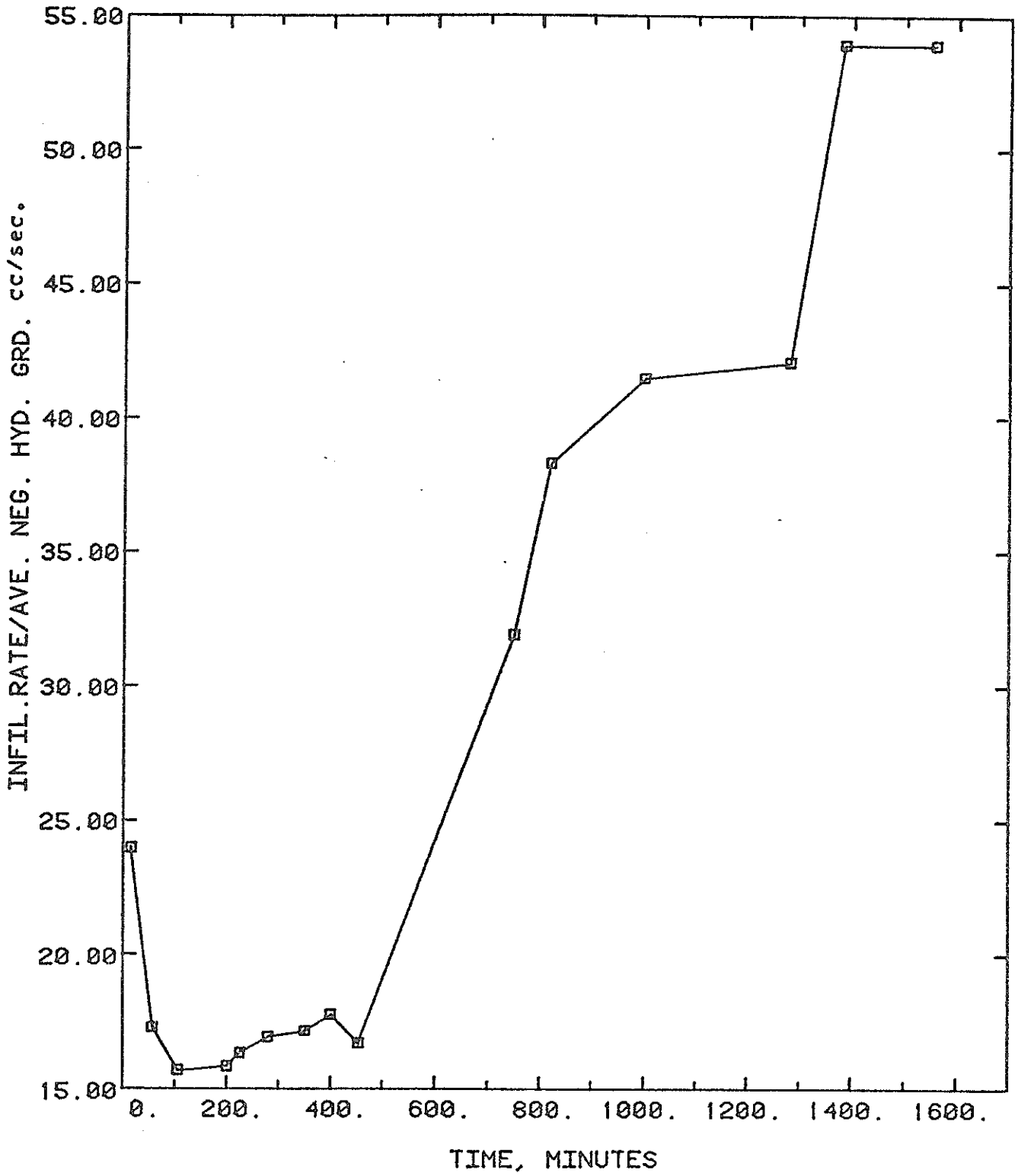

Figure 32. Change in the Ratio Flow Rate and Hydraulic Gradient for S5T3.

constant during this time (figure 32), however no continuous measurements in head were obtained. Similar behavior occurred for S5T5 and S5T7.

If the volume of trapped air is presumed to decrease during phase 2 of an infiltration test and K increases as a result, then the volumetric water content should increase during a test. Furthermore, experiments with CO_2 injection also should be expected to exhibit a larger water content in the soil surrounding the borehole. In fact, an increase in water content after 400 minutes and higher water content with a CO_2 flood is demonstrated for S5T3 in figures 33 and 34 and for S5T8 in figures 35 and 36. (Porosity and maximum water content are about 40 percent.) A comparison of the late time results for these tests (figures 34 and 36) shows that the CO_2 injection has the greatest influence on water content in the vicinity of the borehole. This is to be expected inasmuch as most air entrapment will occur in the near-saturated region (Cary 1967).

One of the most interesting observations during the borehole infiltration tests at S5T3 and S5T8 is the coincidence of increasing infiltration rate at the beginning of phase 2 behavior and decreasing temperature of the air and infiltrating water after about 300 minutes, as dusk approached (figures 30 and 37). This relationship was previously recognized in the field by Robinson and Rohwer (1959).

Water temperature is known to affect the concentration of dissolved gas. At $10^{o}C$ the saturated dissolved oxygen concentration in water should be about 11.3 mg/l; the dissolved oxygen concentration determined by a Bausch and Lomb spectrokit was only 4 mg/l, which indicates that the infiltrating water is capable of dissolving oxygen. However, Peck (1968) indicates that dissolution of gas plays a minor role in reducing the size of air bubbles, and diffusion will eventually cause many bubbles to collapse. In S5T3 when water

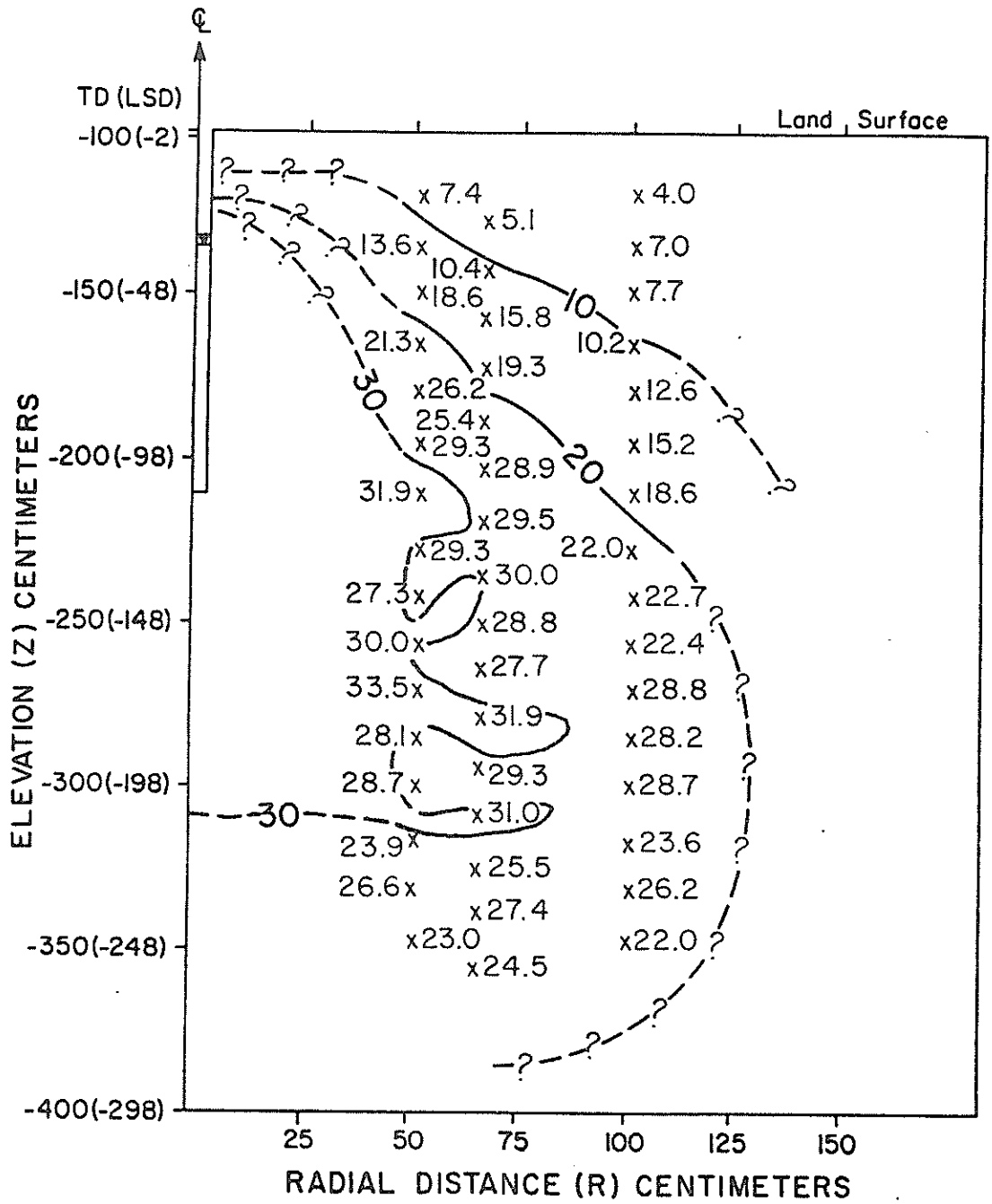

Figure 33. Percent Water Content Distribution after 400 Minutes at S5T3. (TD = Elevation with respect to transducer datum; LDS = elevation with respect to land surface.)

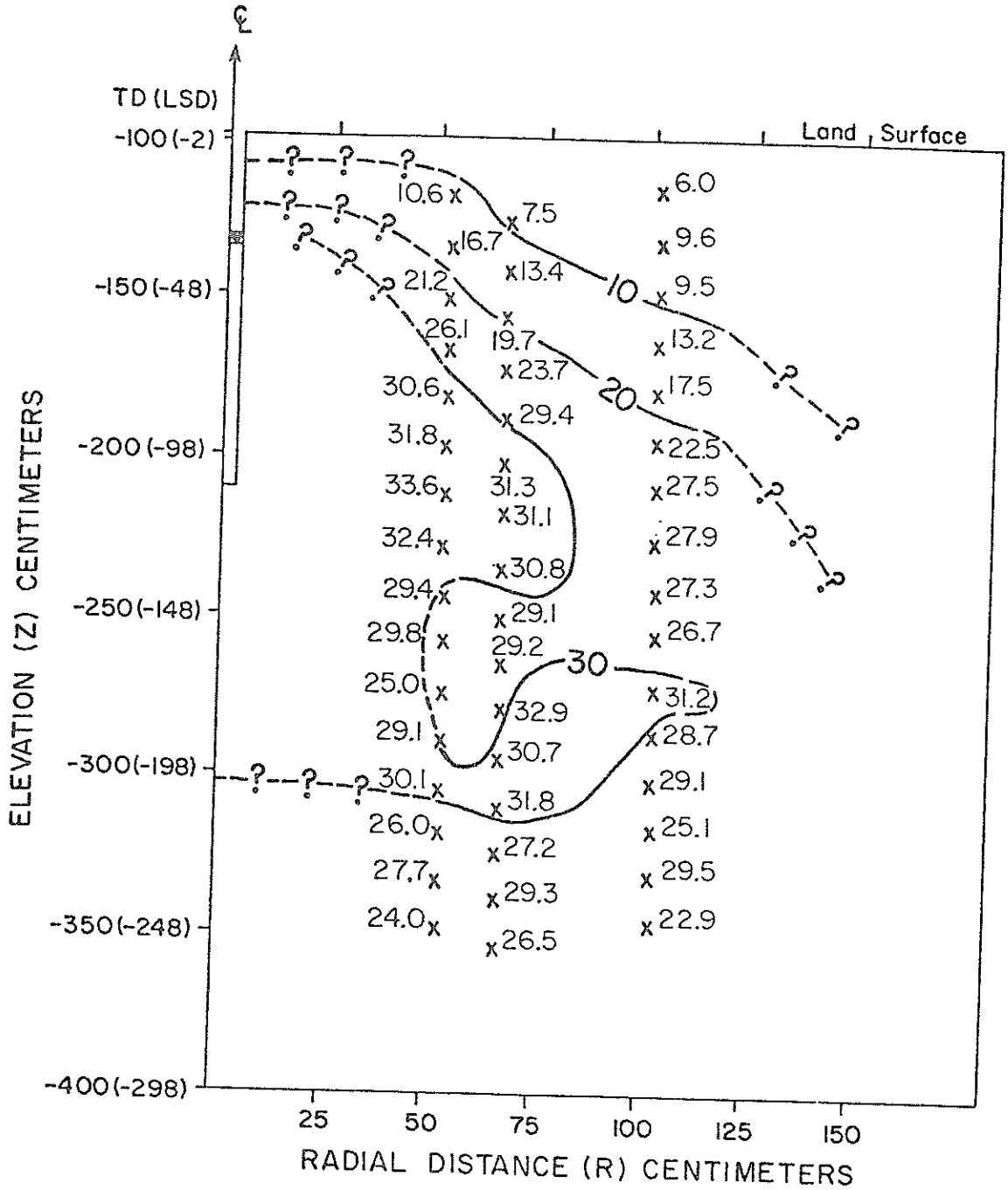

Figure 34. Percent Water Content Distribution after 1400 Minutes at S5T3. (TD = Elevation with respect to transducer datum; LDS = elevation with respect to land surface.)

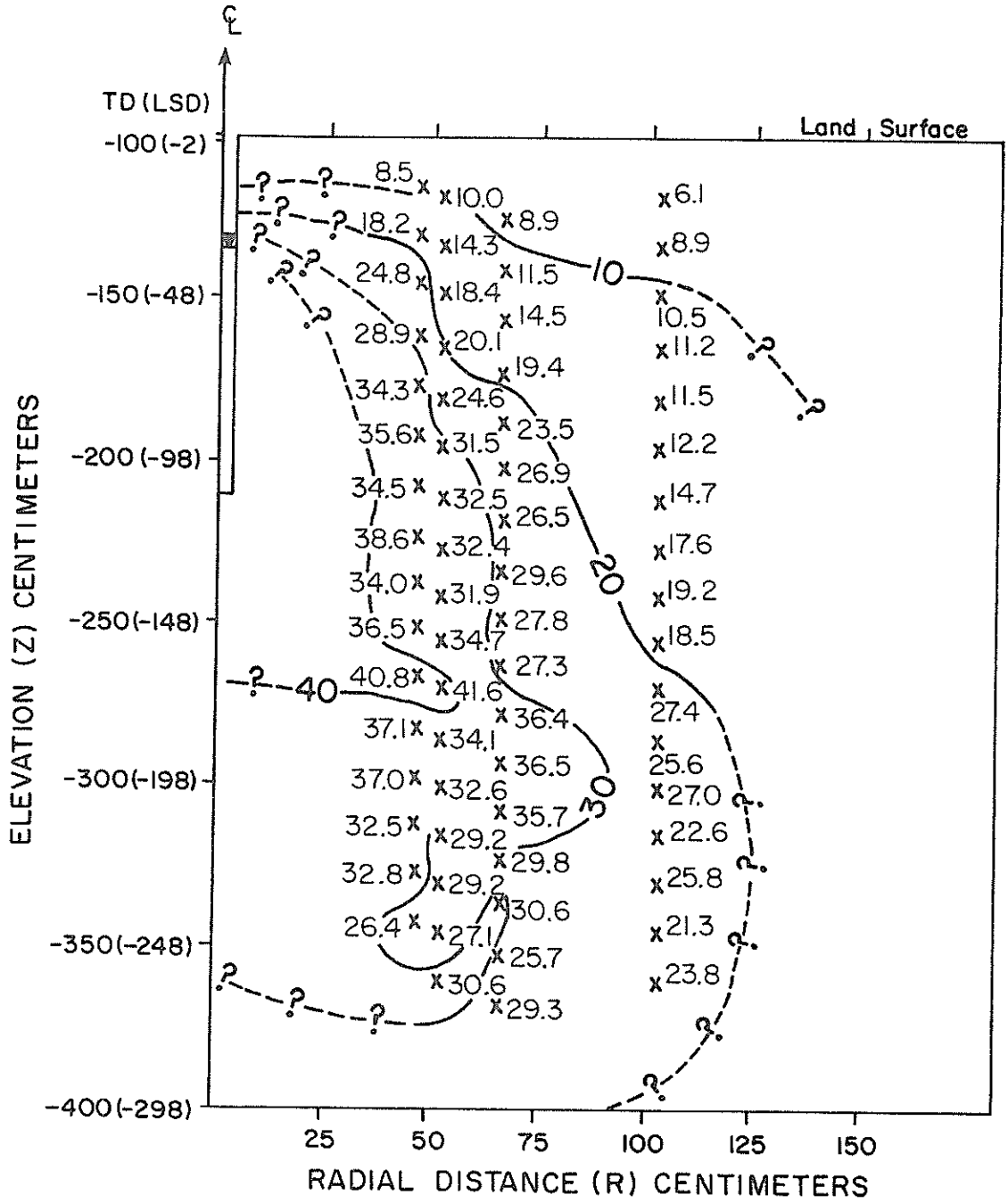

Figure 35. Percent Water Content Distribution after 400 Minutes at S5T8. (TD = Elevation with respect to transducer datum; LSD = elevation with respect to land surface.)

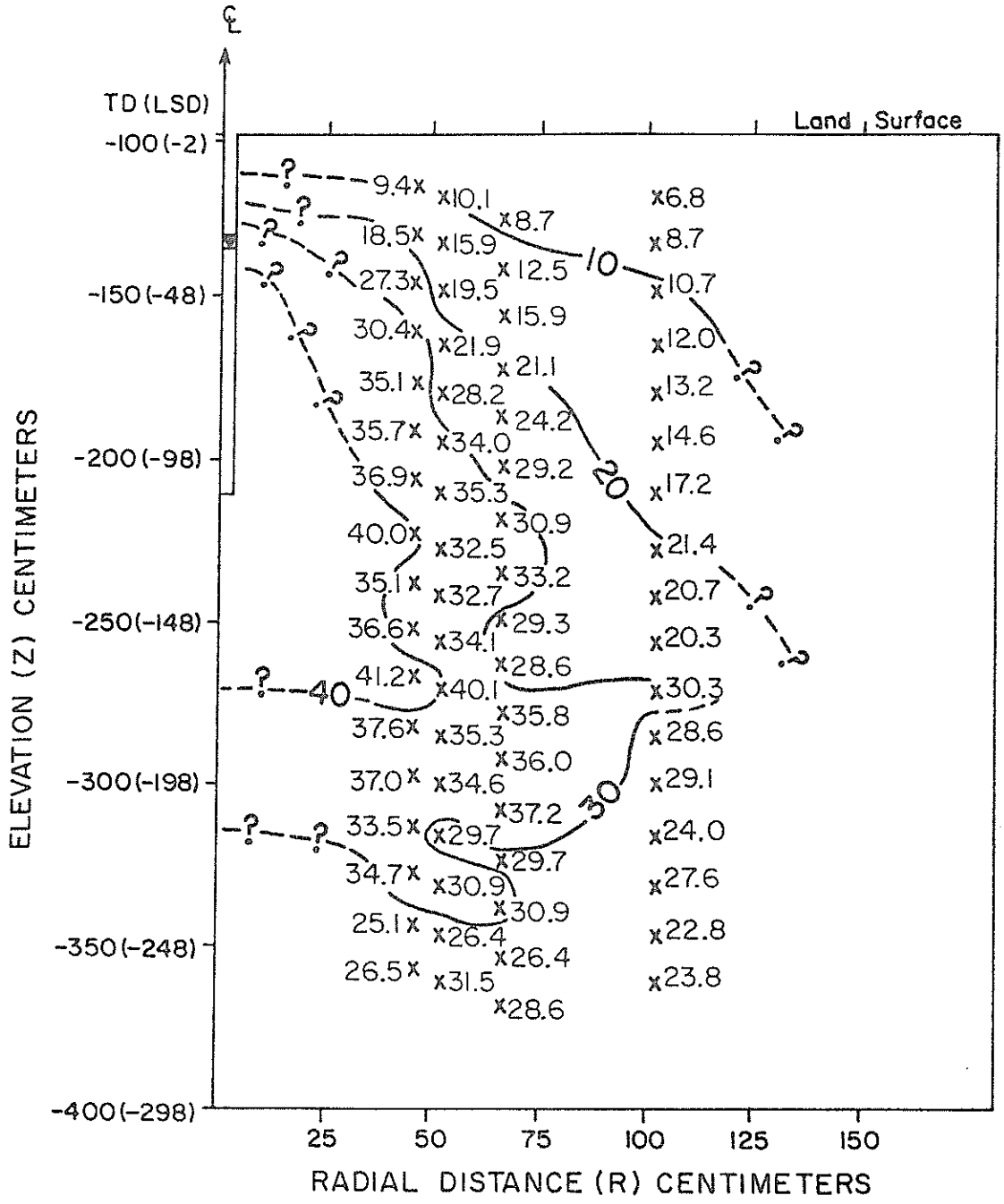

Figure 36. Percent Water Content Distribution after 700 Minutes at S5T8. (TD = Elevation with respect to transducer datum; LSD = elevation with respect to land surface.)

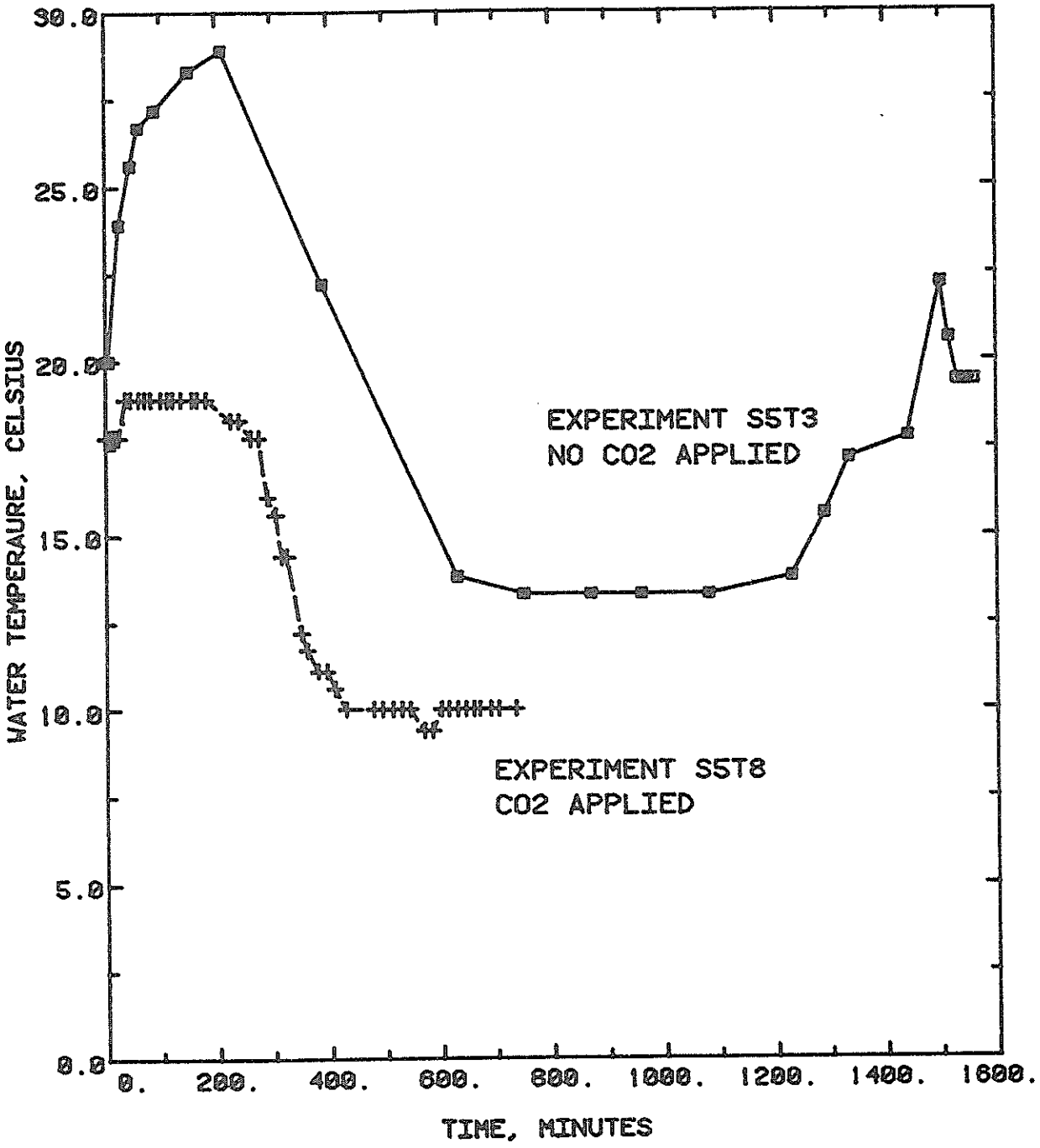

Figure 37. Temperature of Injected Water at S5T3 and S5T8.

temperatures increased again after about 1300 minutes (figure 37), no significant change in infiltration rate occurred. This may mean that entrapped air was already removed from the pore space. It also should be pointed out that if CO_2 is completely effective in removing trapped air during the initial wetting, then the phase two infiltration for S5T8 should not occur.

Subsequent experiments at site 6 were designed to investigate in greater detail in influence of the pressure head in the borehole and water temperature on the occurrence of entrapped air during borehole infiltration tests. Table 11 is a summary of the carbon dioxide treatments at site 6. S6T2 was terminated because of screen clogging probably caused by a wind and dust storm. During S6T3 the rapid release of carbon dioxide froze the regulator, causing uncertainty in the volume of CO_2 injected; however, it is believed that the volume of CO_2 injected was less than S6T1. The same problem occurred to a lesser extent during S6T4. On the basis of previous experiments at site 5 (table 10), the volume of CO_2 injected at S6T1 and S6T3 was insufficient to eliminate entrapped air and achieve maximum infiltration rate. From field experience, the general effectiveness of a CO_2 flood can be evaluated on the basis of the rate of borehole filling. If the flood is poor or no CO_2 is used, the water level in the borehole rises roughly one meter within one to ten minutes when the pumping rate is on the order of 15 liters per minute. On the other hand, if the flood is effective, the borehole may not fill for a few tens of minutes to one or two hours, depending on the casing diameter. For example, the water level at S6T1 rose to 155cm in 120 minutes with an average pumping rate of more than 20 lpm (figures 38 and 39) whereas at S6T3 the water level rose to 122cm in 10 minutes with a pumping rate of about 18 lpm (figures 40 and 41). Therefore, it appears that the CO_2 flood at S6T3 was much less adequate than at S6T1.

TABLE 11
CARBON DIOXIDE INJECTION AT SITE 6

Test	Depth to Base of Hole (cm)	H (cm)	A (cm)	L[1] (cm)	CO_2 Volume (l)	Pore Volume[2] (l)	CO_2 Pore Volumes[3]
S6T1	185	155	122	122	2645	595.8	5.3
S6T3	185	122	121	122	-	290.5	-
S6T4	185	61	58	122	1620	36.3	22.0
S6T5	122	61	57	122	1620	36.3	22.1
S6T6	122	85	85	122	0	0	0

1) Screen length
2) 40% x $0.4H^3$, H(meters)
3) $\left[(\text{volume of } CO_2 - \text{volume of borehole}) \div \text{pore volume}\right] \times \left[H \div L^1\right]$

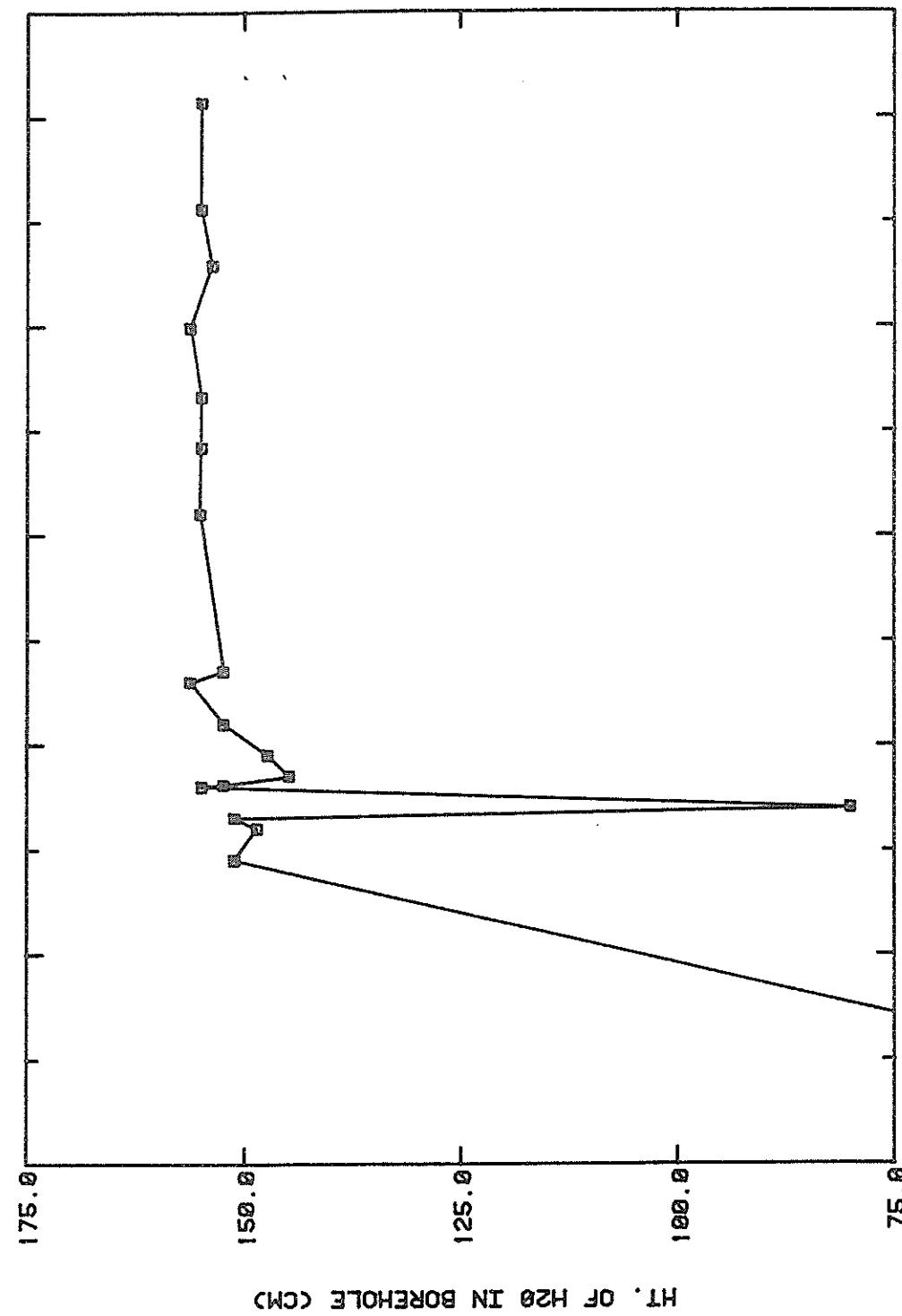

Figure 38. Water Depth in Borehole for S6T1.

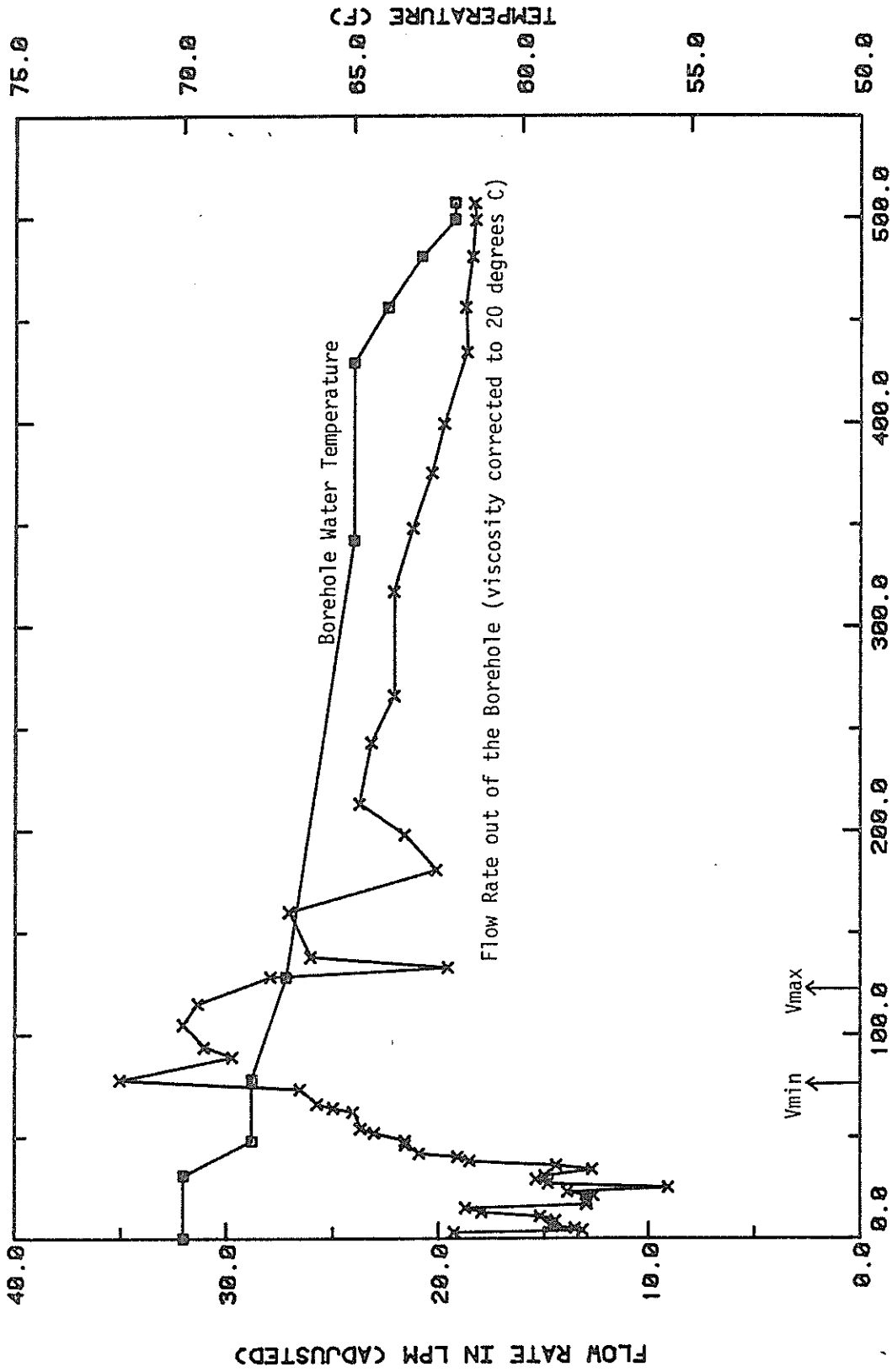

Figure 39. Infiltration Rate and Borehole Water Temperature for S6T1.

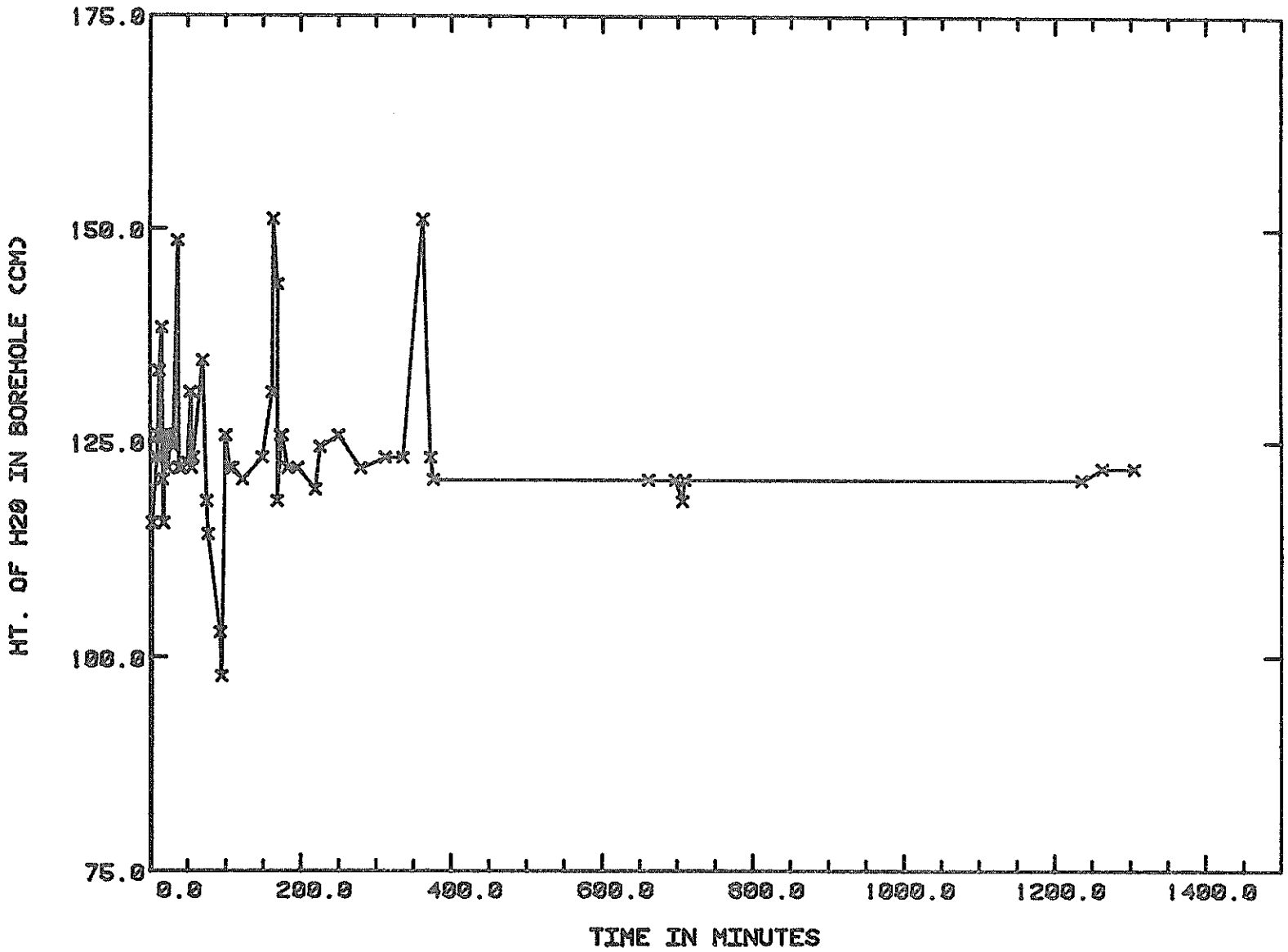

Figure 40. Water Depth in Borehole for S6T3.

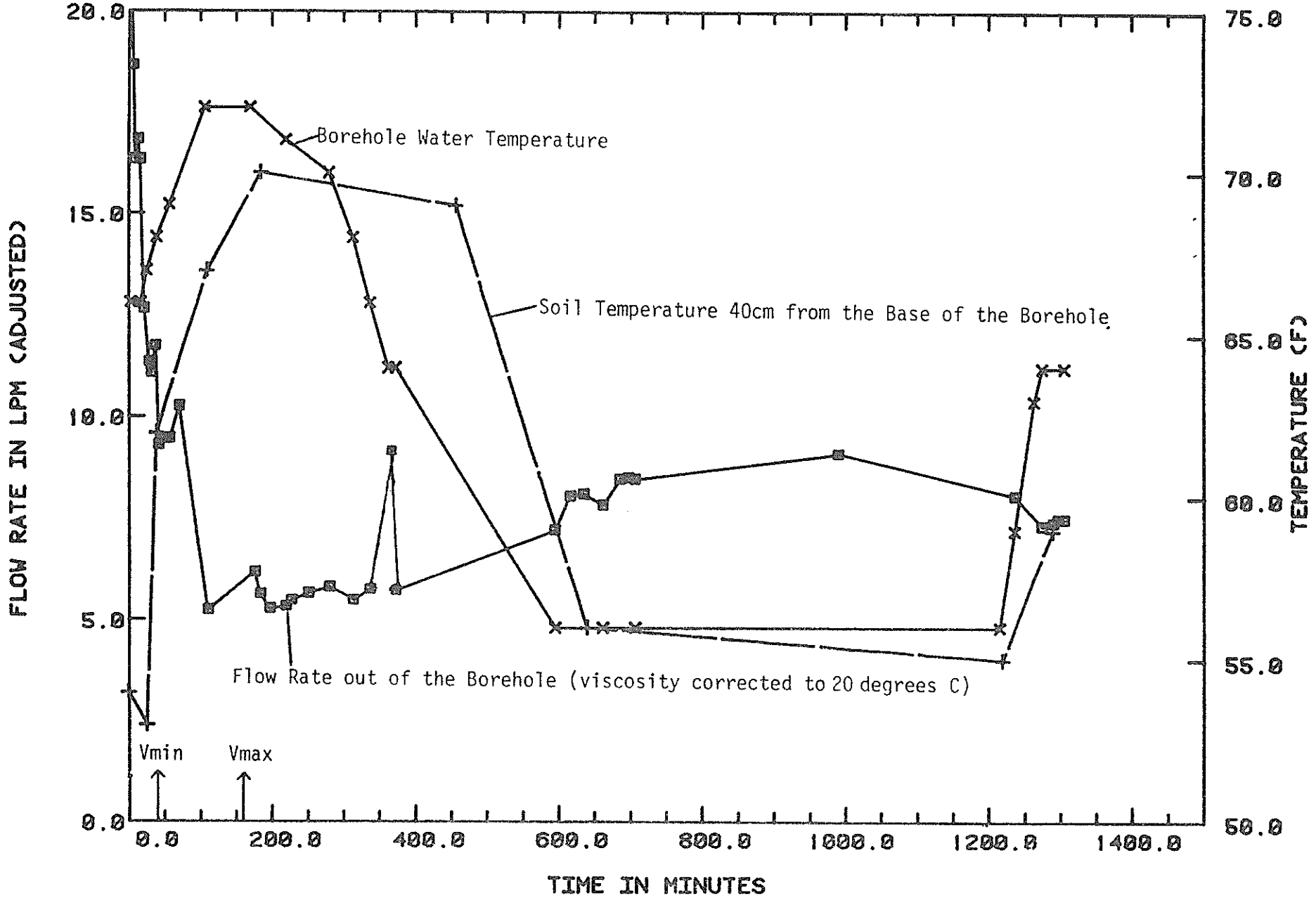

Figure 41. Infiltration Rate and Borehole Water Temperature for S6T3.

Because of the variability of the effectiveness of CO_2 flooding at site 6, soil stratification, and the few number of tests, no definitive results were obtained, beyond the shelby tube laboratory experiments, regarding the role of height of water in the borehole in reducing trapped air.

Transient Phenomena. The site 6 experiments appear to have demonstrated a hydrodynamic phenomenon which has not been described previously by other researchers, at least for three-dimensional infiltration. That is, the soil outside the borehole does not wet monotonically (for example, figures 42 and 43). During the first phase of infiltration and after the wetting front has passed, the soil reaches a maximum wetness and then unpredictably, drains. This response is detected by tensiometers and the neutron probe. Looking back through our experiments this same general behavior occurred in nearly all cases. Although this type of response in one-dimensional problems is attributed to air pressure ahead of the wetting front, a soil air pressure manometer at sites 2 and 6 did not detect any significant pressure changes during the tests. Utilizing data from S6T3 which had a rather ineffective CO_2 flood, the typical pressure head and moisture response with time is shown in figure 44. Both sets of data were taken at a depth of 183cm and 30cm from the borehole. It is apparent that changes in moisture content are coupled to pressure head.

Over the duration of the experiment at S6T3, and other experiments of long duration, the moisture content-pressure head response over time consists of three stages. These stages of soil-water response are distinguished from the three phases of infiltration described earlier. During the stage A at S6T3 there is a rapid wetting of the soil around the borehole for the first 10 minutes; the soil then stays very wet, or at a higher pressure head, until about 75 minutes into the test (figure 44). Stage B at S6T3 is characterized

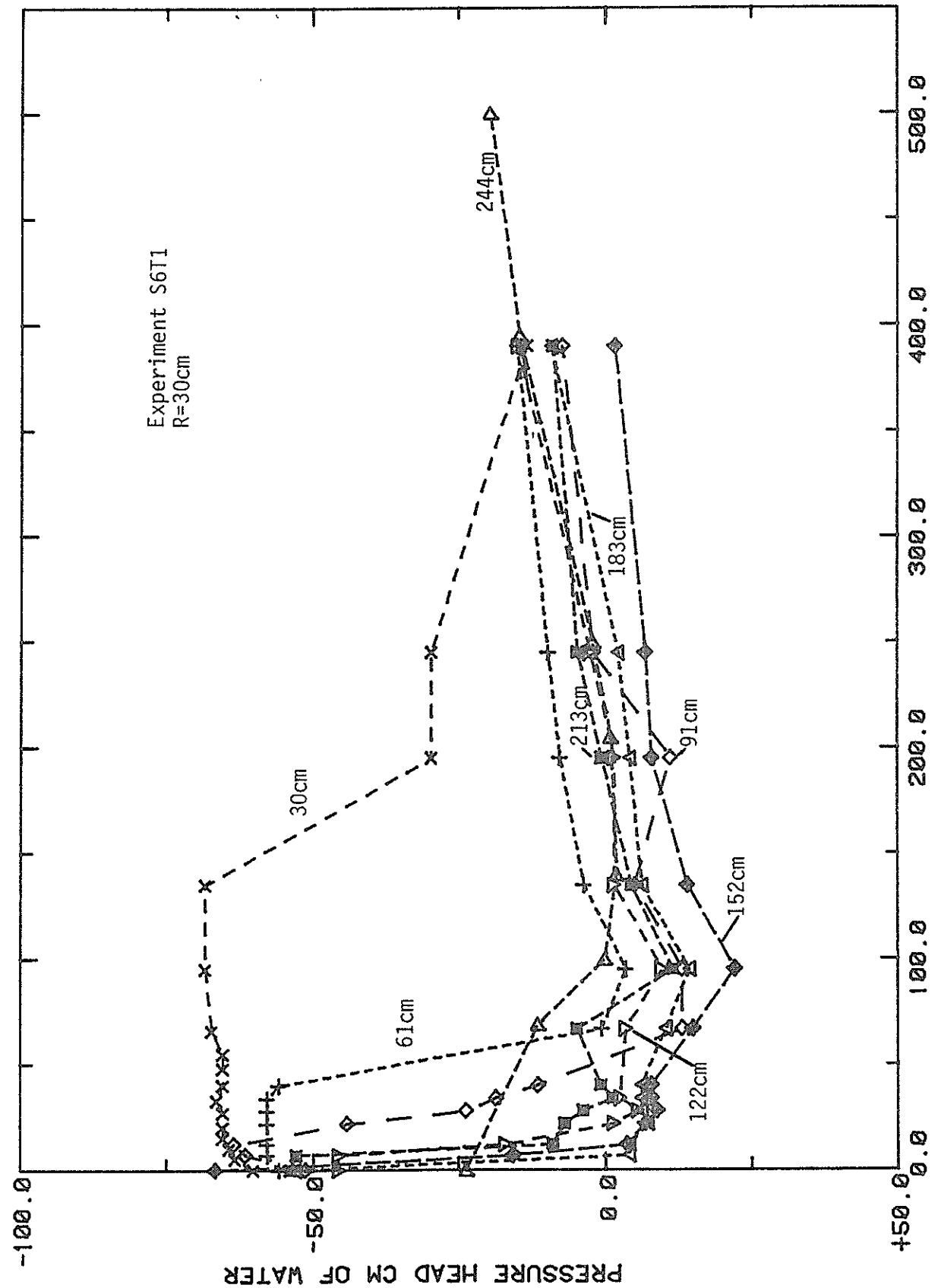

Figure 42. Pressure Head Versus Time at 30cm Radius from the Borehole at S6T1.

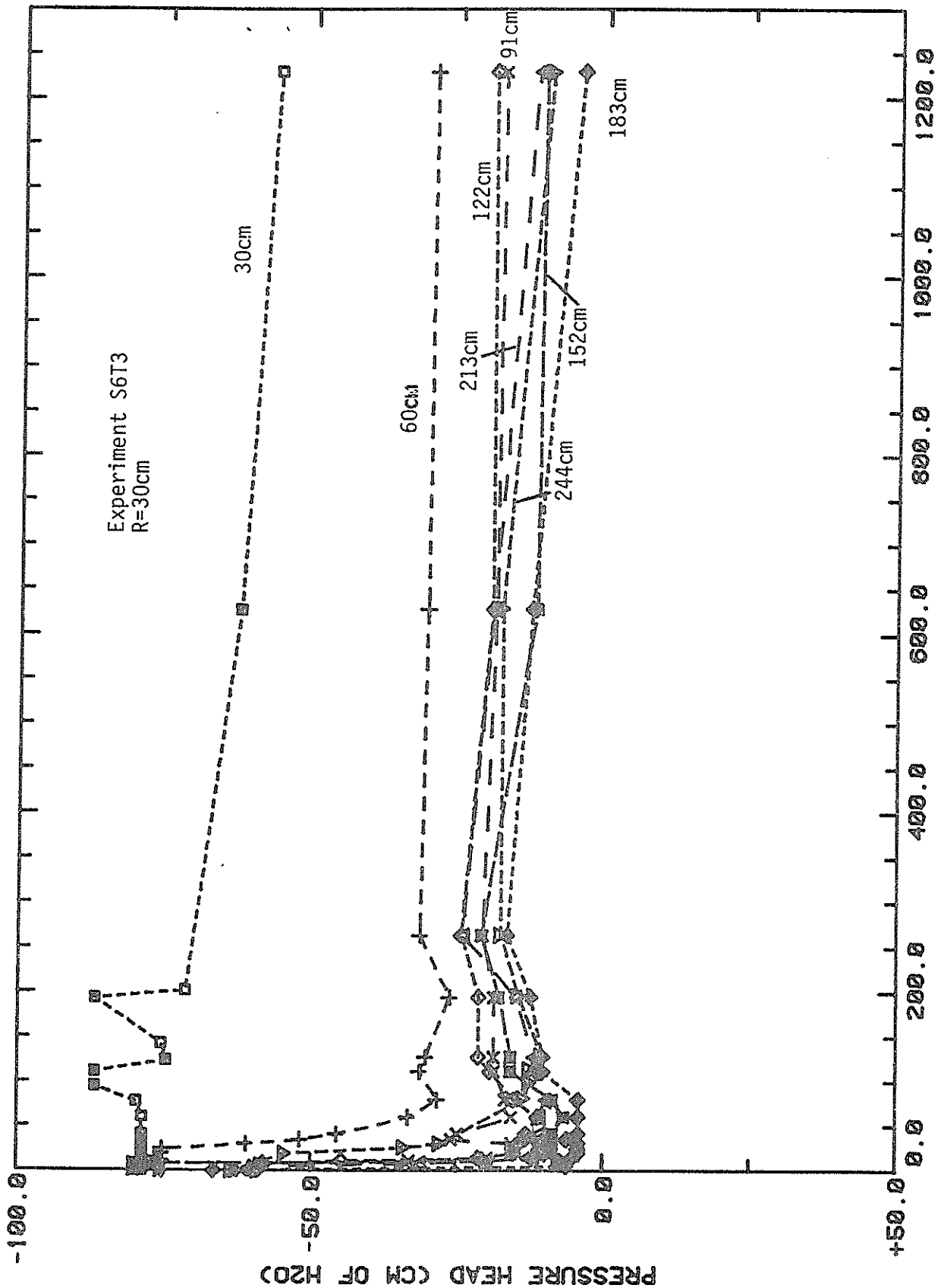

Figure 43. Pressure Head Versus Time at 30cm Radius from the Borehole at S6T3.

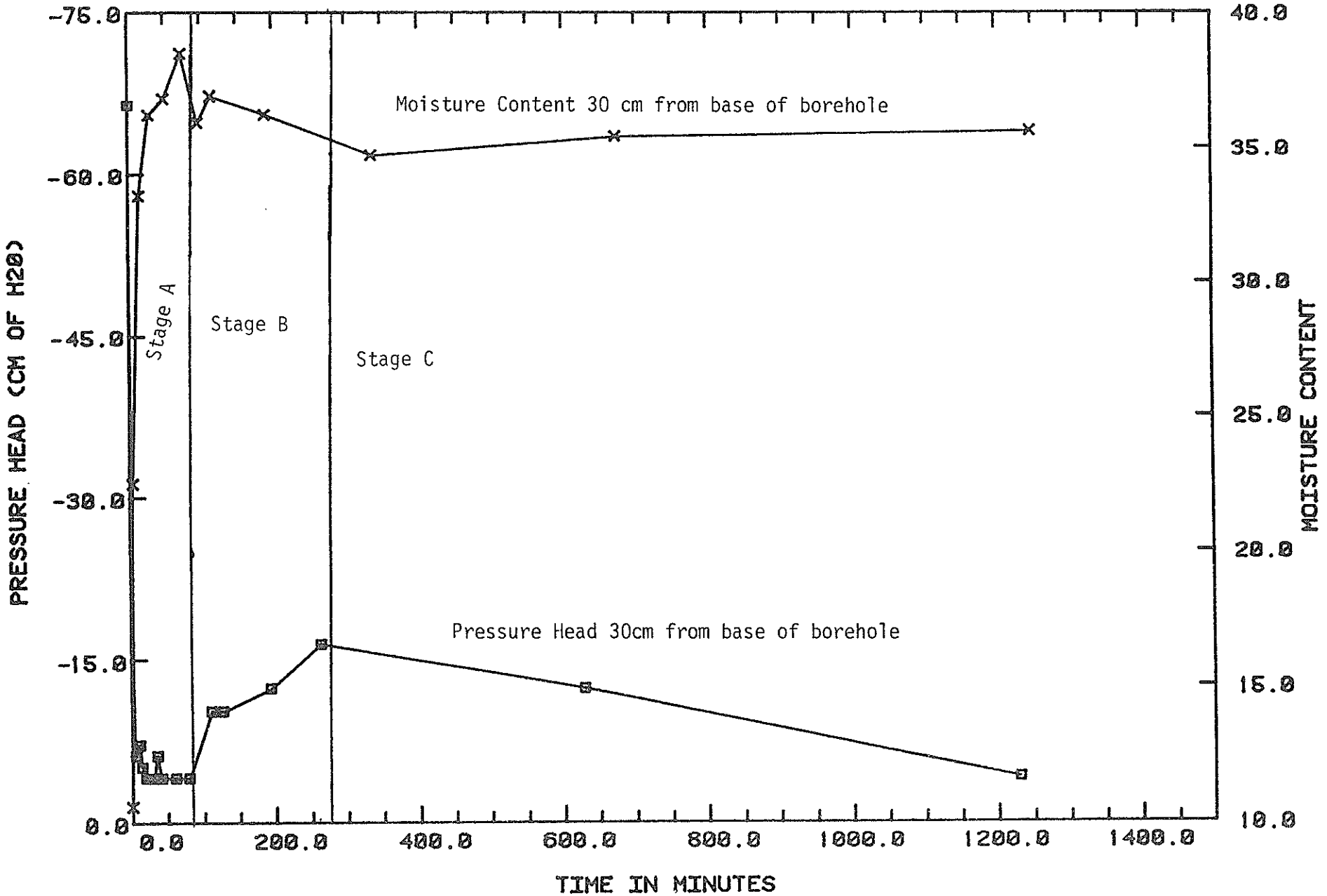

Figure 44. Comparison of Pressure Head and Moisture Content Versus Time at S6T3.

by a gradual drying of the soil around the borehole from 75 minutes until about 275 minutes after the start of the test. The stage C consists of a slow wetting of the soil until the end of the test. During this third stage the pressure head can change appreciably as it does in figure 44; however, this change is not always apparent as indicated by some of the other pressure head data (e.g., figures 42 and 43). Figures 45 through 47 show the pressure head distribution at S6T3 after 20, 265 and 1230 minutes, and total hydraulic head at these time is shown in figures 48 through 50. The 20 minute maps (figures 45 and 48) are representative of the end of stage A when the soil in proximity to the borehole is at a maximum wetness; the 265 minute maps (figures 46 and 49) are representative of the end of stage B when the rate of drying has diminished appreciably; and the 1290 minute maps (figures 47 and 50) show the flow field during stage C at the end of the experiment.

Major differences can be recognized when comparing the 20 and 260 minute maps. During stage A the saturated zone is larger and more symmetric than during stage B. The wetted zone during stage A is relatively small, but most of this zone is nearly saturated. The wetted zone at the end of stage B is relatively large, but most of the wetted zone is unsaturated. In comparison with stage A, the zone of maximum saturation at the end of stage B is closer to the borehole and elongated downward. The maximum decrease in pressure head from stage A to B occurs at the base of the borehole, and contours of equal magnitude of pressure head decrease during stage B plot concentrically around the borehole.

The stage C saturated zone has a similar shape to stage B; however, the saturated zone of stage C is slightly larger than stage B. The zone of increased wetness above the 167cm silty zone has also migrated laterally much further from the borehole during stage C.

Streamlines have been drawn in figures 48, 49 and 50 to illustrate the

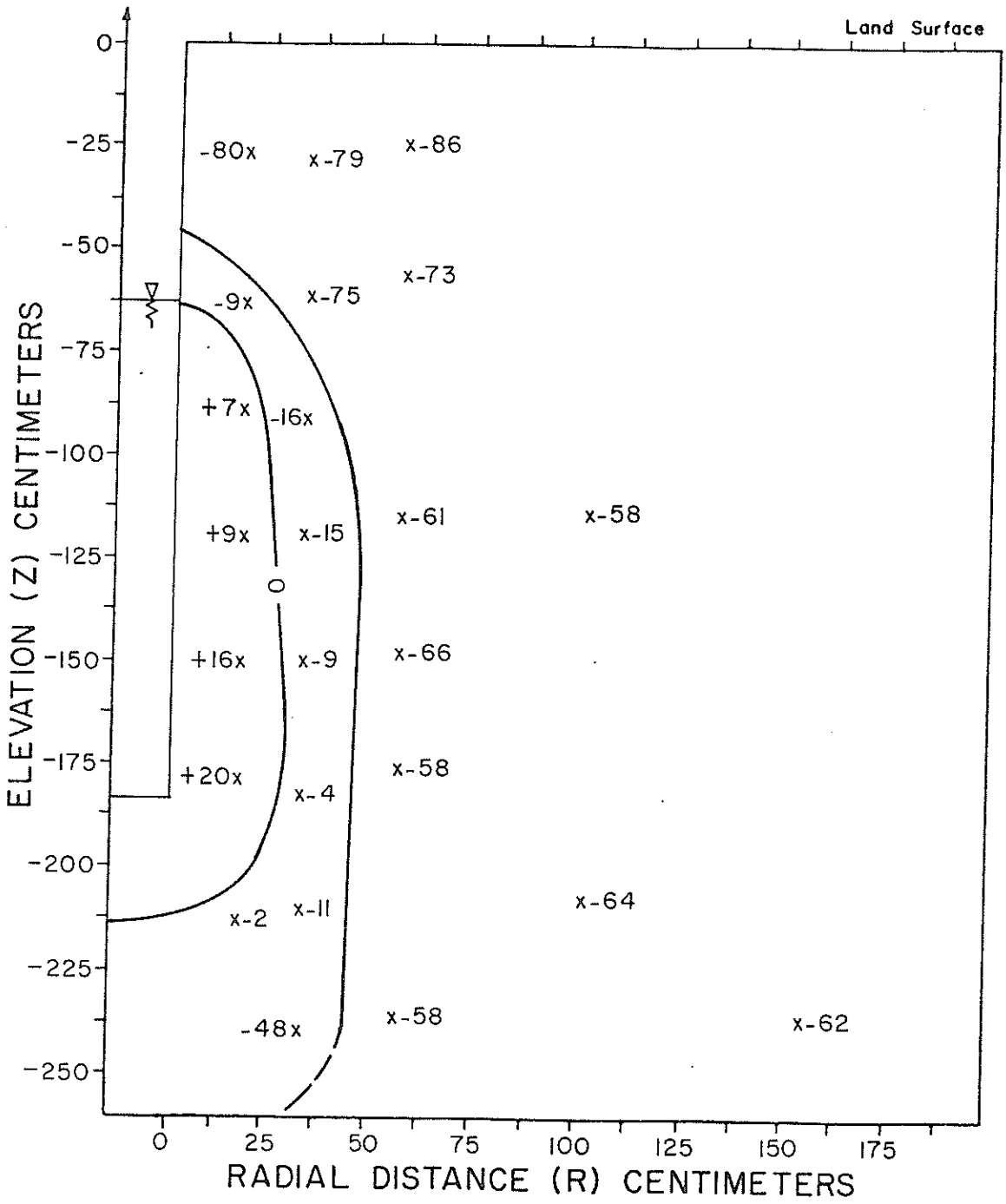

Figure 45. Pressure Head (cm) Profile after 20 Minutes at S6T3.

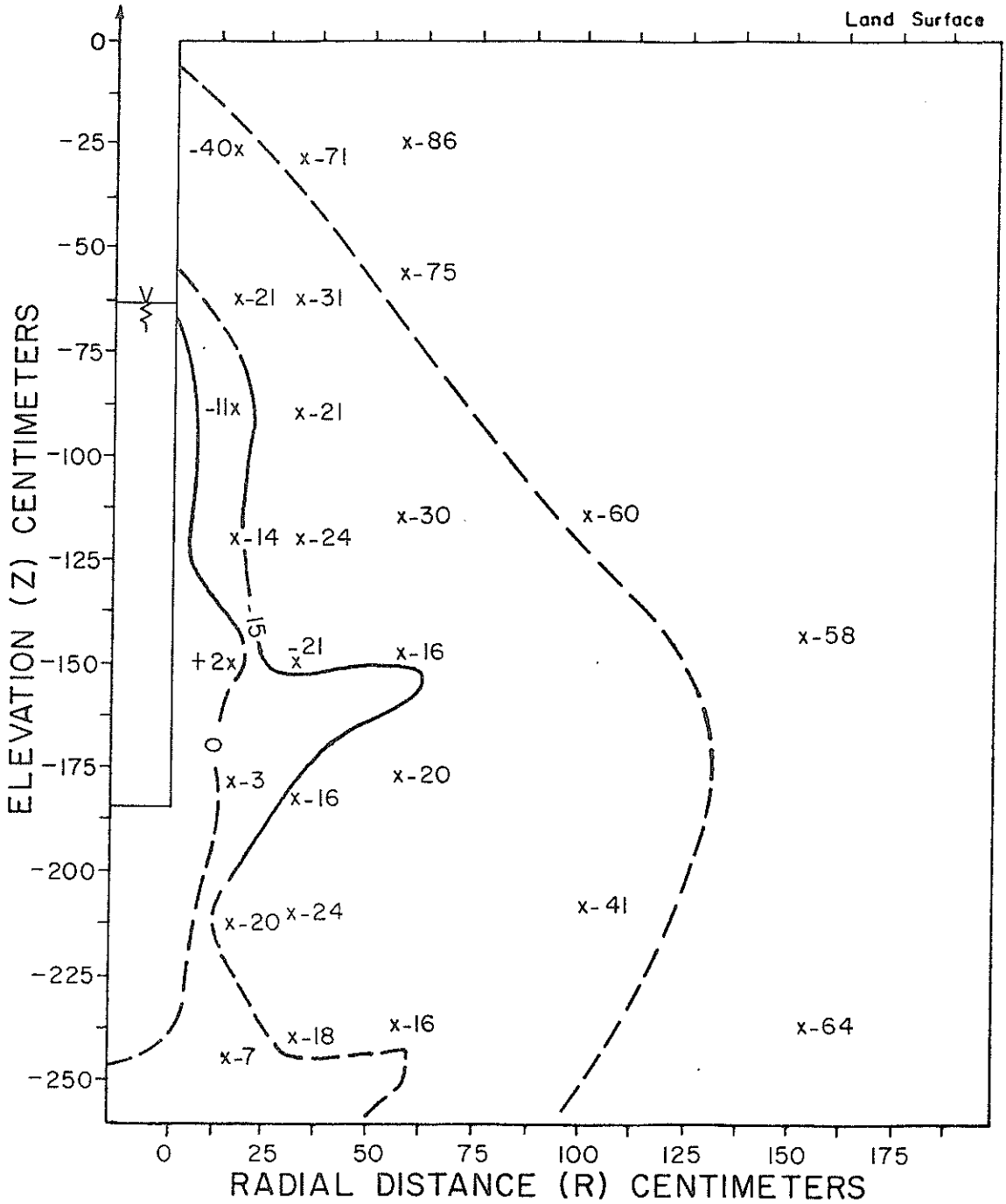

Figure 46. Pressure Head (cm) Profile after 260 Minutes at S6T3.

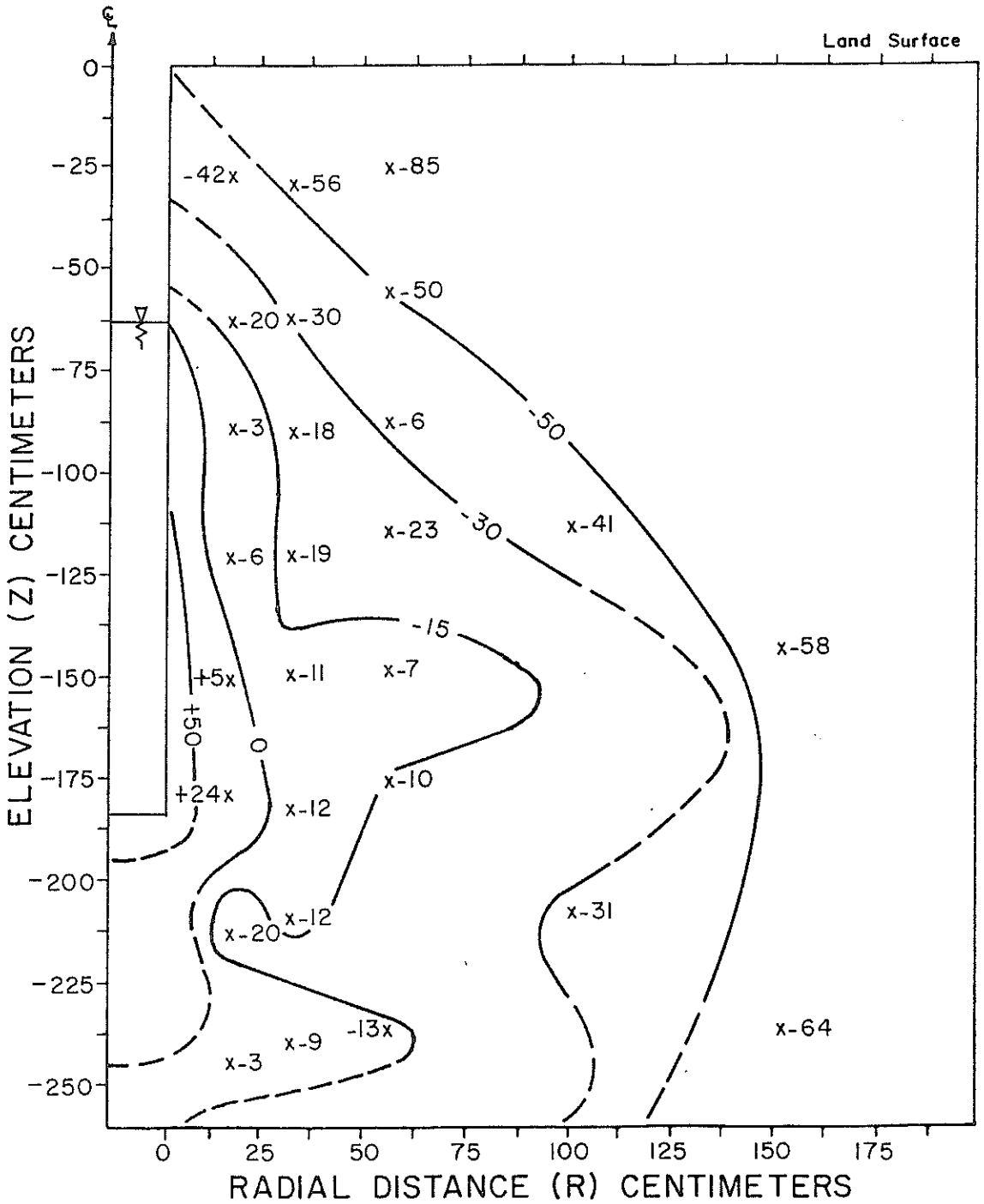

Figure 47. Pressure Head (cm) Profile after 1230 Minutes at S6T3.

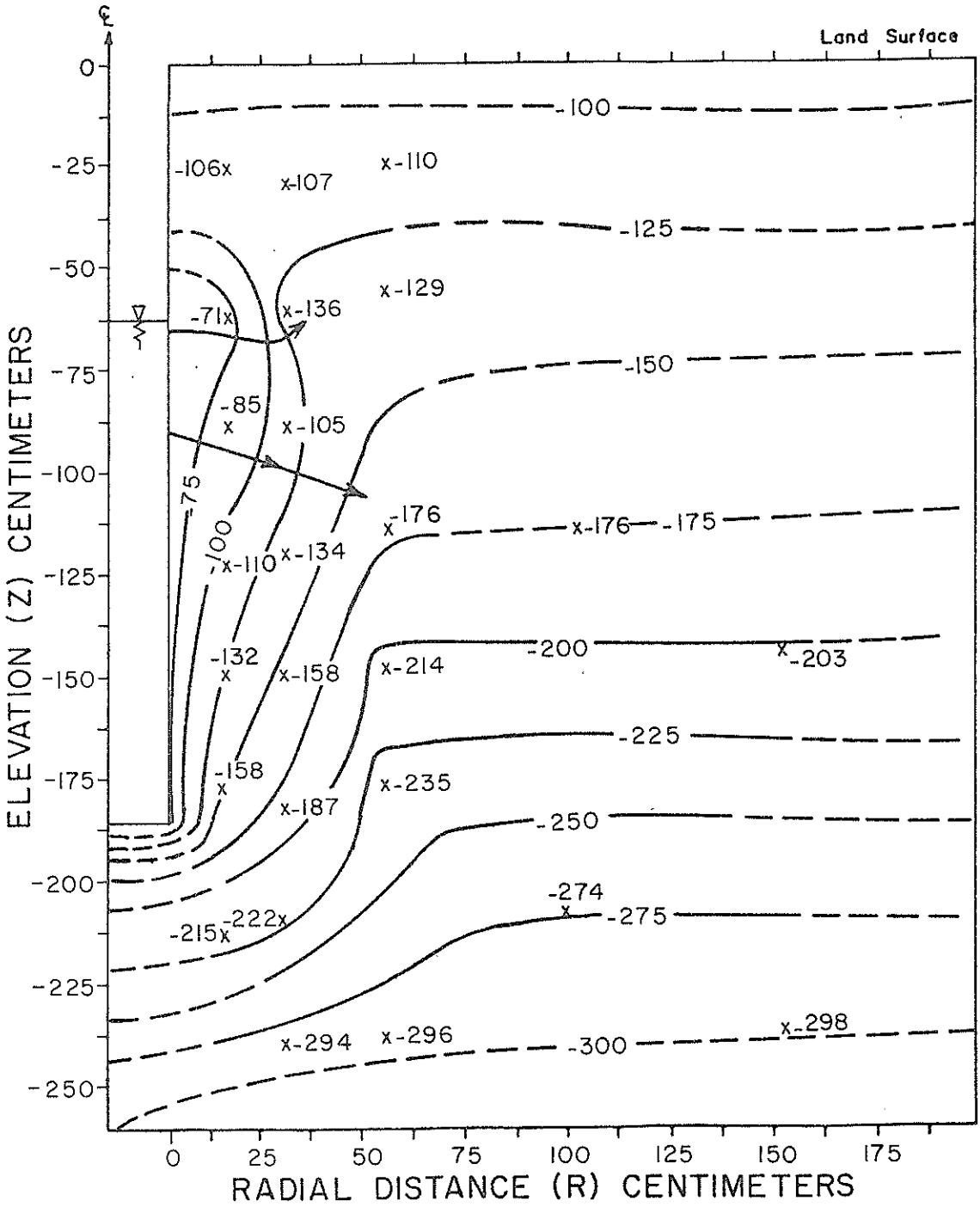

Figure 48. Total Hydraulic Head (cm) after 20 Minutes at S6T3.

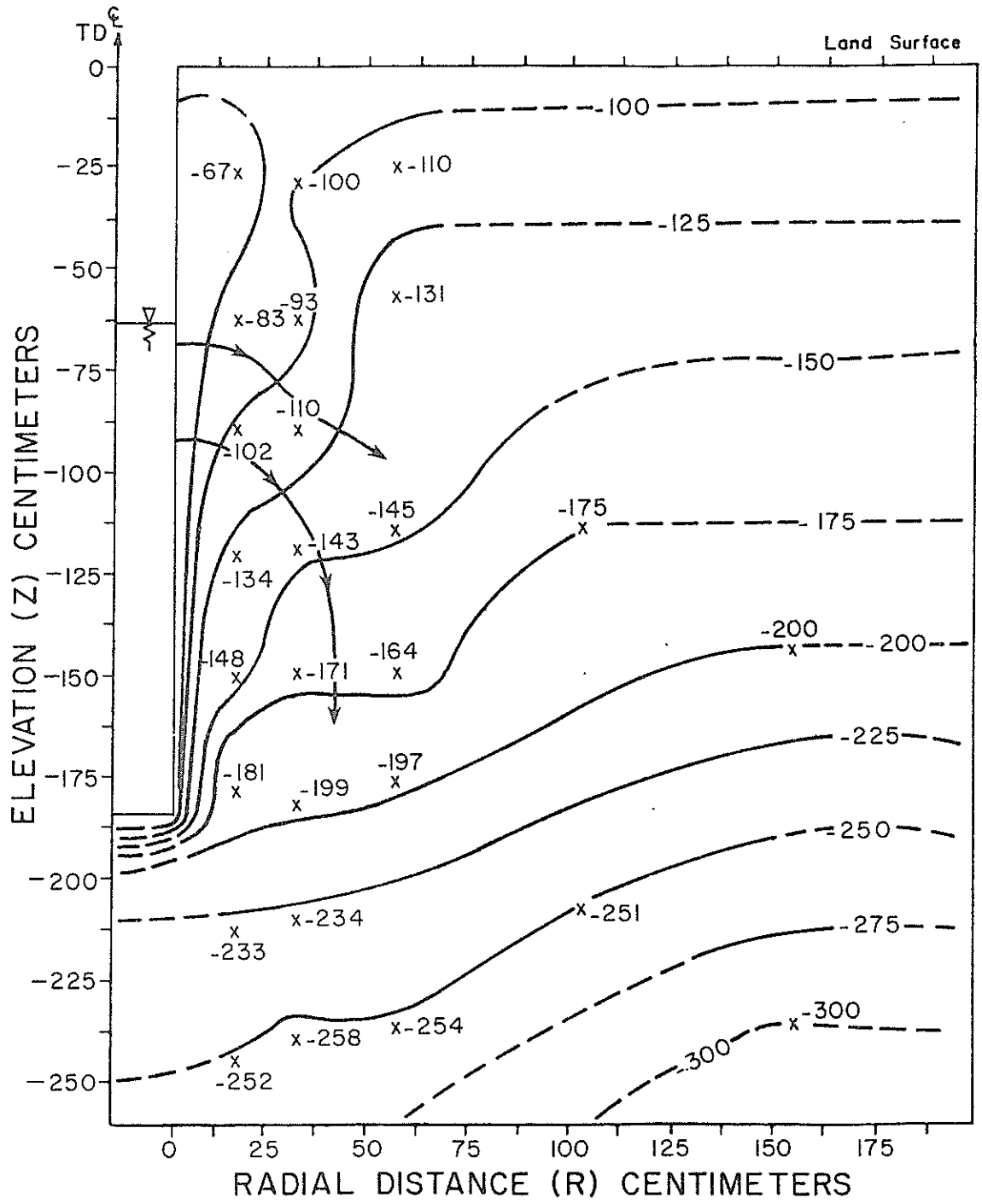

Figure 49. Total Hydraulic Head (cm) after 260 Minutes at S6T3.

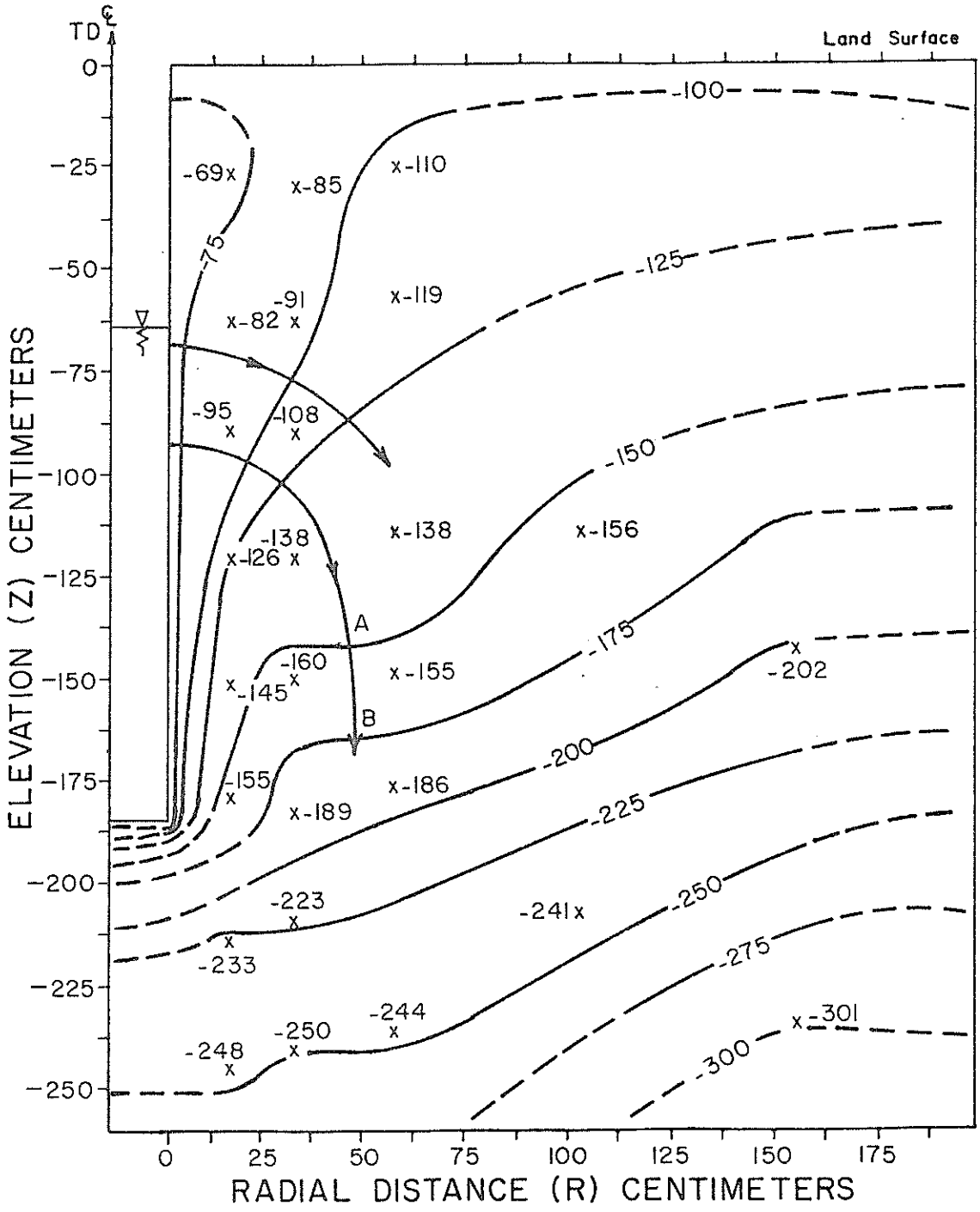

Figure 50. Total Hydraulic Head (cm) after 1230 Minutes at S6T3.

changes in gradient from stage A to stage C. During stage A, horizontal flow components dominate; during stage B and C, vertical flow components are dominant at distances greater than about 25cm from the borehole. During stages B and C when gradients have a larger vertical component, a zone of enhanced wetness develops on top of the silty layers. During stage A perched moisture above the silty layers was not observed because gradients are mostly horizontal and parallel to the silty layers.

From S6T3 infiltration rate and soil-water responses, it is evident that hydraulic conductivity changes with time, even after the wetting front has passed through a particular soil zone. During stage A, average hydraulic gradients close to the borehole decrease rapidly and so does flow rate (figures 41 and 43). During stage B, average hydraulic gradients in close proximity to the borehole are increasing, but flow rate is becoming steady and decreasing slightly. At 20 minutes, gradients near the borehole are actually smaller than at 260 minutes, even though flow rate at 20 minutes is three times greater than at 260 minutes. According to Darcy's law flow rate is directly proportional to hydraulic gradient, if hydraulic conductivity is constant. During stage C, the average hydraulic gradient near the borehole decreases but flow rate increases. This behavior is also counter to Darcy's law if a constant hydraulic conductivity is assumed. Nearly the same response occurred at site 5 as indicated in figures 30, 31 and 32.

One explanation of this behavior is as follows. The stage A soil-water response is due to the passage of a wetting front and the gradual reduction in capillary pressure gradients with increased wetting. Air bubbles become entrapped mostly within the near-saturated zones behind the wetting front and are immediately subjected to a rapid increase in water pressure. This tends to reduce the bubble volume and to increase the water content and hydraulic

conductivity. In response to the gradual increase in K_s, flow from the constant head source increases while gradients adjust to the changing hydraulic conductivity. The amount of change in K_s depends upon how much air is trapped and which portions of water conducting pores are blocked by air. The reason for the transient nature of K_s, and stage B behavior, is believed to be related to the complex factors which affect the amount and distribution of trapped air. From the analysis of Peck (1968) it is evident that bubbles entrapped during infiltration from a borehole may expand until constrained by pore geometry, or they may dissolve completely or partially, depending upon pressure in the bubble and in the atmosphere and pore geometry. Entrapped air bubble volume may also be perturbed by changes in air pressure, temperature or water pressure. In the unsaturated zone bubbles may be stable, although they may also expand due to increasing temperature, decreasing atmospheric pressure, and decreasing soil-water pressure head, and visa versa. Peck's (1968) study also estimates that when the ratio of the volumetric air content to volumetric water content exceeds about 0.01, as it does in our field experiments, the equilibrium process of bubble growth or dissolution would require exchange of air between bubbles and the external atmosphere. The time required to reach equilibration is on the order of 10^4 seconds, but this may range between about 20 minutes and more than a day. This time frame is within the duration of our experiments. During this and subsequent stages, bubbles may also be removed from the pores by bouyancy or translocation to an external air-water interface (Peck 1968, Smith et al. 1966). Removal of entrapped air from the unsaturated zone will change the distribution of water in the pores, and hence change the effective K-ψ relationship. If this change causes the K-ψ curve to become steeper, then some of the pores are likely to drain and pressure heads will decrease, as during stage B.

During stage C changes in pressure head are much smaller than the earlier

stages and are much less predictable. That is, in some tests pressure head decreases and in others it increases or does not change appreciably after the end of stage B. Stage C apparently corresponds with phase 3 infiltration behavior which is influenced by temperature fluctuations in the infiltrating water as shown for S6T1 and S6T3 (figures 39 and 41), for the two day experiment without CO_2 injection at S6T6 (figures 51 to 54), and for the large diameter casing test S7T1 (figures 55 and 56).

There are several factors which cause temperature fluctuations to affect the hydraulic properties of soil containing entrapped air. All tend to cause a decrease in hydraulic conductivity and flow rate with increasing temperature. These temperature sensitive factors include dissolution, the gas laws, surface tension, soil-water characteristic curve (θ-ψ), and unsaturated hydraulic conductivity-pressure head relationship, among others. As the temperature of the infiltrating water increases, the soil-water warms and the gases dissolved in the soil water tend to come out of solution and form bubbles; the bubbles obstruct the pore space and decrease hydraulic conductivity. According to the ideal gas laws, once a bubble has formed its volume will increase with increasing temperature. As temperature increases, soil-water pressure head increases; in the wet range of soil water contents this is due to a decrease in surface tension. Thus, hydraulic gradients may decrease if there are temperature gradients in the soil. Temperature affects surface tension even if there is no trapped air. The dependence of the soil water characteristic curve on temperature when trapped air is present was demonstrated by Chahal (1965): as temperature increases, the soil water content decreases for a given pressure head. There has been little experimental work on the temperature dependence of unsaturated hydraulic conductivity in the presence of trapped air. However, we can infer this

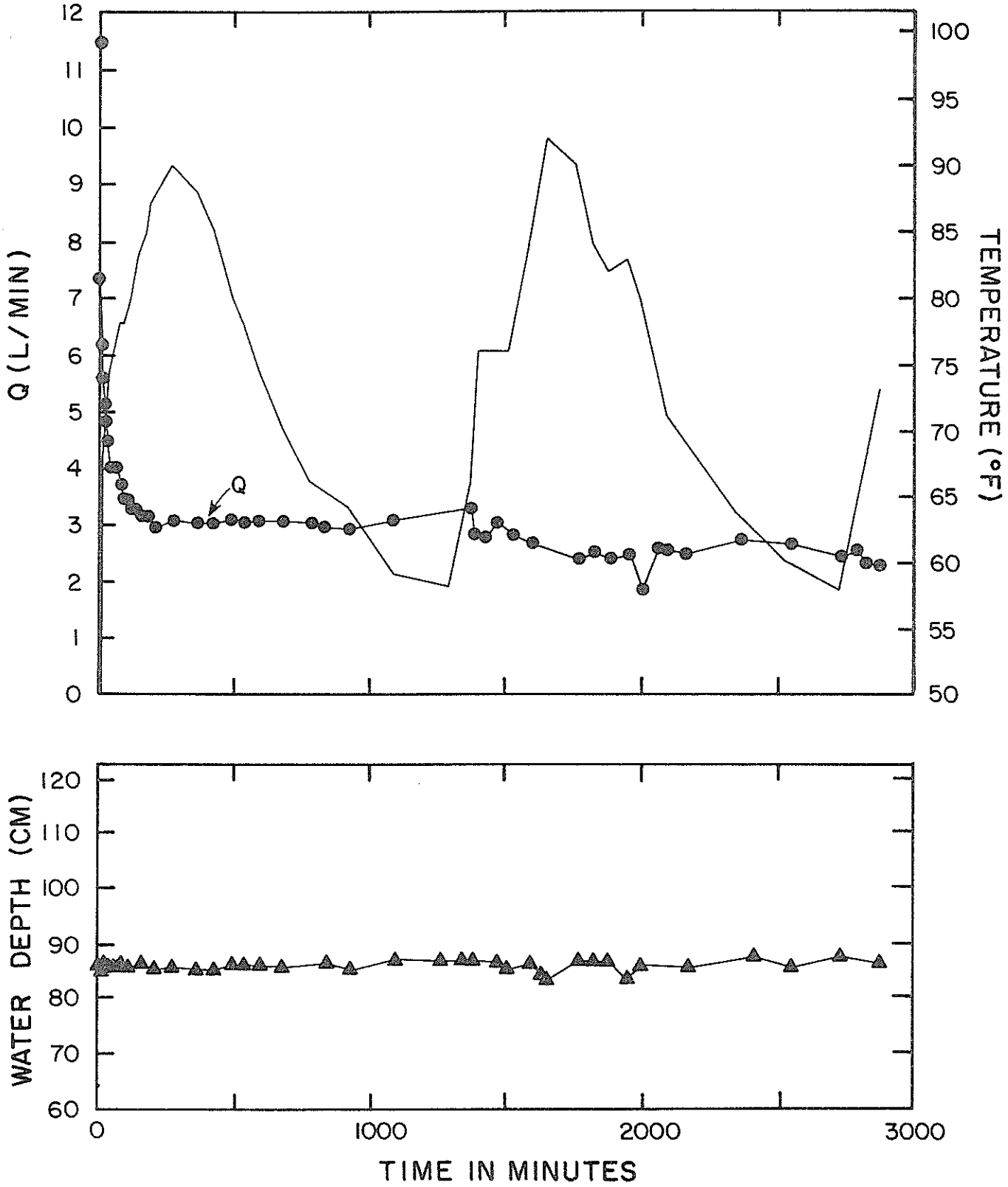

Figure 51. Infiltration Rate, Borehole Water Temperature, and Depth at S6T6.

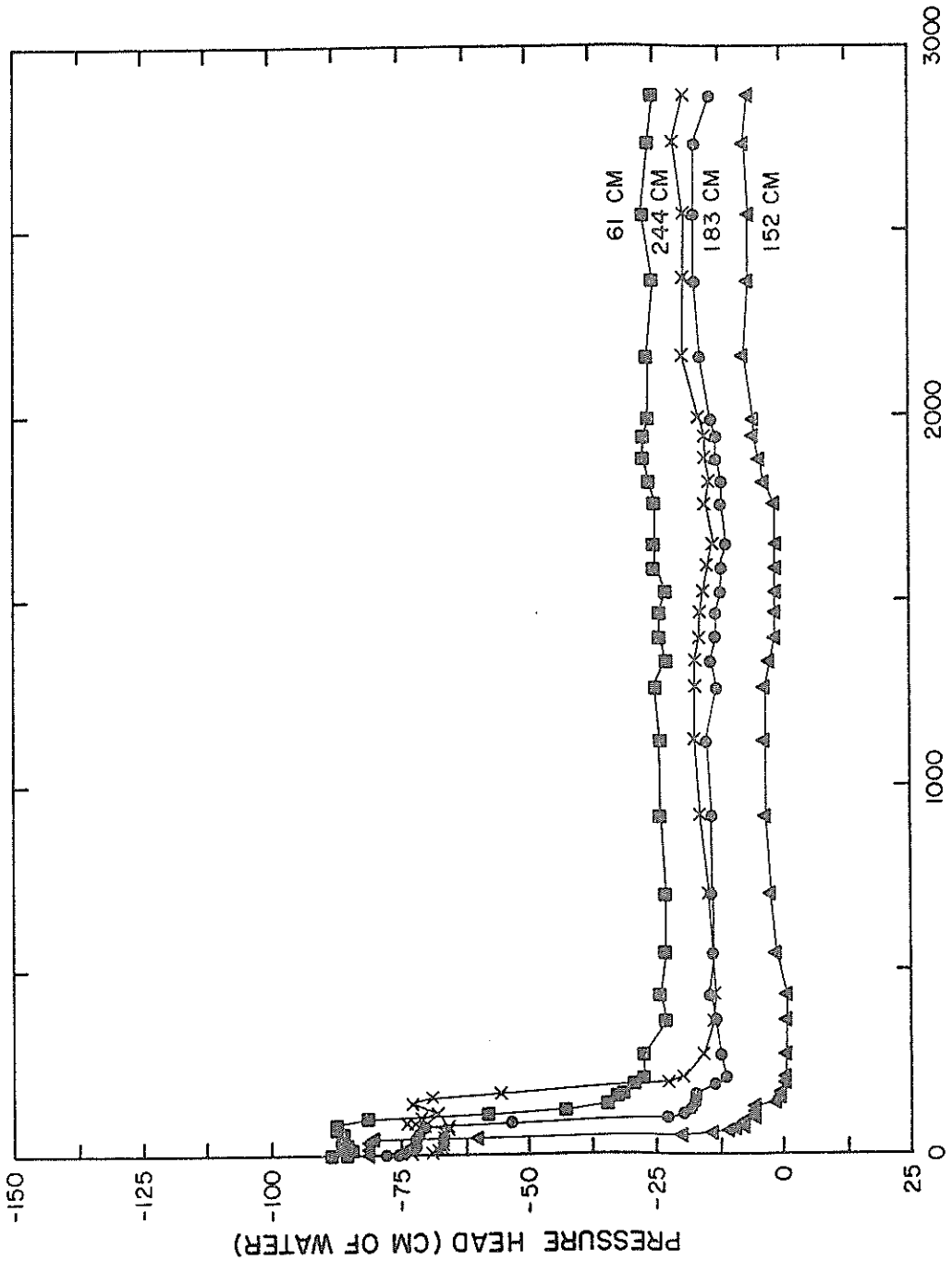

Figure 52. Pressure Head Versus Time 15cm from the Borehole at S6T6.

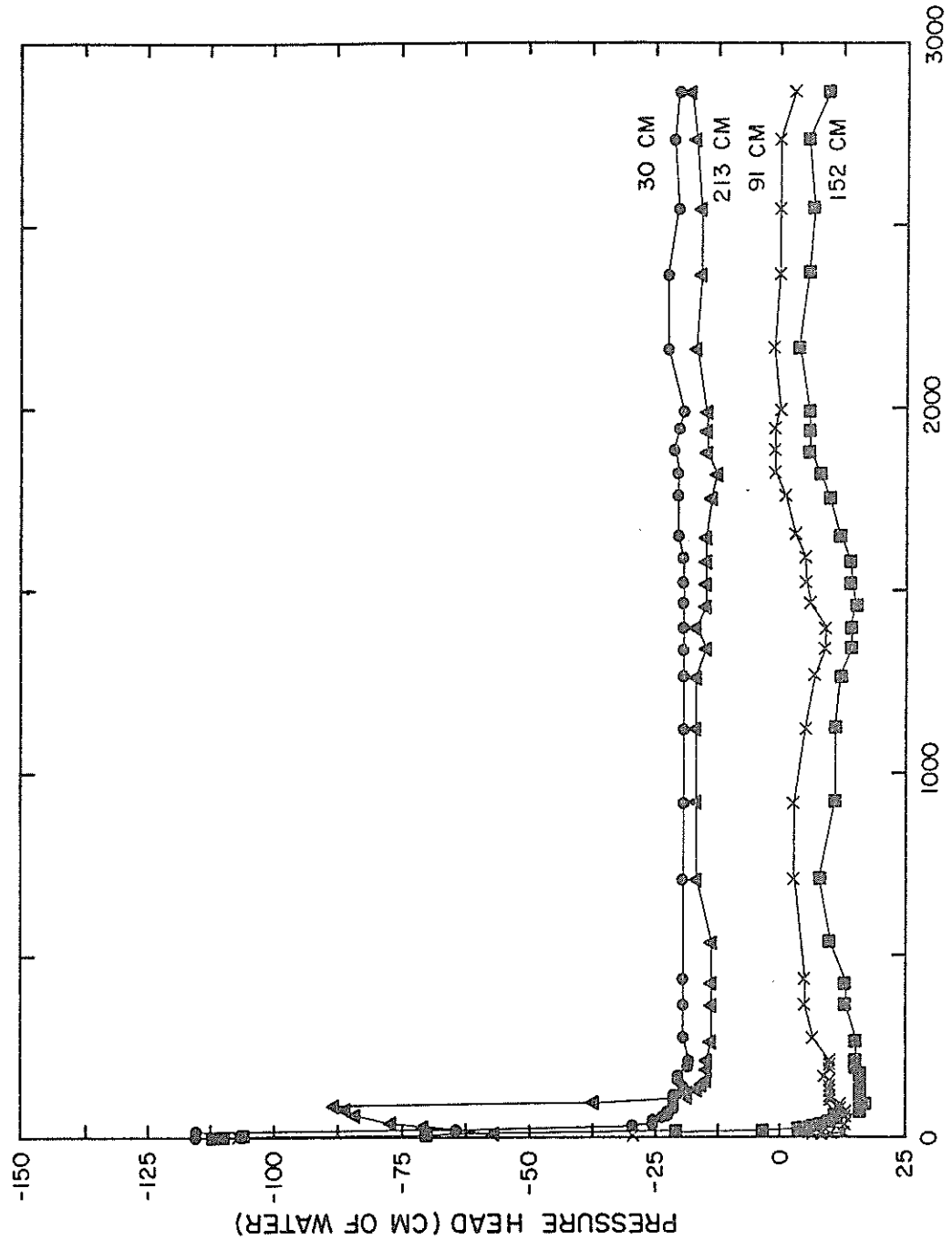

Figure 53. Pressure Head Versus Time 60cm from the Borehole at S6T6.

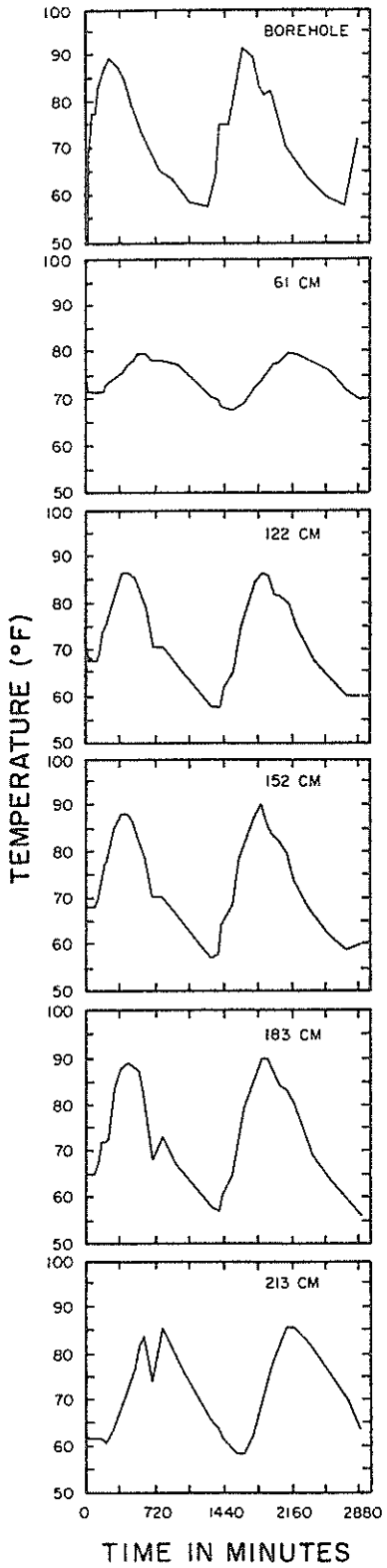

Figure 54. Soil Water Temperature 40cm from the Borehole at S6T6.

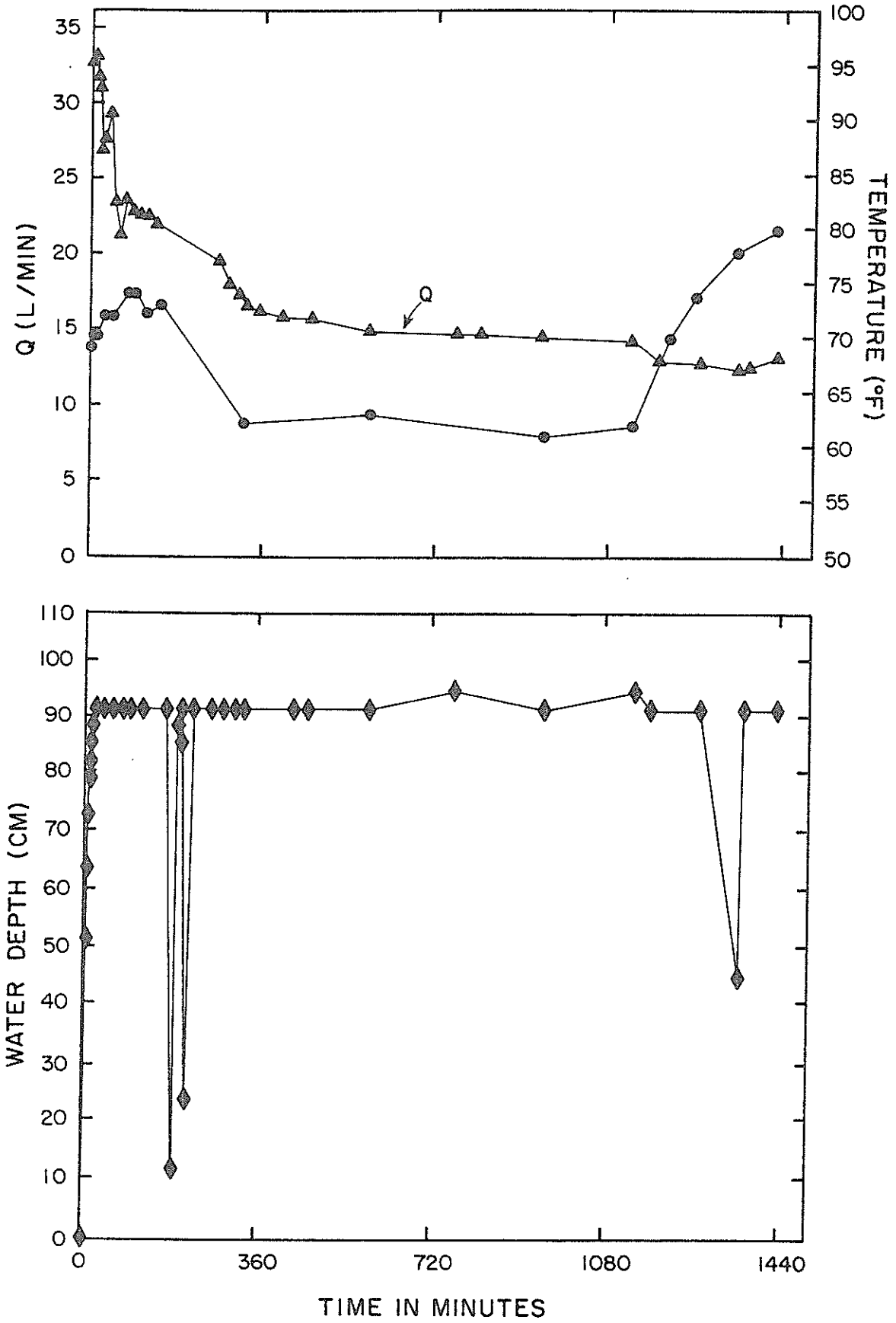

Figure 55. Infiltration Rate, Borehole Water Temperature and Depth at S7T1.

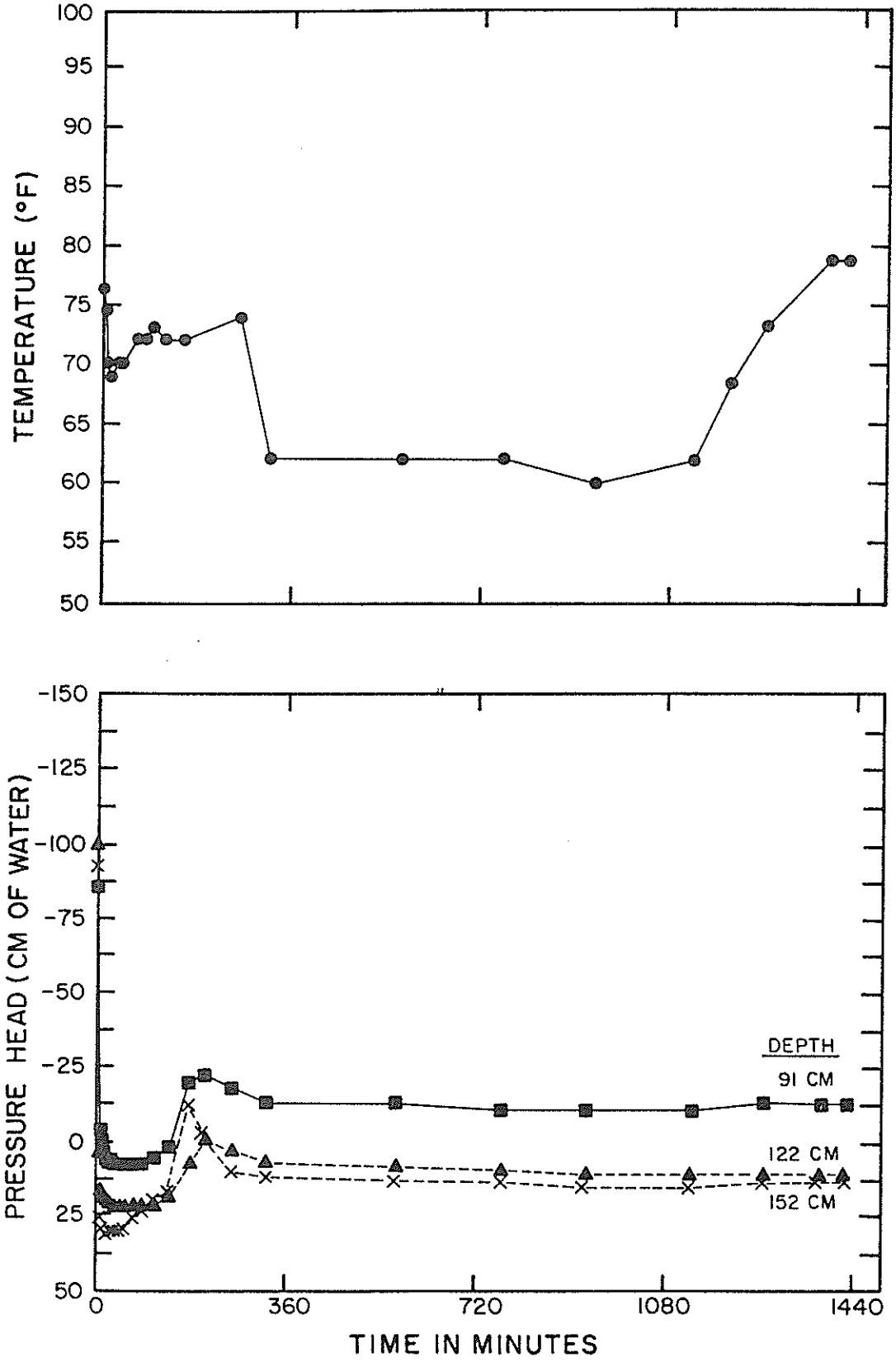

Figure 56. Soil Water Temperature (r=25cm, d-122cm) and Pressure Head (r=15cm) at S7T1.

relationship from the influence of temperature on θ-ψ. As temperature increases the θ-ψ curves are shifted in a direction which gives the impression that the soil is behaving more like a coarser texture soil (Chahal 1965). This shift would tend to steepen the slope of the K-ψ curve. From the results of numerical simulations (Stephens 1979), such a shift during a constant head borehole infiltration test could increase the size of the saturated zone and modify hydraulic gradients. The net result would be a slight decrease in flow rate with increasing temperature. Air temperature increases may also expand tensiometer manometer tubing and alter the density of mercury or other manometer fluids; these effects are generally discounted, inasmuch as most tensiometers in the unwetted zones far from the borehole did not fluctuate significantly with air temperature. Another process which may occur to further complicate interpretation is air bubble nucleation during infiltration (Chahal 1963, Peck 1968).

The experiments at S6T6 (without CO_2) and S7T1 (with approximately 10.5 pore volumes of CO_2 injected) did not exhibit phase two infiltration behavior, as indicated by figures 51 and 55, respectively. Both, however, show the three stages of pressure head and water content fluctuations; for S7T1 these changes are indicated in figures 57 through 62. (The S7T1 is almost identical to the conditions simulated to produce figure 2b. The distribution of water around the borehole in the field is quite similar to simulated results.) The absence of phase 2 for these last two experiments cannot be fully explained at this time. It is possible that much of the air-trapping pore spaces became filled with water during the five experiments prior to S6T6, and that the CO_2 flood at S7T1 was more effective than expected on the basis of pore volumes of injected CO_2.

A much more detailed experimental procedure is warranted to fully explain or predict the influence of air entrapment on measurement of K_s from borehole

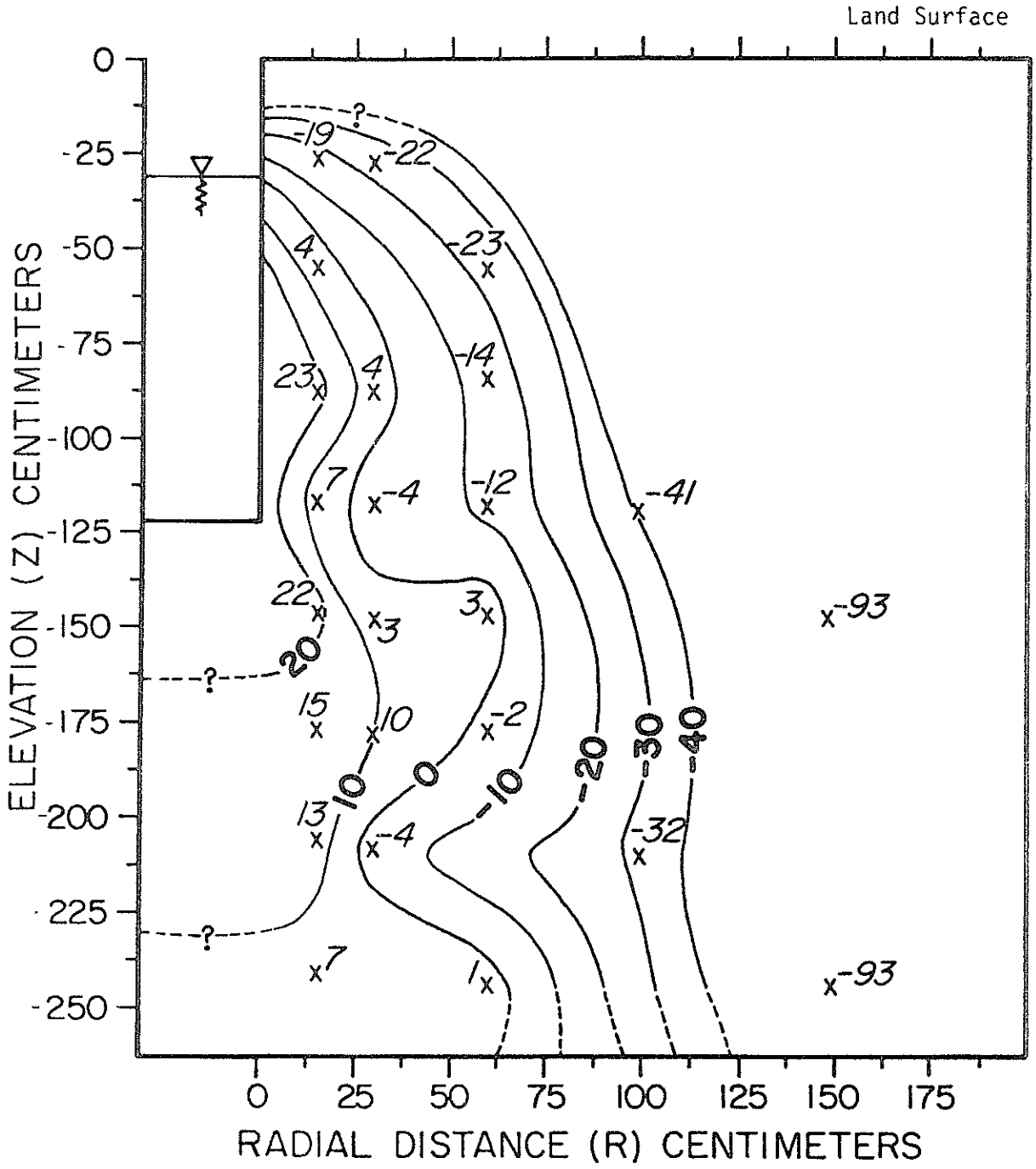

Figure 57. Pressure Head (cm) after 90 Minutes at S7T1.

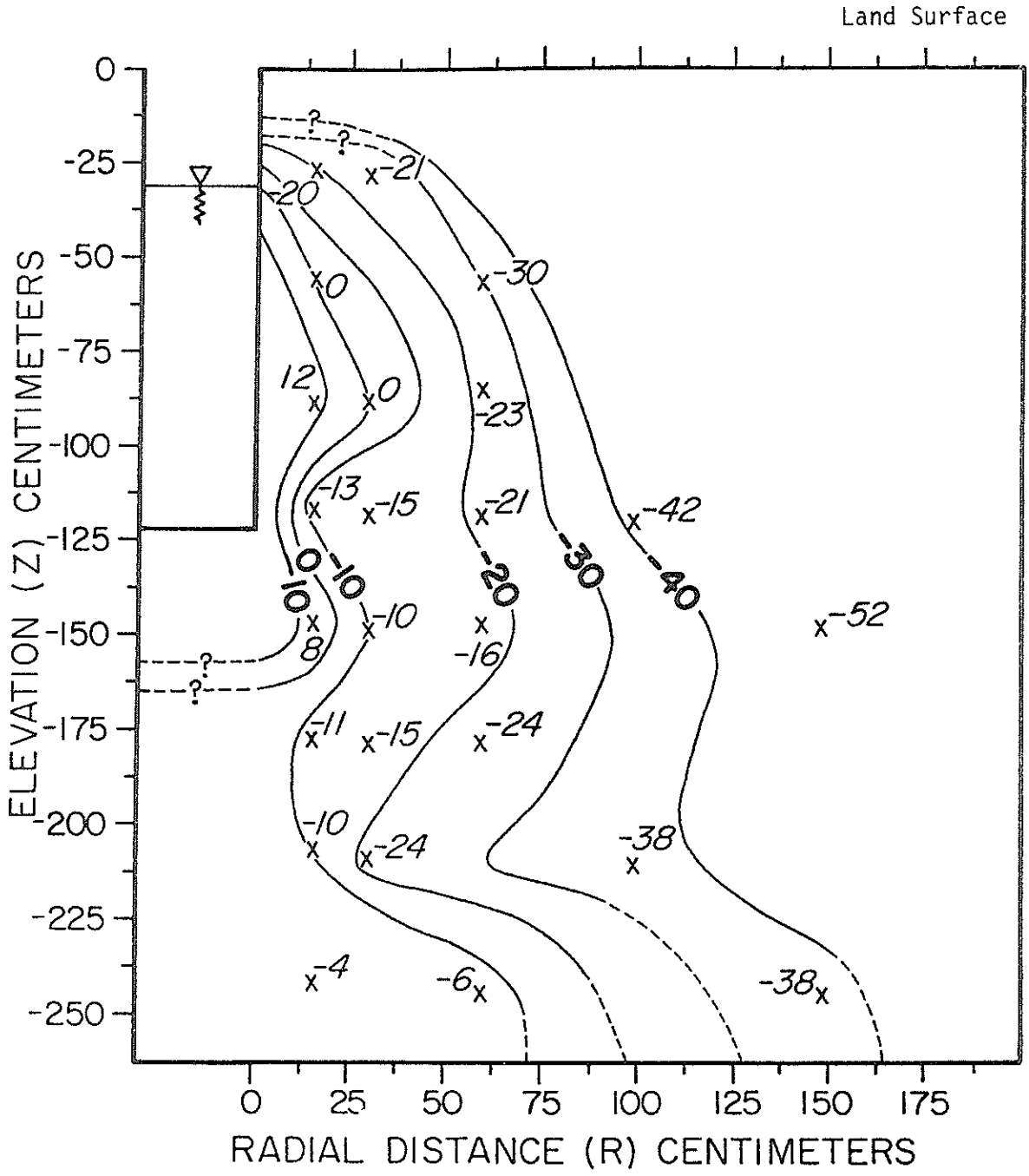

Figure 58. Pressure Head (cm) after 360 Minutes at S7T1.

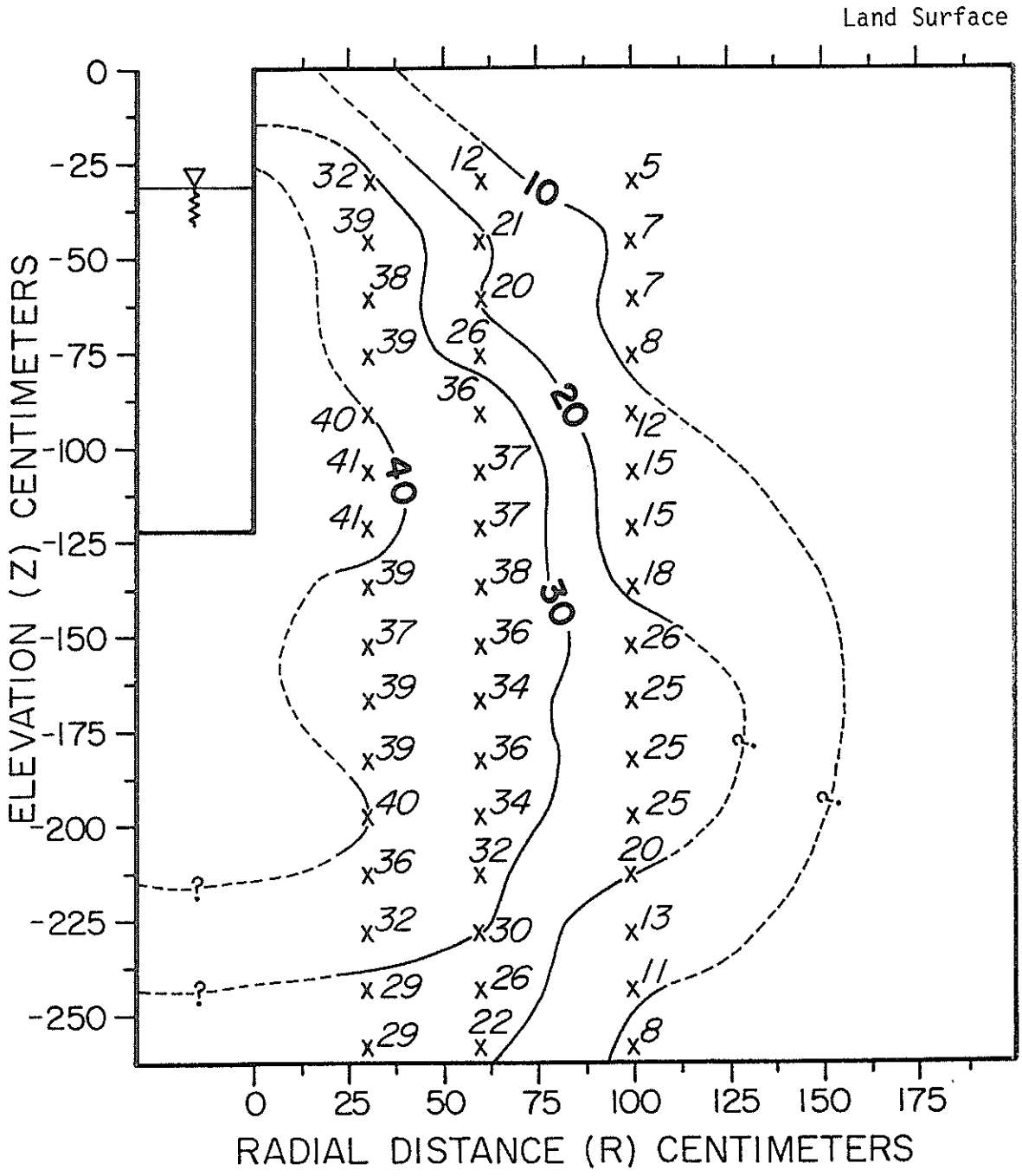

Figure 59. Percent Water Content after 90 Minutes at S7T1.

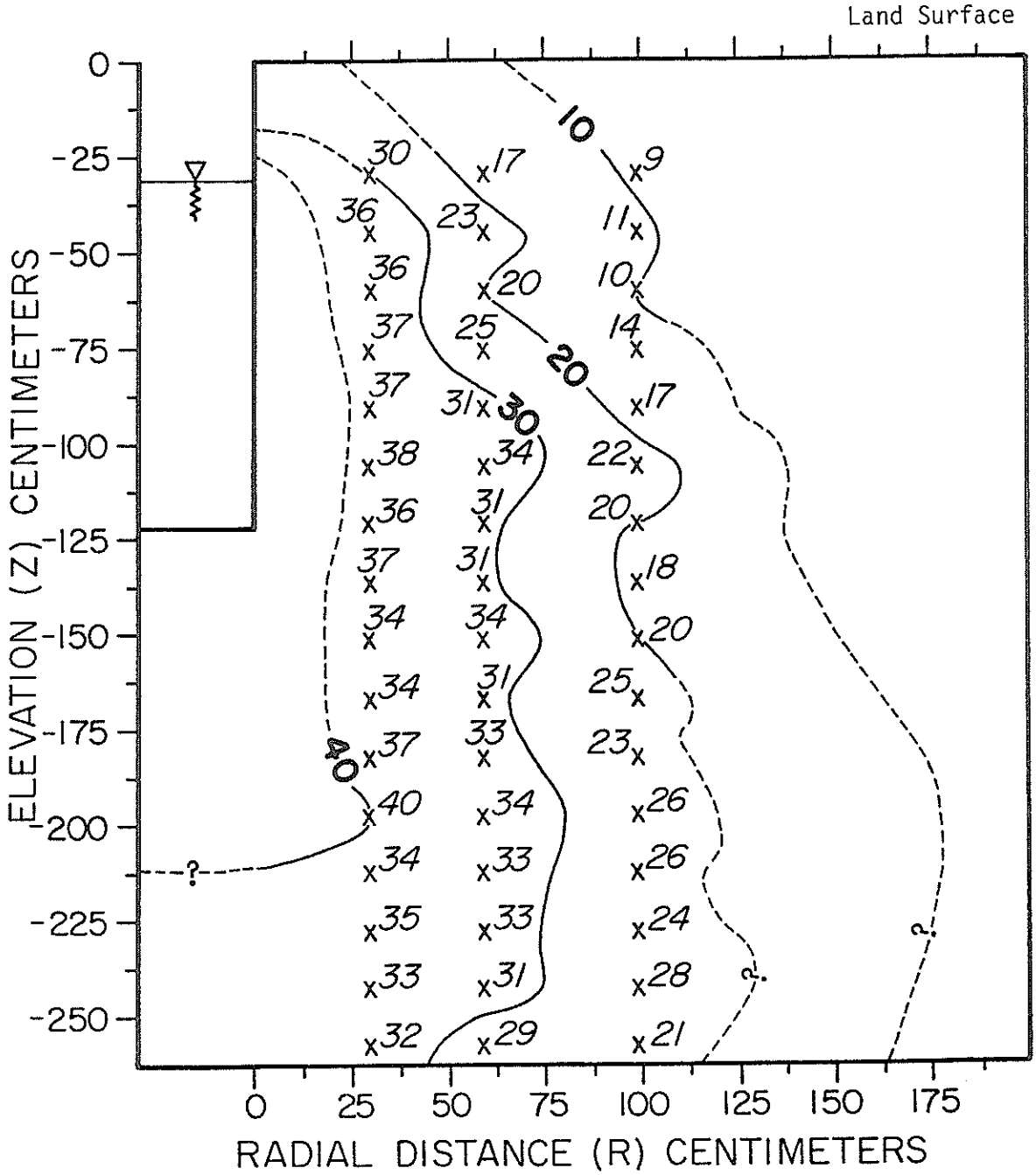

Figure 60. Percent Water Content after 360 Minutes at S7T1.

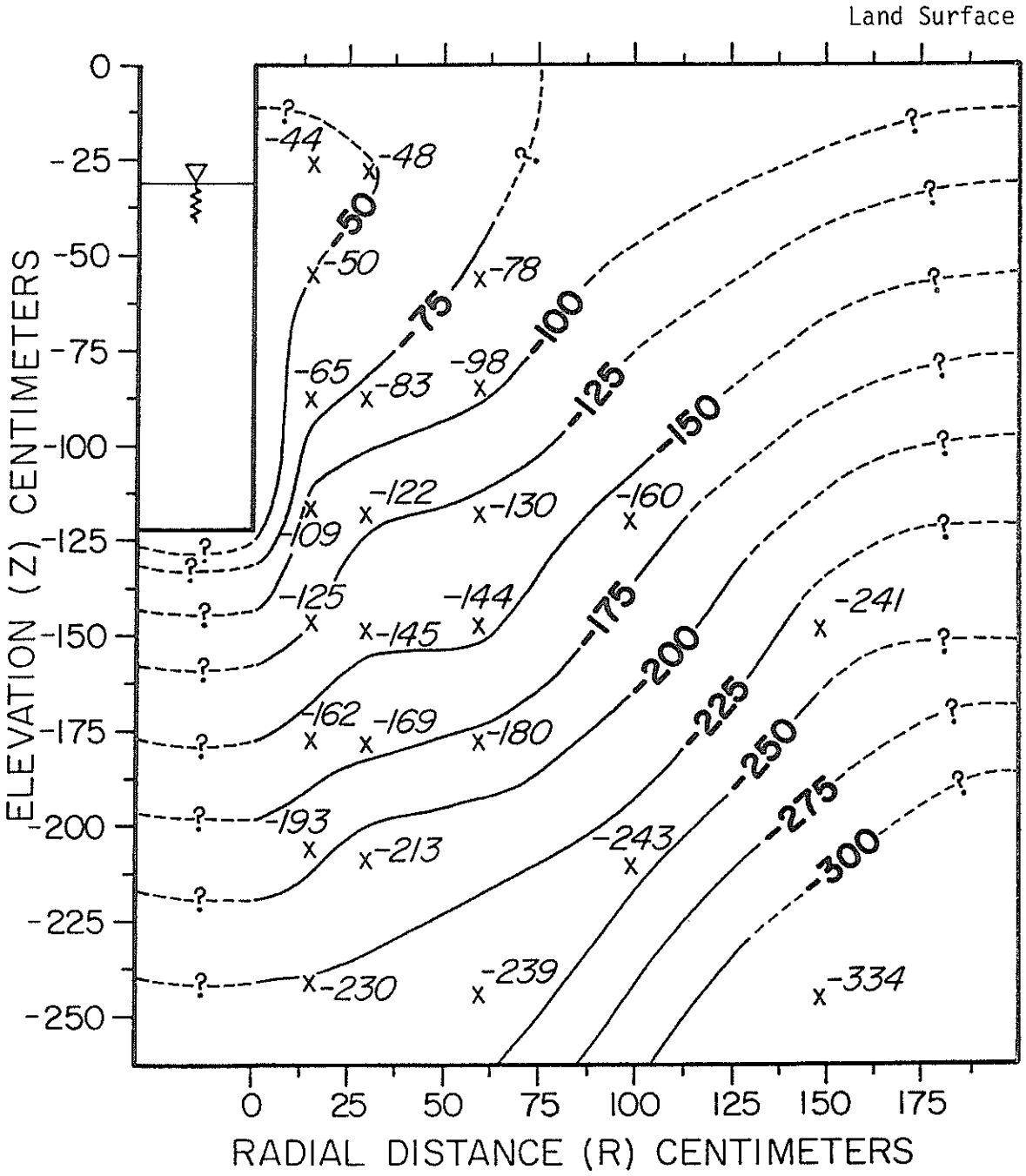

Figure 61. Total Hydraulic Head (cm) after 90 Minutes at S7T1.

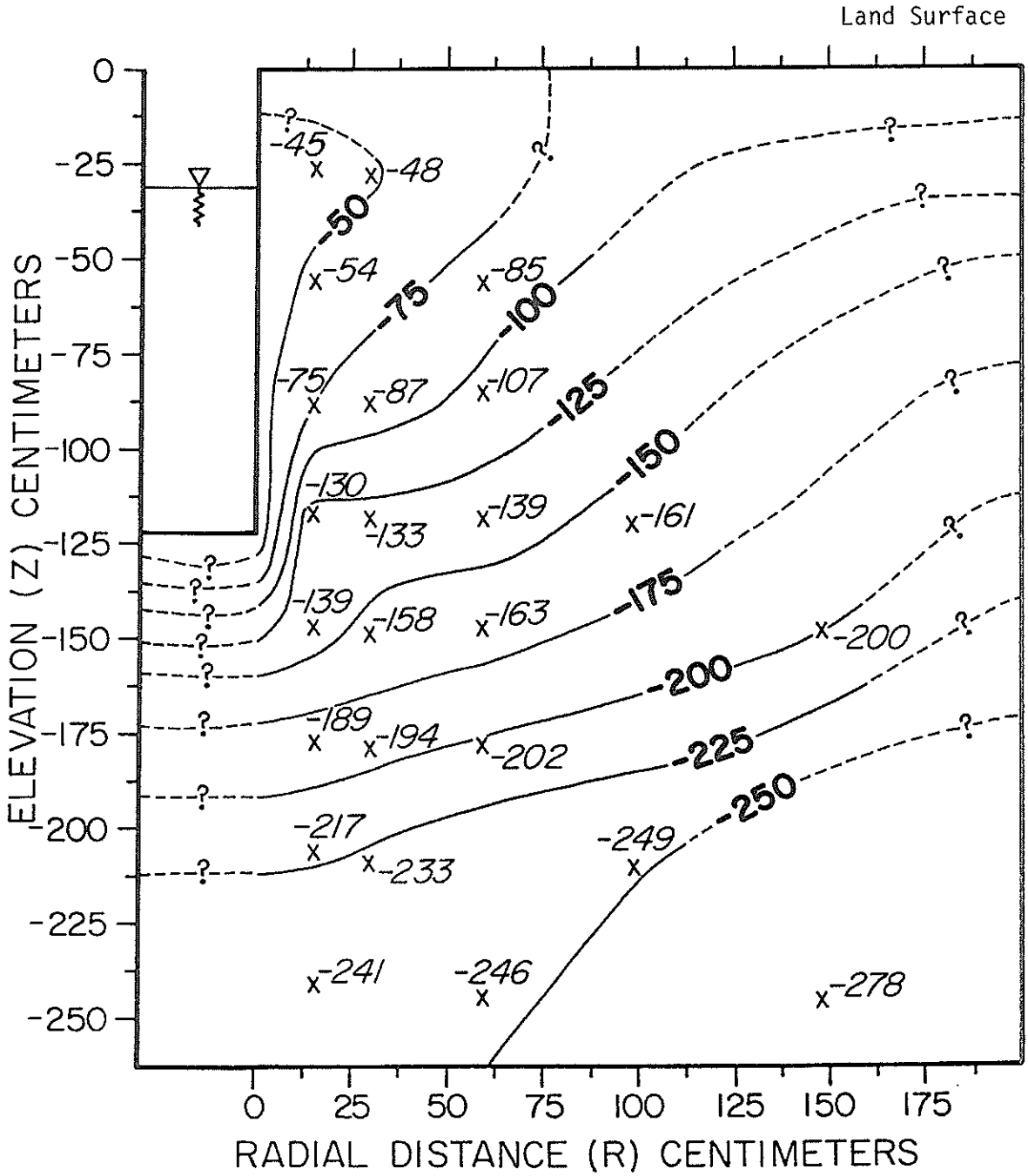

Figure 62. Total Hydraulic Head (cm) after 360 Minutes at S7T1.

infiltration tests. Such work is beyond the scope of the research proposal; nevertheless a great deal of data have been collected for further analysis.

Influence of Borehole Construction

The first four tests were conducted according to USBR (1974) procedures which prescribed the use of gravel in the borehole to prevent the borehole from sloughing. Unfortunately, slight water level fluctuations caused erosion of the upper part of the hole and formation sand filter into the gravel. The 6mm size gravel apparently was too coarse to keep out the 0.25mm sand, even though attempts were made to minimize the impact of water on the wall of the borehole with a perforated hose centered in the gravel pack along the entire length of the borehole. The sloughing problems were solved by using a Johnson plastic well screen with 0.20mm slot sizes. In S2T4, S2T5, S3T1 and S3T2, however, the calculated hydraulic conductivities did not seem to be significantly different with the well screen. PVC casing densely slotted with a hack saw and wrapped with door screen strapped to the outside was used in the remaining site 3 experiments. The percent open area is more than twice as great as the Johnson screen. Compared with the results for the same diameter casing at S2T5 and S3T2, the calculated hydraulic conductivities at S3T3 and S3T4 are about 25 to 50 percent larger (table 8). Some of this difference certainly could be due to spatial variability. This notwithstanding, these results suggest that the open area of well casing can have a significant influence on calculated K_s. A 30cm diameter No. 40 slot steel well screen was used at S7T1 with no apparent sand caving problem.

Another borehole construction factor is whether the bottom of the casing is plugged. Table 8 shows that calculated hydraulic conductivities in open bottom Johnson well screen at S3T1 and S3T2 are 70 percent greater than at S2T4 and S2T5 where the bottom was plugged. Again, owing to spatial

variability, the hydraulic conductivity at site 2 may be 70 percent less on the average than at site 3. On the other hand, K_s calculated for closed-bottom experiments at S3T3 and S3T4 (hack-saw cut PVC casing) is greater than for tests with open bottom Johnson screen at S3T1 and S3T2 (table 8). Thus, it is not clear whether the plugged bottom significantly affects flow rate.

Estimating Final Infiltration Rate from Early Time Data

Stephens (1979) recognized, on the basis of computer simulations and a few field experiments, a reasonably linear relationship between infiltration rate and inverse square root of time. To further evaluate this relationship in the field five borehole infiltration experiments were selected for analysis as shown in table 12. To calculate steady infiltration rate by extrapolation to $t^{-0.5} = 0$ using simple linear regression, data were collected from the time the borehole filled completely until the time when V_{max} (= 2.05 V_{min} table 8) occurred. This limit was selected because V_{max} is easy to calculate, the corresponding time is simple to measure in the field, and it usually is reached before flow rate stabilizes. The steady flow calculated by this extrapolation method, Q_s, the infiltration rate at V_{max}, Q_{vmax}, and the average steady infiltration rate near the end of phase 1, Q_{s1}, are given in table 12. A linear regression between Q and $t^{0.5}$ indicates a fairly good straight line fit (table 12). The two experiments which produced the smallest percent error in Q_{sc} with respect to Q_{s1}, S5T8 and S7T1, also were believed to be effective CO_2 floods. The largest error occurred for S6T5 where the height of water in the borehole (57 cm) was much less than the other experiments.

It is apparent that more work is necessary before the Q versus $t^{-0.5}$ extrapolation procedure can be recommended with predictable results. For our sandy soil the flow rate at V_{max} may be a fair estimate of Q_{s1}, although it consistently overestimates (table 12). In low-permeable materials it may not be practical to wait until V_{max} is achieved, and the extrapolation procedure

TABLE 12
STEADY INFILTRATION RATE (IN LITERS PER MINUTE)
PREDICTED FROM EARLY TIME DATA

Test	Data Points	Q_{sc}	R^2	Standard Error of Est.	Q_{vmx}	t_{vmx} (min)	Q_{s1}	t_{s1}	Q_{max}	$\frac{Q_{sc}-Q_{s1}}{Q_{s1}} \times 100$ (%)	$\frac{Q_{vmx}-Q_{s1}}{Q_{s1}} \times 100$ (%)
S5T3	11	1.11	0.87	1.93	3.92	67	3.50	180	8.45	-68	12
S5T8	5	5.15	0.81	1.29	8.80	33	6.17	260	8.94	-17	43
S6T3	14	3.92	0.88	1.41	5.84	180	5.27	196	9.10	-26	11
S6T5	4	5.94	0.81	0.56	7.06	45	2.13	72	-	179	135
S7T1	7	13.91	0.72	2.22	21.10	57	12.31	1352	-	13	67

Q_{sc} = Calculated flow rate
Q_{vmx} = Measured flow rate when V_{max} infiltrated
Q_{s1} = Minimum flow rate during phase 1
Q_{max} = Maximum flow rate during phase 3

may be more efficient. However, it has already been shown that carbon dioxide injection prior to water infiltration can reduce appreciably the time to reach any stage of infiltration. Carbon dioxide injection and running the test through phase 1 of infiltration may be preferred to the conventional procedure.

Plots of Q^{-1} versus logarithm of time generally fit the S-shape curve predicted by Stephens (1979) when sufficient data are collected. Unfortunately, the curves were not smooth enough to be useful to predict the final Q_s.

Packer Testing

Beginning at 1400 hours April 16, 1982, and after 150 minutes of infiltration, the packer assembly was emplaced to measure flow rate out of 12.7cm packer interval zones in the borehole. The temperature of the infiltrating water was 82°F and initial soil temperatures were about 62°F. Flow rates out of the packer were measured for one minute intervals at five depths within the borehole and are shown in table 13, after correction to 68°F. Total head measurements from tensiometers at radial distances of 15 and 25cm from the packer interval are also given in table 13. The hydraulic conductivities listed are calculated using equation 15. The hydraulic conductivities are very consistent with the results of the conventional borehole infiltration test of S3T4 (table 6). The geometric and arithmetic mean hydraulic conductivities from the five packer intervals with head data at 15cm are 4.31×10^{-3} and 4.82×10^{-3}cm/sec, respectively. The two new empirical solutions for the borehole test developed in this study give 4.3×10^{-3}cm/sec (equation 12) and 4.5×10^{-3}cm/sec (equation 11). Glover's solution tends to slightly underestimate the mean K_s and the Nasberg-Terletskata solution overestimates. Calculated K_s by the Packer test solution

TABLE 13
PACKER TEST RESULTS

Depth to Center of Packer (cm)	Flow Rate Out of Packer (cm_3/sec)	Total Hydraulic Head in Borehole, H (cm)	Total Hydraulic Head @ 15cm radius, h' (cm)	K @ 15cm Radius (cm/sec)
71.4	25.00	-96	-122	8.1×10^{-3}
81.7	25.00	-96	-130	6.2×10^{-3}
91.8	20.83	-96	-136	4.2×10^{-3}
107.0	16.66	-96	-171	1.9×10^{-3}
117.0	33.30	-96	-171	3.7×10^{-3}

Total Hydraulic Head @25cm radius, h'	K @ 25cm Radius (cm/sec)	K_{LAB} Horizontal** @ 25mc (cm/sec)	K_{LAB} Vertical** @ 25cm (cm/sec)	K(h)/K(vert) (Laboratory)
-130	1.1×10^{-2}	2.54×10^{-2}	2.26×10^{-2}	1.12
-135	9.6×10^{-3}	2.04×10^{-2}	1.89×10^{-2}	1.08
-138	7.4×10^{-3}	1.38×10^{-2}	1.56×10^{-2}	0.88
-138	5.9×10^{-3}	2.12×10^{-2}	5.09×10^{-3}	4.16
-197	4.9×10^{-3}	1.46×10^{-2}	1.98×10^{-2}	0.74

** Arithmetic mean of two samples.

at the 25cm distance are greater than at the 15cm distance because of the influence of vertical flow components.

The vertical distribution of flow rate along the borehole neither increases linearly nor is it uniform, as assumed in the Glover and Nasberg-Terletskata analytical solutions, respectively (table 13). The variation in flow rate from the packers appears to be partly related to variability of soil hydraulic conductivity, as indicated by laboratory results from 100cc ring samples collected at the 25cm radius. Variability in hydraulic conductivities calculated from the packer tests follow the general trend in vertical hydraulic conductivity of core samples, although the ring sample results are consistently greater than the packer results. The greatest flow rate occurs near the base of the borehole, as assumed by Glover (1953) and predicted by Stephens (1979).

The excellent agreement between the packer test and conventional borehole infiltration test suggest that the soils is not highly anisotropic. This conclusion is supported by the laboratory analysis of ring samples in table 3.

The results of 20 core samples taken at a 25cm radius at site 3 in both the horizontal and vertical direction indicates that with the exception of packer location 4 (173cm below the datum), the soils at the site are not highly anisotropic.

A source of error during the packer test was the poor resolution of the total hydraulic head as measured by the tensiometers. To overcome this problem, more tensiometers may be required to define the flow field near the borehole. Error due to hydraulic gradient could be reduced by increasing the height of water in the borehole during the tests. This approach would also increase the size of the region where horizontal flow dominates.

PRINCIPAL CONCLUSIONS

The following general conclusions were developed from our research:

1. Soil-water instrumentation surrounding a borehole indicates that the free surface concept of the flow field is inappropriate. Water flowing from the borehole passes through a saturated envelope which is fixed around the borehole and then through unsaturated soil. This result was predicted by numerical simulation using saturated-unsaturated flow models.
2. Entrapped air occurs in both field and laboratory permeameters. Carbon dioxide injection into soil prior to water infiltration is a practical means to reduce trapped air. Carbon dioxide treatment may increase calculated hydraulic conductivities by about two to more than three-fold.
3. For the sandy soil investigated, many of the conventional constant head borehole infiltration experiments exhibited a relatively rapid increase in infiltration rate after the flow rate appeared steady for a few hours. This increase in flow rate from the borehole, which may be on the order of two-fold, is attributed to the expulsion of a significant amount of trapped air. During this period, hydraulic gradients near the borehole actually decrease. Thus, hydraulic conductivity from borehole infiltration tests is a dynamic characteristic of the soil which is sensitive to test procedures.
4. After borehole infiltration begins, the soil wets rapidly, as indicated by tensiometers and neutron probe measurements. Following a brief period of stability, the same instrumentation indicates that the soil drains slightly. This unpredicted non-monotonic behavior occurred in nearly all experiments and may be attributed to the

influence of entrapped air.

5. Soil-water temperature varied considerably due to changes in the temperature of the water supply. Diurnal temperature increases and decreases generally correspond to respective decreases and increases in infiltration rate, even after correcting for viscosity.
6. Air pressure build-up ahead of the wetting front was not observed by a water manometer and air piezometer during borehole infiltration experiments.
7. Boreholes filled with coarse gravel were not effective in preventing caving of the sand. Fine slotted well screen, which keeps sand from the borehole, may slightly restrict water movement and cause somewhat lower apparent hydraulic conductivities. Our experiments regarding the influence of a plug at the base of the borehole are inconclusive.
8. The method to predict the steady flow rate from a graph of infiltration rate versus inverse square root of time produces unpredictable results in fine to medium sand. This procedure may be more relevant to low-permeable media. Carbon dioxide flooding may reduce the test duration and water volume required by about one-half.
9. New empirical solutions to calculate saturated hydraulic conductivity from borehole tests were developed. These new equations account for unsaturated flow effects.
10. Hydraulic conductivities calculated from borehole tests using two new empirical solutions and the Glover solution are quite similar, as predicted by numerical simulations for this soil and the range of test conditions. These borehole methods are generally in good agreement with other field tests, including prolonged ponding. Laboratory experiments on large undisturbed samples collected in shelby tubes also give results similar to field tests. Small

undisturbed samples collected in 100cc rings and placed in an Eijkelkamp constant head permeameter produced hydraulic conductivities on the order of two-fold greater than other results; this may be due to a relatively large amount of flow along the contact between the soil and ring sample.

11. A custom-designed packer assembly showed that the flow rate is greatest near the base of the borehole, but that variability in hydraulic conductivity also has a significant influence on the flow rate distribution. A new field permeameter was developed to calculate horizontal hydraulic conductivity in discrete zones utilizing tensiometers near the borehole. The mean conductivity from five zones along the borehole agrees almost exactly with the hydraulic conductivities calculated from the two new empirical solutions for the conventional borehole infiltration test.

SUMMARY

Experiments were conducted in the field to evaluate the reliability of the borehole infiltration method of determining saturated hydraulic conductivity above the water table. The field site is in a semi-arid sandy terrain north of Socorro, New Mexico, where the depth to the water table is about six meters.

The apparent saturated hydraulic conductivities calculated from the borehole method, as well as results from other commonly used field and laboratory permeameters, are less than at complete saturation due to air entrapment. Without accounting for entrapped air, the calculated hydraulic conductivities may be underestimated by a factor of about two or three. Injecting carbon dioxide into the field soil or laboratory sample is an effective means to remove most of the entrapped air. If no carbon dioxide is

available, entrapped air content may be reduced eventually if borehole infiltration tests are run substantially longer than is generally recommended. Pretreatment with carbon dioxide also offers the advantage of reducing the volume of water required to complete a test by about a factor of two.

New empirical solutions to predicting saturated hydraulic conductivity from borehole infiltration tests were developed. These take into account the influence of capillarity, which other solutions neglected. A new field procedure using packers and tensiometers was also developed to determine hydraulic conductivity in discrete zones of the soil; results from the new packer test procedure is practically identical to that predicted by our new empirical solutions. The new procedures and solutions developed in this study and experimental observations should be of great value to geotechnical and agricultural engineers and hydrologists who work in the vadose zone.

ACKNOWLEDGEMENTS

The cooperation of Ron Perry, John Keiger, William Hutchinson and Ted Stans of the U.S. Department of Interior Bureau of Sport Fisheries and Wildlife in San Acacia and San Antonio, New Mexico, who provided access to the study area, is most appreciated. The work of Gretchen Smith, an undergraduate student at New Mexico Institute of Mining and Technology who performed tedious computations and simulations, is also gratefully acknowledged. Daniel Feinstein, Mustafa Faik Karasarlioglu, and Gregory Lewis conducted field and laboratory studies, which contributed significantly to our project. Lynn Brandvold of the N. M. Bureau of Mines and Mineral Resources supervised chemical analyses of water. We also would like to thank many other New Mexico Institute of Mining and Technology graduate students who were not supported financially on the project, but who volunteered to participate in field experiments.

REFERENCES

Arya, L. M. and Paris, Jack F. 1981. A physioempirical model to predict the soil moisture characteristic from particle size distribution and bulk density data. Soil Sci. Soc. Amer. Jour. 45:1023-1030.

Bouwer, H. 1961. A double tube method for measuring hydraulic conductivity of soil in situ above a water table. Soil Sci. Soc. Amer. Proc. 25:334-339.

Bouwer, H. 1962. Field determination of hydraulic conductivity above a water table with the double tube method. Soil Sci. Soc. Amer. Proc. 26:330-335.

Bouwer, H. 1966. Rapid field measurements of air entry value and hydraulic conductivity of soil as significant parameters in flow system analysis. Water Resources Res. 2(4):729-738/

Bouwer, H. 1978. Groundwater Hydrology. McGraw-Hill, New York, NY. 480 pp.

Bouwer, H. and Jackson, R. 1974. Determining soil properties. IN Drainage for Agriculture. J. van Schilfgaarde (ed.). Am. Soc. Agro. Monograph 17:611-672, Madison, WI.

Bouwer, H. and Rice, R. C. 1967. Modified tube diameters for the double tube apparatus. Soil Sci. Soc. Amer. Proc. 31:437-439.

Brooks, R. H. and Corey, A. T. 1964. Hydraulic properties of porous media. Colo. State Univ. Hydrology Paper 3, Ft. Collins, CO. 27 pp.

Cary, J. W. 1967. Experimental measurements of soil-moisture hysteresis and entrapped air. Soil Sci. Soc. Amer. Proc. 104:1974-1980.

Chahal, R. S. 1965. Effect of temperature and trapped air on matric suction. Soil Sci. Soc. Amer. Proc. 104:262-266.

Christianson, J. E. 1944. Effects of entrapped air upon the permeability of soils. Soil Sci. Soc. Amer. Proc. 58:355-365.

Clapp, R. B. and Hornberger, G. M. 1978. Empirical equations for some soil hydraulic properties. Water Resources Res. 14(4):601-604.

Freeze, R. A. and Cherry, J. A. 1979. Groundwater. Prentice-Hall, Inc., Inglewood Cliffs, NJ. 604 pp.

Glover, R. E. 1953. Flow from a test-hole located above groundwater level. IN Theory and Problems of Water Percolation, D. Zanger (ed.), U. S. Bur. Rec. Eng. Monograph 8:69-71, U. S. Bur. Rec., Denver, CO.

Glover, R. E. 1973. Ground-Water Movement. U. S. Bur. Rec. Eng. Monograph 31:76 pp. U. S. Bur. Rec., Denver, CO.

Gupta, R. P. and Swartzendruber, D. 1962. Flow-associated reduction in the hydraulic conductivity of quartz sand. Soil Sci. Soc. Amer. Proc. 16:6-10.

Gupta. R. P. and Swartzendruber, D. 1964. Entrapped air content and hydraulic conductivity of quartz sand during prolonged liquid flow. Soil Sci. Soc. Amer. Proc. 28:9-12.

Hillel, D. 1980. Fundamental of Soil Physics. Academic Press, New York, NY. 413 pp.

Kim, J. and Kohout, F. J. 1975. Multiple regression analysis: subprogram regression. IN Statistical Package for the Social Sciences. 2nd Edition. Nie, N. H. et al. (eds.) McGraw-Hill Book Co., New York, NY. p. 320-367.

Kozminski, G. 1973. Contribution a l'etude de projets de puits d'injectin en milieu non sature, Bureau de Recherches Geologiques et Minieres, 71 SGN 279 HYD. 72 p.

Kunze, R. J. and Kirkham, D. 1962. Simplified accounting for membrane impedance in capillary conductivity determinations. Soil Sci. Soc. Amer. Proc. 26:421-426.

Lamachere, J. M. 1971. Mesur "in situ" de la permeabilite d'un sol non sature, Bureau de Recherches Geologiques et Minieres, 71 SGN 279 HYD. 79 p.

Machette, M. C. 1978. Geologic map of the San Acacia Quadrangle, Socorro County, NM, Map number GQ-1415. U. S. Geol. Survey, Washington, DC.

McCuen, R. H., Rawls, W. J. and Brakensiek, D. L. 1981. Statistical analysis of the Brooks-Corey and the Green-Ampt parameters across soil textures. Water Resources Res. 17(4):1005-1013.

Miller, I. and Freund, J. E. 1965. Probability and Statistics for Engineers. Prentice-Hall, Inc., Inglewood Cliffs, NJ.

Mualem, Yechezkel. 1976. A new model for predicting the hydraulic conductivity of unsaturated porous media. Water Resources Res. 12(3):513-533.

Mualem, Y. 1976b. A catalog of the hydraulic properties of unsaturated soils. Research Proj. 442, Technion-Israel Inst. Technol., Haifa, Israel. 100 pp.

Mualem, Y. and Dagan, G. 1976. Methods of predicting the hydraulic conductivity of unsaturated soils. Technion-Israel Institute of Technology, Haifa, Israel.

Nasberg, V. M. 1951. The problem of seepage during injection under pressure into an unsaturated soil. Izvestia Akademia Nuak USSR, Otdiel Tekhnicheskyk Nauk, No. 9.

Orlob, G. T. and Radhakrishna, G. N. 1958. The effects of entrapped gasses

on the hydraulic characteristics of porous media. Trans. Amer. Geophys. Union 39(4):648-659.

Peck, A. J. 1966. Diffusivity determination by a new outflow method. IN Water in the Unsaturated Zone, Proc. Wageningen Gentbrugge, Belgium, 191-202.

Peck, A. J. 1968. Theory of the spanner psydrometer, 1. The thermocouple. Agriculture Meteorology 5:433-447.

Robinson, A. R. and Rohwer, C. 1959. Measuring seepage from irrigation channels. USDA-ARS Tech. Bull. 1203. 82 pp.

Seginer, I. and Levine, G. 1964. Infiltration of water under pressure from a piezometer cavity into a homogeneous soil: 1. Soil Sci. Soc. Amer. Proc. 97:48-57.

Smith, W. O., Olse, H. W., Bagnold, R. A., and Rice, J. C. 1966. Certain flows of air and water in sands during infiltration. Soil Sci. Soc. Amer. Proc. 101(6):441-449.

Stephens, D. B. 1979. Analysis of constant head bubble infiltration tests in the vadose zone. Univ. of AZ, Ph.D. Dissertation.

Stephens, D. B. and Neuman, S. P. 1982a. Vadose zone permeability tests: summary. Amer. Soc. Civ. Engrs. Proc., J. Hyd. Div. 108(HY5):623-639.

Stephens, D. B. and Neuman, S. P. 1982b. Vadose zone permeability tests: steady state. Amer. Soc. Civ. Engrs. Proc., J. Hyd. Div. 108(HY50:640-659.

Stephens, D. B. and Neuman, S. P. 1982c. Vadose zone permeability tests: unsteady flow. Amer. Soc. Civ. Engrs. Proc., J. Hyd. Div. 108(HY5):660-667.

Terletskata, N. M. 1954. Determination of permeability in dry soils. Hydroelectric Waterworks, No. 2, Feb., Moscow.

Todd, D. K. 1980. Groundwater Hydrology. 2nd Ed. John Wiley & Sons, New York, NY.

Topp, G. C. and Binns, M. R. 1976. Field measurements of hydraulic conductivity with a modified air-entry permeameter. Can. J. Soil Sci. 56:139-147.

U. S. Bureau of Reclamation. 1974. Earth Manual. 2nd Ed. U. S. Gov't. Printing Office, Washington, DC. 810 pp.

U. S. Dept. of Agriculture Soil conservation Service. Map numbers S4-R-33582 and 4-R-33714. Gross Annual Lake Evaporation and Normal Annual Precipitation, NM Apr. 1972.

van Genuchten, M. 1978. Calculating the unsaturated hydraulic conductivity with a new closed-form analytical model, Dept. of Civ. Eng. Res. Rept. No. 78-WR-08, Princeton Univ., Princeton, NJ.

van Genuchten, M. 1980. A closed-form equation for predicting the hydraulic conductivity of unsaturated soils. Soil Sci. Soc. Amer. Jour., 44(5):892-898.

Watson, K. K. 1966. An instantaneous profile method for determining the hydraulic conductivity of unsaturated porous materials. Water Resources Res. 2(4):709-715.

Winger, R. J. Jr. 1960. In-place permeability tests and their use in subsurface drainage. Internat'l. Comm. on Irr. and Drainage, 4th Cong., Madrid, Spain, 3.

Winger, R. J. Jr. 1965. In-place permeability tests used for subsurface drainage investigations. U. S. Bur. Rec., Div. of Drainage & Groundwater Engrg., Off. of Chief Engineer, Denver, CO.

Zanger, C. N. 1953. Theory and problems of water percolation. U. S. Dept. of the Interior, Bur. of Rec. Engrg. Monograph 8, U. S. Bur. Rec., Denver, CO.